MINIMUM-ERROR, ENERGY-CONSTRAINED SOURCE CODING BY SENSORY NEURONS

BY

ERIK C. JOHNSON

DISSERTATION

Submitted in partial fulfillment of the requirements
for the degree of Doctor of Philosophy in Electrical and Computer Engineering
in the Graduate College of the
University of Illinois at Urbana-Champaign, 2016

Urbana, Illinois

Doctoral Committee:

Professor Douglas L. Jones, Chair
Professor Stephen E. Levinson
Assistant Professor Lav R. Varshney
Professor Mark E. Nelson
Dr. Rama Ratnam

ABSTRACT

Neural coding, the process by which neurons represent, transmit, and manipulate physical signals, is critical to the function of the nervous system. Despite years of study, neural coding is still not fully understood. Efforts to model neural coding could improve both the understanding of the nervous system and the design of artificial devices which interact with neurons. Sensory receptors and neurons transduce physical signals into a sequence of action potentials, called a spike train. The principles which underly the translation from signal to spike train are still under investigation.

From the perspective of an organism, neural codes which maximize the fidelity of the encoded signal (minimize encoding error), provide a competitive advantage. Selective pressure over evolutionary timescales has likely encouraged neural codes which minimize encoding error. At the same time, neural coding is metabolically expensive, which suggests that selective pressure would also encourage neural codes which minimize energy. Based on these assumptions, this work proposes a principle of neural coding which captures the trade-off between error and energy as a constrained optimization problem of minimizing encoding error while satisfying a constraint on energy.

A solution to the proposed optimization problem is derived in the limit of high spike-rates. The solution is to track the instantaneous reconstruction error, and to time spikes when the error crosses a threshold value. In the limit of large signals, the threshold level is a constant, but in general it is signal dependent. This coding model, called the neural source coder, implies neurons should be able to track reconstruction error internally, using the error signal to precisely time spikes. Mathematically, this model is similar to existing adaptive threshold models, but it provides a new way to understand coding by sensory neurons.

Comparing the predictions of the neural source coder to experimental data

recorded from a peripheral neuron, the coder is able to predict spike times with considerable accuracy. Intriguingly, this is also true for a cortical neuron which has a low spike-rate. Reconstructions using the neural source coder show lower error than other spiking neuron models. The neural source coder also predicts the asymmetric spike-rate adaptation seen in sensory neurons (the primary-like response). An alternative expression for the neural source coder is as an instantaneous-rate coder of a rate function which depends on the signal, signal derivative, and encoding parameters. The instantaneous rate closely predicts experimental peri-stimulus time histograms.

The addition of a stochastic threshold to the neural source coder accounts for the spike-time jitter observed in experimental datasets. Jittered spike-trains from the neural source coder show long-term interval statistics which closely match experimental recordings from a peripheral neuron. Moreover, the spike trains have strongly anti-correlated intervals, a feature observed in experimental data. Interestingly, jittered spike-trains do not improve reconstruction error for an individual neuron, but reconstruction error is reduced in simulations of small populations of independent neurons. This suggests that jittered spike-trains provide a method for small populations of sensory neurons to improve encoding error.

Finally, a sound coding method for applying the neural source coder to timing spikes for cochlear implants is proposed. For each channel of the cochlear implant, a neural source coder can be used to time pulses to follow the patterns expected by peripheral neurons. Simulations show reduced reconstruction error compared to standard approaches using the signal envelope. Initial experiments with normal-hearing subjects show that a vocoder simulating this cochlear implant sound coding approach results in better speech perception thresholds when compared to a standard noise vocoder. Although further experiments with cochlear implant users are critical, initial results encourage further study of the proposed sound-coding method.

Overall, the proposed principle of minimum-error, energy-constrained encoding for sensory neural coding can be implemented by a spike-timing model with a feedback loop which computes reconstruction error. This model of neural source coding predicts a wide range of experimental observations from both peripheral and cortical neurons. The close agreement between experimental data and the predictions of the neural source coder suggests a fundamental principle underlying neural coding.

To my beautiful, dearest Sarah, for being the rock of my life and my constant companion in a turbulent world. To my parents, Brad and Vicki, and to my sisters, Cori and Sam, for the family that has always been there for me and provided me with more than I can ever repay. To Milanti, for his valuable aid in writing this thesis. To Edmund and Faye, for their constant distractions.

ACKNOWLEDGMENTS

This research was supported by National Science Foundation (NSF) grant EFRI-BSBA-0938007, NSF grant IGERT-0903622, research funds from the College of Engineering, University of Illinois at Urbana-Champaign (UIUC) and the Coordinated Science Laboratory, UIUC. The electric fish data studied in this document were collected in the laboratory of Professor Mark E. Nelson, UIUC, through National Institutes of Health grant R01MH49242 and NSF grant IBN-0078206. The rat cortical pyramidal neuron data has been graciously made available in the public domain through the International Neuroinformatics Coordinating Facility (INCF) 2009 Spike Time Prediction Challenge, École Polytechnique Federale de Lausanne (EPFL). I have benefited greatly from the guidance of my advisor, Douglas L. Jones, as well as Dr. Rama Ratnam and my committee. My labmates Long Le, David Jun, David Cohen, Michael Friedman, Duc Phan, Alex Asilador, Jamie Norton and Cagdas Tuna have also been a great source of help on this project. Daniel Lee and Professor Justin Aronoff were instrumental in testing the vocoding strategy.

TABLE OF CONTENTS

LIST OF ABBREVIATIONS

ACE	Advanced Combinational Encoder
ATP	Adenosine Triphosphate
AHP	After-Hyperpolarizing Potential
BMI	Brain-Machine Interface
CIS	Continuous Interleaved Sampling
CV	Coefficient of Variation
DC	Direct Current
dB	Decibel
dBV	Signal-level in dB compared to 1 V
ELL	Electrosensory Lateral Line
EE	Envelope Enhancement
EOD	Electric Organ Discharge
EPFL	École Polytechnique Federale de Lausanne
FPGA	Field Programmable Gate Array
HINT	Hearing in Noise Test
Hz	Hertz, Cycles/s (see also, kHz)
IACUC	Institutional Animal Care and Use Committee
IIR	Infinite Impulse Response
IRB	Institutional Review Board
ISI	Inter-Spike Interval

INCF	International Neuroinformatics Coordinating Facility
kHz	Kilo-Hertz, Kilo-Cycles/s (see also, Hz)
L5	Layer 5 of cortex
LIF	Leaky Integrate-and-Fire
LIF-DT	Leaky Integrate-and-Fire with Dynamic Threshold
ms	Milli-Seconds (see also, s)
MSE	Mean Squared-Error
mV	Milli-Volts (see also, V)
pALLN	Posterior branch of Anterior Lateral Line Nerve
PSTH	Peri-Stimulus Time Histogram
RMS	Root Mean-Square
s	Seconds (see also, ms)
SCC	Serial Correlation Coefficient
V	Volts (see also, mV)

CHAPTER 1

INTRODUCTION

In response to sensory stimuli, sensory neurons generate abrupt changes in the voltage measured across the cell membrane, known as action potentials or spikes. These waveforms propagate along the entire length of the neuronal axon, allowing for communication over long distances. Since action-potential waveforms have short duration and are essentially stereotyped for a given neuron, it is assumed that any meaningful information about a stimulus is carried in the timing of the spikes. When a spike arrives at a synapse (the junction between two neurons) it causes release of vesicles containing neurotransmitters, exciting or inhibiting the target neuron [1]. In this sense, information about a stimuli is encoded as action potentials and propagated to downstream neurons. Although critical for communication between neurons, the process of generating action potentials is also metabolically expensive, requiring the activation of ATP-driven mechanisms to restore the equilibrium ion concentrations.

Understanding neural encoding (how stimuli are represented as spike trains) and neural decoding (how stimuli can be reconstructed from spike trains) is critical to understanding information processing in the nervous system [2, 3]. In sensory systems, stimuli typically activate sensory receptors. These receptors release neurotransmitters which stimulate sensory neurons. This thesis will consider encoding of signals by single sensory neurons and small populations of neurons. Especially in sensory neurons, neural codes should represent real-world signals with high fidelity (alternatively with minimal error). This implies that it would be possible to estimate, or decode, the input signal given a spike train from a sensory neuron with minimal error.

As action potentials are largely stereotyped for a given neuron, the spike train from a single neuron can be reasonably modeled as a sum of Dirac delta functions $\sum_{i=1}^{N} \delta(t - t_i)$, where t_i are the spike times of the N spikes. The process of neural encoding is defined here as the process of mapping

a finite-energy, non-negative, continuous-time signal $s(t)$, defined over the interval $[0, T]$, into a sequence of spike times. This continuous-time signal might represent the membrane voltage of the neuron near the site of spike generation. The spike times are a vector of N real values bounded between 0 and T. The process of neural decoding "reads" a spike train and produces a reconstructed signal $r(t)$ [4]. Neural decoding is a mapping between the vector of N spike times and a finite-energy, non-negative, continuous-time signal $r(t)$ defined over $[0, T]$. This reconstruction process could represent stimulation of a downstream neuron by neurotransmitter released at synapses. An illustration of this process can be seen in Fig. 1.1.

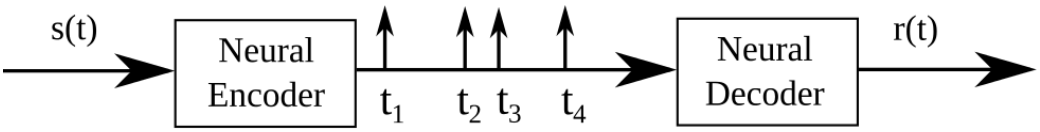

Figure 1.1: Illustration of the neural encoding and decoding processes. The neuron is stimulated by an input signal $s(t)$, which could, for instance, represent the membrane voltage induced in the cell by neurotransmitter released from a sensory receptor. The encoding process maps the signal $s(t)$ to a sequence of spike times, $\sum_{i=1}^{N} \delta(t - t_i)$. The neural decoding process maps a spike train into a reconstructed waveform $r(t)$, and could represent the membrane voltage induced in downstream neurons by neurotransmitter released at synapses.

1.1 Proposed Minimum-Error, Energy-Constrained Neural Encoding by Single Neurons

What principles govern neural encoding and decoding in sensory systems? This thesis posits that sensory neurons have been subjected to millions of years of selective pressure resulting in strategies which encode stimuli with minimum error. An optimized neural encoder should time spikes such that the signal can be decoded with minimum error. Neurons, however, are also constrained by physiology. A critical constraint for neurons is the amount of available metabolic energy [5]. Every action potential generated by a neuron consumes energy, as ATP-driven sodium-potassium pumps work to restore the cell's ion concentrations and resting membrane potential. It has been suggested that metabolic energy consumption has placed selective pressure

on the development of sensory systems and neural codes [6]. This thesis develops a model of neural encoding and decoding by sensory neurons which minimizes encoding error subject to a constraint, or penalty, on the metabolic energy consumed.

Traditionally, the problems of neural encoding and decoding have been approached separately. However, an encoding scheme which is designed without knowledge of the decoding scheme may be suboptimal. This thesis supposes that the processes of neural encoding and decoding are closely related. Here it is assumed that neurons attempt to minimize the error between a finite-energy, non-negative, continuous-time signal $s(t)$ defined over $[0, T]$ and a reconstruction of the signal, $r(t)$, given only the spike times. This interpretation is most relevant to primary sensory neurons, but may have implications for many other kinds of neurons as well. Millions of years of selective pressure suggest that the spike times, t_i, should be timed such that the error $s(t) - r(t)$ is minimized. This thesis uses a squared-error criterion. Although other error measures may be relevant, there is currently little experimental evidence to suggest which criterion should be used. Neurons are also constrained by the energy they can expend. A possible model is that a neural code must use energy e less than a total energy budget E. This leads to the following general optimization problem for a fixed decoding process

$$\min_{t_1,t_2,\ldots,t_N} \int_0^T (s(t) - r(t))^2 dt \qquad (1.1)$$
$$\text{subject to } e \leq E$$

What form might the decoding strategy take? One possibility to generate $r(t)$ is to filter the spike train with a linear filter $h(t)$, $r(t) = h(t) * (\sum \delta(t - t_i))$. This approach, though simple, is based on post-synaptic filtering of spike trains, where the post-synaptic neuron membrane passively filters spikes to create a time-varying membrane voltage [7]. Such a passive filter can be approximated as a linear, time-invariant filter $h(t)$. Existing neural decoding methods such as stimulus reconstruction [4] and reverse correlation [8] also model the decoding process as a linear filter. The simplest biologically plausible reconstruction filter is a first-order low-pass filter with impulse response $h(t) = A \exp(-t/\tau)$. This reconstruction filter form comes from modeling a cell membrane as an RC circuit, which is a well-established model of the

passive electrical properties of cell membranes [7]. For example, a first-order passive component is included as the leak term in the Hodgkin-Huxley model of membrane voltage [9].

Intuitively, firing more spikes provides more degrees of freedom for encoding an input signal and should lead to lower reconstruction error. Why, then, are there such a variety of spike rates observed experimentally? Generating action potentials is an energy-intensive process for neurons, consuming a considerable amount of a neuron's metabolic energy [10, 11]. Prior work has estimated that 20%-50% of a neuron's energy is expended generating and propagating action potentials. Other sources of energy consumption include maintaining the baseline ion concentrations and functions of the cell, generating post-synaptic potentials, and recycling vesicles. Neural energy expenditure can then be broadly divided into two categories that are relevant for neural encoding. The first category consists of the baseline metabolic processes which are not affected by spiking activity, at least on short time scales. From the perspective of an encoding scheme, this energy expenditure is a fixed component b. The other major category consists of energy costs incurred for every spike fired. This includes generating and propagating the action potentials, as well as releasing and recycling vesicles. As post-synaptic potentials are generated in response to spiking activity, these costs could also be considered to be incurred when a spike is fired. These costs are generally proportional to the number of spikes fired, and can be roughly approximated by a per-spike cost k. This leads to a model of the energy consumption rate in a neuron as $E = b + kR$ [12], where R is the average spike-rate in spikes per second. A neural encoder can therefore control its energy consumption by limiting the mean rate at which spikes are fired. This results in a trade-off between the number of spikes used to encode a signal and the encoding error.

In this thesis, a minimum-error, energy-constrained neural encoding scheme is developed in which the encoder uses knowledge of the decoded signal to track the encoding error. Spikes are fired whenever the error signal reaches a (potentially time-varying) error threshold, $\gamma(t)$.

$$s(t) - r(t) = \gamma(t) \tag{1.2}$$

This system is closely related to dynamic threshold spike-timing models [13, 14]. These models, however, are not optimized to minimize reconstruction

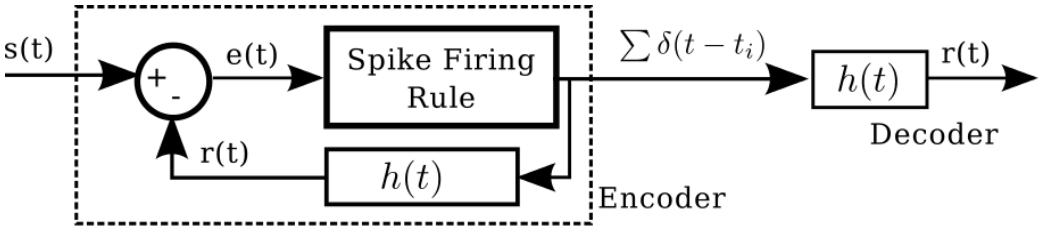

Figure 1.2: The proposed minimum-error, energy-constrained neural encoding system, which is related to dynamic-threshold neural models [13, 14]. The reconstruction filter is $h(t)$. In this model, the decoding filter is used to generate $r(t)$ and also to compute the error $e(t) = s(t) - r(t)$. Spikes are generated when $s(t) - r(t) = \gamma(t)$, where $\gamma(t)$ is a potentially time-varying threshold. The parameters of the proposed model must be optimized to achieve minimum error for a given energy constraint.

error. A block diagram of the proposed encoding and decoding scheme can be seen in Fig. 1.2. In Chapter 3, the optimality of the proposed model is proved and the optimal parameter values are derived under the assumption of a high spike-rate.

The proposed minimum-error, energy-constrained neural encoding scheme tracks the error between the reconstructed waveform and the input signal. When this error gets too large, a spike is fired. An optimal encoder should time spikes to minimize encoding error while also limiting the spike rate. An example encoding of a signal can be seen in Fig. 1.3. Figure 1.3A shows the input stimulus in black and a possible reconstructed signal in red. The reconstructed waveform shows discontinuities whenever a spike is fired. This is due to the first-order form of the reconstruction filter. Figure 1.3B shows the spike times for this example, and Fig. 1.3C shows the reconstruction error. In this example, the threshold level γ is a constant, which does not vary with time.

1.2 Overview

The goal of this thesis is to investigate models of minimum-error, energy-constrained neural encoding. This thesis hypothesizes that sensory neurons maintain a trade-off between reconstruction error and energy consumption. This suggests that any model of neural encoding, or spike timing, should explicitly consider possible reconstruction error and energy expenditure when

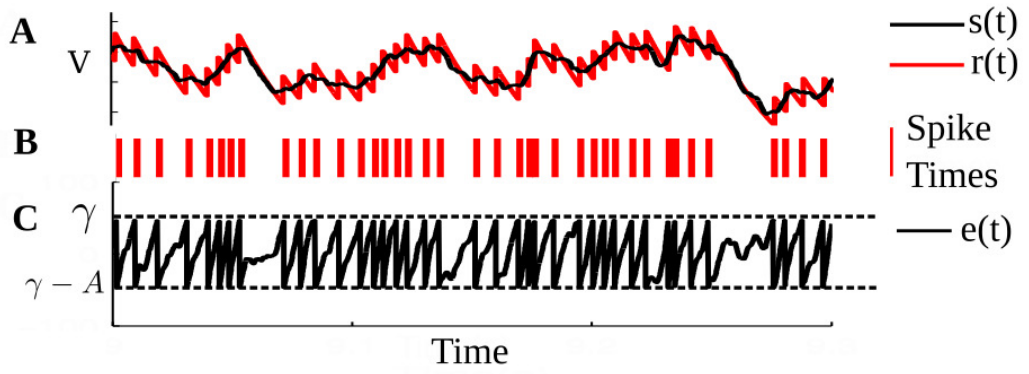

Figure 1.3: Example encoding of an input signal $s(t)$ by the neural encoder shown in Fig. 1.2. The input signal is shown in black and the reconstructed signal in red. The spike times predicted by the model are shown in Panel B. One can see that the reconstructed signal has a discontinuity at the spike times, corresponding to the arrival of a spike at the reconstruction filter. This approach creates an approximation of the original input signal. Panel C shows the error term, $e(t) = s(t) - r(t)$. In this example γ is assumed to be constant and the error is bounded between γ and $\gamma - A$. This thesis hypothesizes that an optimal neural encoder should time spikes such that the error is minimized, subject to an energy constraint.

deriving an optimal encoding strategy.

Investigating this hypothesis first requires the development of the energy-constrained neural encoding problem and the derivation of an encoding strategy and optimal parameter values. Equally critical is the comparison of the predicted spike-times and reconstructed waveforms against experimental data and the predictions of other neural encoding models.

The proposed encoding strategy also has many possible extensions. The first extension presented in this thesis is the interpretation of the optimal, energy-constrained neural coder as an instantaneous rate coder of a rate function determined by the input signal and reconstruction filter. The second extension is modeling stochastic spike-firing to study encoding in small populations of sensory neurons. Finally, new models of neural encoding have important implications for Brain Machine Interfaces (BMIs) which encode information to stimulate neurons. One example is encoding auditory signals in cochlear implants. This thesis proposes a strategy to encode sounds in cochlear implants which is consistent with minimum-error, energy-constrained neural coding.

This thesis presents the proposed neural coding model along with several extensions. Chapter 2 begins by reviewing the relevant literature in neuroscience, computational neuroscience and information theory. This background establishes the relevance of the problem and argues for the novelty of the approach. Chapter 3 introduces a simplified version of the encoding model, then presents a more formal development of the theory for this model in the limit of high spike-firing rates. In Chapter 4, the predictions of the model are compared against data from primary sensory neurons and cortical neurons. Chapter 5 introduces an instantaneous rate code which produces identical interspike intervals when compared to the optimal neural coder, suggesting an alternative interpretation of optimal neural coding. To extend the model to stochastic spike-firing, Chapter 6 introduces a stochastic threshold which has implications for encoding in neural populations. Finally, Chapter 7 introduces a possible method to apply the theory of minimum-error, energy-constrained neural coding to sound coding in cochlear implants.

CHAPTER 2

LITERATURE REVIEW

Understanding how physical signals such as light intensities or sound pressure waves are represented and processed in the nervous system has long been a fundamental goal of systems neuroscience. The neurons of the nervous system are the main processing and communication units in the brain. Neurons transmit signals along their axons by firing action potentials, also known as spikes. These action potentials allow for rapid transmission of information over long distances. During an action potential, channels embedded in the cell membrane of the neuron allow ions, such as sodium and potassium, to flow into and out of the cell. The action potential consists of a rapid depolarization of the cell membrane voltage followed by a somewhat slower re-polarization. This change in membrane potential propagates down the axon of the neuron due to the action of voltage-gated ion channels. Following the action potential, the neuron must restore the resting concentrations of the ions, which requires the ATP-driven activity of sodium-potassium pumps [7].

Neurons use spikes to encode and transmit information throughout most of the nervous system. When the dendrites of a neuron are stimulated by a neurotransmitter (usually released by another neuron or sensory receptor), the cell membrane voltage is changed. In the simplest case, when the cell membrane voltage in the cell body, or soma, is sufficiently depolarized, an action potential is generated. This action potential is propagated down the axon of the neuron to its axon terminals. Here, the neuron interfaces with other neurons, forming a connection called a synapse. When an action potential reaches the synapse, the pre-synaptic neuron releases vesicles containing neurotransmitters. The neurotransmitters then excite or inhibit the post-synaptic neurons. In this way, neurons use spikes to transmit information about the stimulus at their dendrites to post-synaptic neurons [1].

Spike shape and propagation speed vary significantly across neuron types

and geometry [15], but the spike shape is largely fixed for a given neuron geometry. Some conditions, such as rapid bursts of spikes or complex axonal geometries, can alter the action-potential shape [16], but spike shapes are generally fixed for a given neuron. Unlike experimental extracellular recordings, the shapes of the spikes do not play a major role and spike-sorting is not done by the nervous system [17]. A spike train, therefore, can be thought of as a sequence of all-or-none responses. As each spike waveform is essentially the same, the information conveyed by a spike train must be represented in the times of the spikes. Such a signal can be thought of as a sum of Dirac deltas, $\sum \delta(t-t_i)$. The critical question is how neurons, such as sensory neurons, represent continuous signals such as sensory input, receptor potentials, and membrane voltages as a spike train.

Of course, neurons do not simply connect one neuron or receptor to another neuron. Many neurons have complex dendritic arbors with synapses from hundreds of other neurons. The aggregate activity of all these presynaptic neurons drives the spiking activity of the neuron at the soma [18]. At the terminals, a neuron may again synapse onto hundreds of other neurons, forming a large and complex network. Although the behavior of large populations of neurons is an extremely important problem, this thesis will largely deal with spike generation in a single neuron. In sensory systems, understanding encoding by single neurons is critical to describing the role of primary sensory afferents, the first stage of processing in sensory systems. Another critical point is that the study of single neurons allows for direct comparison to experimental data where the activity of individual neurons can be measured in response to known stimuli.

2.1 Spiking Neuron Models

Attempts to model the membrane voltage in neurons date back at least to Lapicque [19]. Measuring the membrane potentials of frog nerves, Lapicque began to model the membrane of the cell as an integrator. Studying the giant squid axon, Hodgkin and Huxley [9] greatly expanded on this concept to model the cell membrane as a resistive and capacitive circuit with variable resistance terms. This results in a coupled set of nonlinear differential equations which determine the voltage across the cell membrane. The resistance

terms model different ionic channels, and the model is capable of predicting action-potential waveforms. Over the years, the Hodgkin and Huxley model has been expanded many times with the addition of more terms capturing different ionic currents to model phenomenon such as spike-rate adaptation (see, for example [20]). These models are closely coupled to the biophysics of cells, modeling the flows of individual ion currents. These models predict not only the times at which action potentials occur, but also the shape of the action potential and the membrane voltage in response to an input current. These models are biophysically plausible, but also require a large number of parameters to accurately reproduce experimental data.

A much simpler model of neuronal spiking is the leaky integrate-and-fire (LIF) model, which has been used extensively (for example, Model 1 of [21]). In this approach, the membrane of the cell is modeled as a low-pass filter, and the membrane voltage is defined as

$$\tau \frac{dV(t)}{dt} = RI(t) - V(t) \tag{2.1}$$

where $V(t)$ is the time course of the membrane potential, $I(t)$ is the input current, R is the membrane resistance, and τ is the membrane time-constant. Whenever the voltage reaches a fixed threshold θ, a spike is generated and the voltage is reset to a resting level V_r. Although it is a very common neural model, the LIF model does not predict the membrane voltage and does not reproduce all of the expected behaviors of experimental neurons, such as spike-frequency adaptation [22]. In general, there are a variety of neural models with varying trade-offs between computational complexity, accuracy, and number of parameters [23].

A promising class of models, which balance relatively low computational complexity with good predictive power, are dynamic-threshold models (also known as adaptive or moving thresholds). The key concept is an extension of the classic LIF model dating back at least to Katz [24], which was then explored further [25, 26]. The goal of these models is to better represent adaptation in spike rates and relative refractory periods. Rather than using a fixed threshold θ as in the standard LIF model, the firing threshold varies with time in response to spiking activity. The intuition is that the threshold should be raised initially following a spike, resulting in a lower probability of firing. The threshold then decays, and further spiking becomes more proba-

ble. This adaptation accounts for the relative refractory period observed in neurons.

More recently, models with dynamic thresholds have been used to model the spike-train statistics of weakly electric fish [14, 27, 28], showing strong negative correlations between interspike intervals as well as spike-frequency adaptation. These models, however, do not explicitly incorporate ion currents as a Hodgkin-Huxley style model does. An alternative approach to introducing spike-frequency adaptation is the addition of an adaptation current model, such as modeling the after-hyperpolarizing potential (AHP) [29] or M current [30]. Previous studies have incorporated such adaptation currents, showing similar results when compared to dynamic-threshold models without explicit ion-channel models [31, 32]. Dynamic threshold models can also be extended to include nonlinear terms in the differential equations which define the model, which help explicitly capture the absolute and relative refractory periods [33, 34, 35].

Dynamic-threshold models have also been used to predict spike times from experimental data with millisecond precision. The Multi-timescale Adaptive Threshold (MAT) model [13], which uses a linear sum of exponentials to model the dynamic threshold, is capable of predicting spike times recorded experimentally from a cortical neuron stimulated by current injection. This model participated in the INCF Quantitative Spike Prediction challenge [36], predicting spike times more accurately than all other tested models. Even though dynamic-threshold models are comparatively simple, these approaches are capable of closely modeling experimental spike-times.

Due to the predictive power of these dynamic-threshold models, they are particularly important to investigate. There are two main distinctions between these models – models with a reset of the input voltage [27, 31] and those which are non-resetting [14, 13]. In both cases the models define a membrane voltage $v(t)$ and threshold process $r(t)$. Spikes are generally fired at a time t_i when

$$r(t_i) - v(t_i) = 0 \tag{2.2}$$

The voltage $v(t)$ is defined as in the classic LIF model

$$\tau \frac{dv(t)}{dt} = Ri(t) - v(t) \tag{2.3}$$

The threshold adaptation is defined by an adaptation function $h(t)$ which models the change in spike threshold. Intuitively, the threshold should be increased immediately following a spike then decay downward. A typical choice is $h(t) = A\exp(-t/\tau), t > 0$ [31]. If the train of spikes up to time t is given by $\sum_k \delta(t - t_i)$, then the threshold process is given by

$$r(t) = h(t) * \big(\sum_k \delta(t - t_i)\big) \tag{2.4}$$

In the resetting models, when a spike is fired, $v(t)$ is reset to V_r as in the LIF model. This extension of the LIF model is commonly referred to as a LIF Dynamic Threshold (LIF-DT) model [32]. The non-resetting models [13] do not include this reset in the input voltage. For these models, the input is simply the filtered version of the input current $I(t)$.

There are a wide variety of spiking neuron models with a range of biophysical detail and computational complexity. Dynamic-threshold models have few parameters and low computational complexity compared to Hodgkin-Huxley style models, but have strong predictive power. It is still unclear, however, what processing principle drives these models. What encoding strategies are implemented by dynamic threshold models?

2.2 Spike-Train Decoding

The problem of decoding a spike train has also received considerable attention. Decoding spike trains is important not only for understanding what information is encoded in a spike train but also for BMIs which rely on decoding strategies to generate commands for artificial systems. The nature of the neural code for single neurons has been widely debated, with two common interpretations being rate and temporal codes [2, 37]. A rate code supposes that variables of interest are encoded in the rate at which spikes are fired over a short window. Temporal codes posit instead that the precise timing of spikes encodes additional information. When decoding a rate code, it is

possible to simply estimate the spike rate in small bins and translate this directly into the quantity of interest.

More sophisticated techniques exist to estimate an input stimulus from a spike train [38] such that squared reconstruction error is minimized. This was attempted using the reverse-correlation technique [8], where a spike-triggered average of the input signal is computed. If the spikes are spaced further apart than the length of the average, the time-reversed average can be used as a reconstruction filter. The spikes are treated as Dirac deltas filtered through the reconstruction filter.

For reconstruction of spike trains, the reverse-correlation approach was extended by the stimulus-reconstruction method [38, 4, 3], which aims to find the filter $h(t)$ for the input signal $s(t)$ such that the squared approximation error $h(t) * (\sum_i \delta(t - t_i)) - s(t)$ is minimized. For stationary input signals and spike trains, this is a standard minimum mean squared-error filtering problem, with the solution given by the well-known Wiener filter

$$H(\omega) = \frac{S_{s,spikes}(\omega)}{S_{spikes}(\omega)} \tag{2.5}$$

where capital letters denote the Fourier transform, $S_{s,spikes}$ is the cross-spectral density of the input signal and spike train, and S_{spikes} is the spectral density of the spike train. If the spike train is convolved with this filter, the estimated reconstruction has minimal error. This approach can estimate amplitude modulations in the sensory systems of weakly electric fish [4].

In general, however, decoding of neural signals has been investigated separately from the process of encoding spike trains. Neural decoding approaches are designed to work with spike trains that have already been generated. Prior work generally does not use direct knowledge of the encoding process. One would expect biological systems, over evolutionary time-scales, to have jointly optimized the encoding and decoding process.

An alternative approach to reconstruction was developed for encoding with populations of simple neural models with randomized parameters [39]. This thesis showed that using knowledge of the encoding scheme and parameters across the entire population, it was possible to design a reconstruction scheme based on the theory of frames. This was extended to Hodgkin-Huxley neurons [40] and encoding of video data [41]. These approaches are closely related to filter-bank reconstructions and are not necessarily physically realizable, nor

do they imply neurons use a similar approach.

Another view of neural encoding and decoding is the noise-shaping neuron hypothesis proposed by Shin et al. [42, 43, 44]. In this model, a negative feedback signal is defined as $L(s(t)) - Y(t)$, where $Y(t)$ is a filtered spike train (not a dynamic threshold). This feedback signal is used in spike generation, for instance to modulate a Poisson process. This hypothesis proposes that the feedback filter is specifically designed to adapt the neuron's input/output function to the input signal statistics and filter out encoding noise from the signal band. This is similar to the idea of noise shaping in sigma-delta converters [45]. While there are many superficial similarities between the noise-shaping neuron and the source-coding neuron proposed in Chapter 1, previous work on the noise-shaping neuron [43] is not concerned with coding fidelity or an energy constraint.

For realistic models of neuronal coding, it is critical that both the encoding and decoding processes be causal. The causality requirement for decoding requires causal decoding filters. The generation of spikes must also be causal, depending only on the previous history of spiking and the previous input signal.

2.3 Energy-Constrained Neurons

Neural processing of sensory signals is constrained by many factors including metabolic energy expenditure. Metabolic energy is a limited resource in organisms, and minimizing energy consumption is critical. It has been suggested that metabolic cost can be seen as a unifying principle underlying all of neuronal biophysics [46]. Cortical computation can be a large portion of an organism's energy budget [47], with the generation of action potentials accounting for 20-50% of the expended energy of the nervous system [10, 48, 11]. Every time an action potential is generated, sodium and potassium pumps, activated by ATP, work to restore the resting concentrations of the cell membrane. Every spike has an energetic cost for an organism.

The cost of generating action potentials suggests that selective pressure has been applied on evolutionary timescales, resulting in codes which are optimized to minimize energy consumption while operating with a high fidelity [6]. It is very likely that neural codes in sensory systems are optimized to

balance a trade-off between energy and encoding error.

There are different ways to approach questions of energy-efficiency in neurons. Sengupta et al. [11] showed that action-potential shape can have a large influence on the relative energy cost of spiking. They found that the most efficient potentials occurred in mammalian cortical neuron models. A follow-up study [49] showed that balancing excitatory and inhibitory currents limits the energy required to generate post-synaptic potentials. Broadly, these studies have estimated that energy is consumed to generate post-synaptic potentials, spiking activity (including generating and propagating the action potential and releasing and recycling vesicles), and baseline maintenance of cellular processes unrelated to spiking.

At the level of a single neuron, a simplifying assumption is that encoding only influences the energy costs which are incurred by spiking. This includes the generation and propagation of the action potential, the release of vesicles, and recycling vesicles. As action potentials are nearly fixed for a given neuron, the cost per action potential is essentially fixed. This suggests that an energy-efficient encoding scheme must control the mean spike rate of the resulting code to control the mean energy expenditure. Ideally, the code would time spikes to minimize representation error while limiting the overall number of spikes fired.

2.4 Energy-Efficient Encoding Schemes

The idea that a neuron must make efficient use of limited resources is an old one, dating back at least to the ideas of Barlow [50]. It has been hypothesized that a neural code should maximize the information capacity of the resulting spike trains [51]. This idea has been applied at the level of neuronal populations, resulting in ideas such as sparse population coding [52] and receptive fields optimized for particular sets of stimuli [53].

At the level of individual neurons, it is also possible to derive energy-efficient encoding strategies. Previous work has attempted to understand energy-efficient neural processing by modeling the channel capacity of neurons or the entropy of a spike train. Levy and Baxter [12] proposed an energy-constrained encoding model and maximized a ratio of spike-train entropy to energy expended. This was expanded to study optimal interspike-interval

(ISI) distributions [54]. Further work by Berger and Levy [55] proposed modeling an integrate-and-fire neuron as a communication channel. They then derived the interspike interval distribution which maximizes the ratio of bits transmitted to energy expended. This approach has been generalized in several ways, including introducing unequal synaptic weights [56] and generalized inverse Gaussian interspike intervals [57]. These existing theories of energy-efficient neural encoding, however, do not provide a mechanism for predicting spike times from a sensory signal, nor do they predict encoding errors (distortion) of sensory signals.

The neural source coder is also related to prior work on predictive coding in spiking networks [58], which has also been examined in a probabilistic framework [59]. This previous work also proposed an optimization problem which balanced fidelity against spiking activity (as a surrogate for energy), where the goal was to encode the state variables of a dynamical system in the activity of a population of spiking neurons. This population was meant to simulate cortical networks. Assuming a fixed threshold, a neural model similar to the neural source coder was derived and studied in simulated populations of cortical neurons. Here, a more general stimulus-dependent threshold is derived for a single neuron, and this thesis provides a detailed comparison to experimental data from single sensory neurons.

2.5 Contributions of This Thesis

This thesis proposes that sensory neurons balance a trade-off between energy consumption (the average spike-rate of the neuron) and encoding error by incorporating knowledge of the decoding scheme within the encoder. In the limit of high spike-rates, the optimal form of the encoder is derived along with the optimal parameters. This model is used to predict spike times from a primary sensory neuron and a cortical neuron. Extending the model, an instantaneous rate code is also proposed which, in the limit of high spike-rates, produces spike trains with identical intervals. Stochastic spike firing is introduced to explain jittered spikes, and the possible benefits to population coding are explored. Finally, in an example of spiking neuron models being applied to the design of artificial systems, an approach for cochlear-implant stimulation is proposed.

The fundamental motivation for using a decoding filter is the classic pre-synaptic/post-synaptic neuronal pair which could serve as an encoder-decoder system [7]. The encoder neuron communicates a spike train along the length of its axon to the synaptic terminals. The post-synaptic neuron is modeled as recovering the input signal with a simple filtering operation, mimicking the cell membrane and propagation through the dendritic arbor [21, 7]. The filter is usually a single-pole element that models the RC characteristics of the cell membrane. Although this ignores aspects of synaptic processing such as quantal synaptic failure and synaptic adaptation [18], this is a reasonable starting point.

Rather than studying the questions of neural encoding and decoding separately, the proposed approach argues that evolution has jointly optimized the encoding and decoding process within a single neuron to minimize a trade-off between encoding error and energy expenditure. In doing so, neurons may have incorporated a biophysical decoder internally so that the coding error is made available to the neuron. By tracking the encoding error, it is possible to generate an encoded spike train that minimizes reconstruction error. This internal decoder tracks the input stimulus from the encoded spike-train and fires an impulse whenever the coding error reaches a threshold. This is mathematically close to the dynamic-threshold-without-resetting that has been used to predict spike times [13] and the statistical structure of spike trains [14]. Unlike adaptive-threshold models, however, this thesis proposes an encoding principle and derives the optimal form of encoder.

This approach provides a coding framework that has strong analogies to lossy source-coding theory [60, 61]; namely, an internal decoder tracks the coding error and determines an optimum policy for timing the spikes. The extent of permissible error is determined by the constraint on the spike-rate, much in the way that the rate-distortion function determines the trade-off between coding error and bit-rate. Previous work [58] has developed similar predictive coding models of neurons, but the model derived here has a more general form for single neurons and is compared directly to experimental data from sensory neurons.

Unlike many previous studies of energy-efficient encoding schemes [62, 12, 55], the approach proposed in this thesis predicts precise spike-times and estimates reconstructions of input signals. These predictions can be compared with experimental spike-times and reconstructions estimated from experi-

mental spikes. The concept of minimum-error, energy-constrained encoding by single neurons provides a way to understand the principles of neural encoding and decoding.

CHAPTER 3

DETERMINISTIC, OPTIMAL NEURAL SOURCE CODING

The proposed energy-constrained, optimal encoding scheme for neurons results in a spike-firing rule which can be used to predict spike times. Further, the method can predict reconstructed waveforms with highest fidelity for the given constraint on the long-term spike rate. The predicted spike-times are the key outcome of the encoding model and can be directly compared to experimental observations. Reconstructed waveforms can also be estimated from experimental spike-trains and compared to the original signal.

In this chapter, the form of the energy-constrained optimal encoder is derived for the case of a deterministic signal with a high spike-rate. The form of the encoder which minimizes reconstruction error is derived, and the parameters of the reconstruction filter are constrained to satisfy the energy constraint.

Two approaches are taken to derive the optimal neural encoder. The first assumes a constant input, which does not vary between spikes. This approach leads to the development of a stimulus-dependent threshold on the error. The second approach assumes a more formal, first-order linearization of the error signal in the limit of high spike-rates. This approach gives a rule for spike firing which does not depend on the input signal. The error is determined by the signal, signal derivative, and encoder parameters.

It has been shown previously [13, 36] that dynamic threshold models can accurately reproduce experimental spike-times with millisecond precision. These models, however, do not give insight into the principles of encoding and do not predict reconstructed waveforms. The proposed energy-constrained, optimal encoding scheme is closely related to dynamic threshold models without resetting the input voltage [13, 14]. Thus, it seems reasonable to expect the proposed encoder to also accurately predict spike times. The optimal neural encoding model goes beyond existing spike-timing models by predicting a reconstructed waveform with minimal error.

3.1 Formulation of the Optimal Encoder with Stimulus-Dependent Threshold

This chapter develops a formulation of the optimal neural-encoding scheme presented in Chapter 1 in the case of high spike-rates. The assumption for this derivation is that the signal can be approximated as piecewise constant. The procedure results in an optimal spike-firing threshold $\gamma(t)$ which varies with the strictly positive signal level $s(t) > 0$.

The neural source coder generates a sequence of spike times t_i. This spike train is represented as a sum of Dirac delta functions $\sum_i \delta(t - t_i)$. A reconstructed signal is generated by filtering the spike train with a reconstruction filter $h(t)$. The reconstructed waveform $r(t)$ is given by the convolution of the reconstruction filter with the spike train $r(t) = h(t) * (\sum_i \delta(t - t_i))$. The encoding error is therefore given by $s(t) - r(t)$, and spikes are fired when $s(t_i) - r(t_i) \geq \gamma(t_i)$.

The encoding/decoding mechanism is motivated by the classic idea of a pre- and post-synaptic neuron pair [18]. The pre-synaptic neuron encodes the signal $s(t)$, whereas the post-synaptic neuron decodes the signal $r(t)$ by filtering with the post-synaptic membrane. The encoding neuron needs to maintain the error signal $e(t) = s(t) - r(t)$ to ensure spikes are fired to minimize encoding error.

For this formulation, the decoding filter $h(t)$ is restricted to be a first-order filter with impulse response $A \exp(-t/\tau), t > 0$. This form models the post-synaptic membrane as an RC element, which is a well-established model for the passive electrical properties of cell membranes [7, 9].

In this approach, γ will be optimized in its most general form, $\gamma = f(s, t)$. This firing level is allowed to vary as a function of the input signal level, as well as time. By allowing a variable value of γ, encoding error will be minimized.

The proposed optimal neural-encoding strategy must solve the problem of minimizing encoding error subject to a constraint on the energy expended by the neuron. Encoding error is measured by the average squared reconstruction error over an interval $[0, T]$, $\frac{1}{T}\int_0^T (s(t) - r(t))^2 dt$. As a first approximation, encoding energy can be approximated as $E = kR + b$, where R is the average spike-rate in the window of length T. The term b includes the baseline processes of the neurons that are not affected by spiking activity.

The term k is the energy cost per spike and includes the cost of generating the action potential, propagating the action potential, and releasing and recycling vesicles. These costs are roughly proportional to the number of spikes. The rate must then be constrained to $R = (E - b)/k$ to satisfy the energy constraint.

The three parameters A, τ, and γ are unknown and must be chosen to minimize encoding error while achieving the energy constraint. This approach assumes that A, τ, and γ can be varied across neurons to minimize encoding error. Once set by the optimization procedure, however, the parameters A and τ are constant over the window of length T. The optimal encoding scheme can then be written as

$$\min_{\gamma(s(t),t),A,\tau} \frac{1}{T}\int_0^T (s(t) - r(t))^2 dt \qquad (3.1)$$
$$\text{subject to } R = \frac{E-b}{k}$$

In general, this problem is difficult to solve due to the nonlinearity of the encoding strategy. The problem is decomposed into two easier problems. First, the spike-rate constraint is satisfied by adjusting the parameters A and τ. Second, the optimal value of $\gamma(s(t), t)$ is derived to minimize encoding error for a given A and τ.

3.1.1 Average Rate with a First-Order Reconstruction Filter

It is possible to decompose Problem 3.1 by first satisfying the rate constraint, then deriving the optimal form of γ. By computing the average output level for a given spike rate, it is possible to define the rate constraint in terms of A and τ. This simplifying approximation places a constraint on A and τ which will approximately satisfy the rate constraint.

Integrating the filter impulse response $h(t)$ for $t > 0$, the average output level of a single spike is given by $A\tau$. The average filter output should match the average level of the signal over a long time window T. In this case, fluctuations in the signal will contribute minimally to the spike rate. Given a target average rate R_T, the average output level of the reconstructed function is $A\tau R_T$. If the average signal level is $\bar{S}$, then the filter parameters

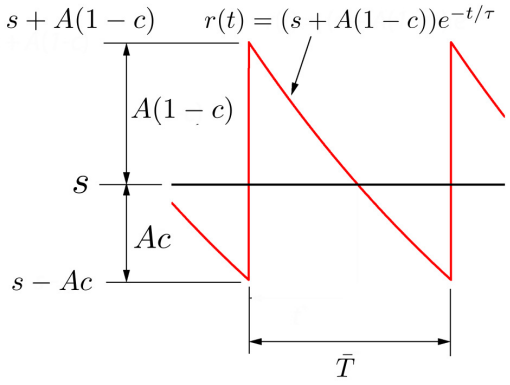

Figure 3.1: Geometrical interpretation of the optimization procedure to achieve a minimum-error reconstruction of a signal given a constraint on the mean firing rate ($\frac{1}{\bar{T}}$). The signal (black line) is assumed to be constant within the interval of interest (between adjacent spikes). The reconstruction $r(t)$ (red) is a single-pole low-pass filter with parameters A and τ. It undergoes a discrete jump of magnitude A whenever the encoder emits a spike. The decoded signal then relaxes until it reaches a firing level of $s - Ac$ when a spike is generated. For fixed s, A, c, and τ, the interspike interval is $\bar{T}$. The parameters A and τ are determined from a constraint on $\bar{T}$. The optimization procedure is applied to find the optimal value of c that minimizes the error between s and $r(t)$.The threshold value of the reconstruction error $\gamma = Ac$ will in general be signal level-dependent.

A and τ should be chosen to satisfy

$$A\tau = \frac{\bar{S}}{R_T} \tag{3.2}$$

This approach does not uniquely define A and τ, leaving one degree of freedom. However, this does define how the rate constraint can be satisfied by adjusting A and τ. To match experimental data, the ambiguity is resolved by selecting the parameters to satisfy Eq. 3.2 while maximizing the coincidence with the experimental spike-train, as described in Chapter 4. Now it remains to determine the optimal value of γ given A and τ.

3.1.2 Derivation of Stimulus-Dependent Firing Threshold

Given the filter values A and τ required to satisfy the rate constraint, the remaining step is to derive the optimal value of γ to minimize the error in

Problem 3.1. This requires further simplification of the input signal, namely the assumption of a piece-wise constant input signal.

In the limit of high spike-rates, the time between spikes decreases. Assuming that the signal $s(t)$ changes much more slowly than the time between spikes, it is possible to assume that the signal is constant between spikes. This leads to a piece-wise constant signal approximation. As the spike rate increases, the approximation error between the signal $s(t)$ and the piece-wise constant signal decreases.

Applying the piece-wise constant approximation, assume the signal has value s. A spike is fired at time 0 when $s(t) - r(t) = \gamma$. For simplicity, define

$$c = \gamma / A \tag{3.3}$$

$$\epsilon = s / A \tag{3.4}$$

These two terms are the threshold and signal values normalized by the spike height A. Figure 3.1 shows a geometrical interpretation of these parameters. Then the reconstructed waveform for $t > 0$ is given by

$$r(t) = (s + A(1 - c)) \exp(-t/\tau) \tag{3.5}$$

The value of c should lie between 0 and 1. This can be seen from Fig. 3.1, where otherwise the entire signal would lie above or below the signal level s, resulting in greater squared error.

Assuming that $s > Ac$, the reconstruction will decay until it reaches the level $s - Ac$. At this time, another spike will be fired. Defining the time $\bar{T}$ as the time where $r(\bar{T}) = s - Ac$, this will be the time of the next spike. This defines the interspike interval. Solving for $\bar{T}$, this yields

$$\bar{T} = -\tau \ln(\frac{\epsilon - c}{1 + \epsilon - c}) \tag{3.6}$$

To minimize reconstruction error, it is possible to minimize the error between 0 and $\bar{T}$. The problem can be written as

$$\min_c A^2 \int_0^{\bar{T}} ((1 + \epsilon - c) \exp(-t/\tau) - \epsilon)^2 dt \tag{3.7}$$

Substituting the value of $\bar{T}$ yields

$$\frac{A^2\tau}{2}(1-2\epsilon-2c-2\epsilon^2 ln(\frac{\epsilon-c}{1+\epsilon-c})) \tag{3.8}$$

Differentiating with respect to c gives

$$\frac{dE}{dc} = A^2\tau(\frac{\epsilon^2}{\epsilon-c} - \frac{\epsilon^2}{1+\epsilon-c} - 1) \tag{3.9}$$

Setting the derivative to 0, with $A > 0$, $\alpha > 0$, and $\epsilon > 0$, gives a quadratic equation for c

$$0 = c^2 - (1+2\epsilon)c + \epsilon \tag{3.10}$$

For $0 \leq c \leq 1$, there is only one valid solution

$$c^* = \frac{(1+2\epsilon) - \sqrt{1+4\epsilon^2}}{2} \tag{3.11}$$

To test if this critical point is a minima, the second derivative is given by

$$A^2\epsilon^2\tau\left(\frac{1}{(\epsilon-c)^2} - \frac{1}{(1+\epsilon-c)^2}\right) \tag{3.12}$$

At the value of c^*, this gives $1+4\epsilon^2$, which is always positive. Hence this critical point is a minima.

In terms of the firing level γ, this gives

$$\gamma(s(t)) = Ac = A\frac{(1+2\epsilon) - \sqrt{1+4\epsilon^2}}{2} \tag{3.13}$$

As the value of ϵ varies with the input signal, this term γ becomes dependent on the signal $s(t)$. The value of γ is also dependent on A.

It is important to note the asymptotic limit of γ as ϵ increases. If the signal level increases, ϵ increases and the limit approaches $A/2$. More formally,

$$\lim_{\epsilon\to\infty}\gamma = A/2 \tag{3.14}$$

For signals which are much larger than A, γ approaches a constant and is no longer signal-dependent. This suggests that a fixed firing level is an approximation of the optimal value of γ for large signals.

The derivation of γ results in a different firing rule than previous adaptive threshold models without resetting [14]. In previous models, spikes were fired when $s(t) - r(t) = 0$. Setting $\gamma = 0$ results in suboptimal reconstructions. Moreover, the value of γ actually varies with the signal level.

3.1.3 Minimum Firing Level

A simple, but meaningful, extension of this derivation is for very small input signals. In many neurons, small input signals only result in subthreshold variations. Equation 3.13, however, predicts spiking for any nonzero ϵ. This may not result in minimal encoding error. A minimum firing level can be derived for piece-wise constant input functions.

To derive a minimum level for spike firing, consider the case where no spikes are fired. The reconstructed signal $r(t)$ will decay to zero. In this case, the reconstruction error is given by

$$E_0 = \int_0^{\bar{T}} (s)^2 dt \tag{3.15}$$

This is an approximation that holds well after the signal has not spiked for some time. This yields a baseline error value of $E_0 = s^2\bar{T}$. From Eq. 3.8, the error when firing a spike, E, is given by

$$E = \frac{A^2\tau}{2}(1 - 2\epsilon - 2c) + s^2\bar{T} \tag{3.16}$$

The point of interest is the value of s_0 such that $E = E_0$. For signals smaller than s_0, firing spikes actually results in additional error. Setting the two equations equal yields

$$1 - 2c - 2\epsilon = 0 \tag{3.17}$$

Substituting in the optimal value of c yields

$$\sqrt{1+4\epsilon^2} - 4\epsilon = 0 \tag{3.18}$$

$$\epsilon = \frac{1}{\sqrt{12}} \tag{3.19}$$

$$s = \frac{A}{\sqrt{12}} \tag{3.20}$$

For signals with s smaller than this level, spikes should not be fired. This provides a lower limit on γ for small signals. A minimum firing level is important from a neural modeling perspective, as it implies the existence of subthreshold variations that are known to exist in neurons.

The expression for the optimal signal-dependent firing-level γ in Eq. 3.13 and the rate constraint in Eq. 3.2 approximate a solution to Problem 3.1 in the limit of high spike-firing rates. This solution varies considerably from previous dynamic threshold models without resetting. In these existing models, spikes are fired when $s(t) - r(t)$ reaches 0, regardless of the encoding error. The minimum firing level in Eq. 3.20 extends the optimal encoding problem in the limit of small signals, which should not elicit spikes.

3.2 Derivation of Optimal Encoder with Linearized Model

Although the derivation of the stimulus-dependent threshold assumes a constant stimulus at high spike-rates, it also is possible to derive results for a linearized signal and reconstruction model. The encoded spikes are reconstructed by convolving them with the filter $h(t)$, and the result is subtracted from the input $s(t)$ to compute $e(t)$. In the limit of high spike-rates, this alternative derivation approach uses a linearization of the encoding error. Critically, this derivation accounts for changes in the derivative of the input signal. This analysis predicts a spike rate versus distortion curve parameterized by the encoder parameters and derives asymptotic expressions, valid at high spike-rates, for the encoder error and the optimal parameter values.

A trade-off between spike rate and encoding error in the optimal neural encoder is similar to the ideas of the bit rate and distortion trade-off in rate-distortion theory. The dynamic threshold also has strong analogies to

source-coding theory; namely, an internal decoder tracks the coding error and determines an optimum policy for timing the spikes. The extent of permissible error is determined by the constraint on the spike rate, much in the way that the rate-distortion function determines the trade-off between coding error and bit rate.

3.2.1 Linearized Encoding Model

In this derivation, it is assumed that a spike train is reconstructed using a causal linear filter of the form $h(t) = A\exp(-t/\tau)$. The spike train is modeled as a sum of Dirac delta functions $\sum_{i=1}^{N}\delta(t-t_i)$. One can then define the reconstructed waveform as

$$r(t) = h(t) * \Big(\sum_{i=1}^{N}\delta(t-t_i)\Big) \tag{3.21}$$

Spikes are fired at time t_i whenever

$$s(t_i) - r(t_i) = \gamma(t_i) \tag{3.22}$$

where $\gamma(t_i)$ is the potentially time-varying signal level. In this formulation, it is assumed that the value of τ is given, as the dynamics of the neuron membrane are relatively fixed. The firing level $\gamma(t_i)$ is a free parameter, as is the parameter A. This parameter represents how large a change a spike induces in the reconstructed signal. In a neuron, this could correspond to the strength of the synapse between the encoding neuron and the post-synaptic neuron. When a spike is fired, there is a discontinuous jump in the signal $r(t)$ of size A.

An optimal neural encoder should minimize the squared reconstruction error $e(t) = s(t) - r(t)$ subject to an energy constraint on the number of spikes fired. This derivation assumes a linearization of the input signal $s(t)$ and reconstruction $r(t)$ using a first-order taylor series approximation, as seen in Fig. 3.2. The signal, following a spike at time t_i is approximated as $s(t_i)+s'(t_i)t$. For the reconstruction, the linearization is $r(t_{i+})+r'(t_i)t$, where $r'(t_i)$ is the first right derivative of the reconstruction. These approximations

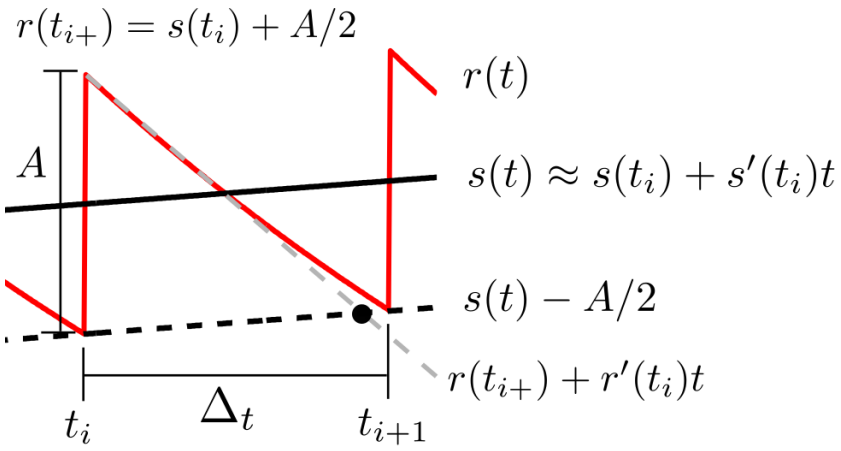

Figure 3.2: Illustration of the linearized input signal $s(t)$ and reconstructed waveform $r(t)$. A spike is fired at time t_i and the next spike is fired at time t_{i+1}, following an interval of Δ_t seconds. In this example, the input signal is assumed to be approximately linear between spike times. At time t_i, a spike is emitted, causing a discontinuity in the reconstructed waveform $r(t)$ of height A. The value of $r(t_{i+}) = s(t_i) + A/2$, as the spike was fired when $r(t_{i-}) = s(t_i) - A/2$. For $t > t_i$, the reconstructed waveform is given by $r(t) = (s(t_i) + A/2)\exp(-t/\tau)$. First-order Taylor series approximations of $r(t)$ and $s(t)$ are used. The linear approximation of $r(t)$ is shown as the dashed gray line. In this case, the predicted time between spikes using the linear approximation is given by the black circle. This leads to a slightly lower estimate of the time between spikes. As spike rate increases, the estimate of the time between spikes using the linearizations approaches the true time between spikes.

lead to a linear form of the encoding error,

$$e(t) = e_0 + kt \tag{3.23}$$

where e_0 is the value of the error immediately following a spike (assumed to be at $t = 0$ without loss of generality), and k is the slope of the error. Examining this linearized error, it is possible to derive some important structural properties about an optimal encoder.

Suppose the error has an initial value of $e_0 = -A/2$. If a spike is fired at time $t_i = A/k + \Delta$, the averaged squared error over the interval $T = 2A/k$

is given by

$$E(\Delta) = \frac{1}{T}\int_0^T e(t)^2 dt \tag{3.24}$$

$$= \frac{k}{2A}\left(\int_0^{A/k+\Delta} (kt + e_0)^2 dt + \int_{A/k+\Delta}^{2A/k} (kt + e_0 - A)^2 dt\right) \tag{3.25}$$

Analyzing this expression will result in the value of Δ which minimizes squared error over this interval. Substituting $-A/2$ for e_0 in Eq. 3.23 gives

$$\frac{k}{2A}\left(\int_0^{A/k+\Delta} (kt - A/2)^2 dt + \int_{A/k+\Delta}^{2A/k} (kt + -3A/2)^2 dt\right) \tag{3.26}$$

$$= \frac{k}{2A}\left(\frac{k^2t^3}{3} - \frac{kt^2A}{2} + \frac{tA^2}{4}\Big|_0^{A/k+\Delta} + \frac{k^2t^3}{3} - \frac{3kt^2A}{2} + \frac{9tA^2}{4}\Big|_{A/k+\Delta}^{2A/k}\right) \tag{3.27}$$

$$= \left(\frac{7A^2}{12} - \frac{k^2}{2}(A/k + \Delta)^2 - Ak(A/k + \Delta)\right) \tag{3.28}$$

Taking the first derivative of the error with respect to the perturbation parameter Δ, the expression is

$$\frac{dE(\Delta)}{d\Delta} = k^2(A/k + \Delta) - Ak \tag{3.29}$$

$$= k^2\Delta \tag{3.30}$$

The second derivative is then given by

$$\frac{d^2E(\Delta)}{d\Delta^2} = k^2 \tag{3.31}$$

The first-order condition for optimality is satisfied when $\Delta = 0$ and the second-order sufficient condition for local minima is satisified for any $k > 0$.

As long as the slope parameter, k, is positive, the error will be minimized when a spike is fired after A/k seconds. This corresponds to a change in the error of A. Regardless of the slope value, this will always give a fixed value of γ. This value of gamma will result in a local minima for the error. For a linearized model, an optimal encoder will track the error and fire after reaching a fixed γ. Given this intuition, the following section formally establishes the linearized model and derives the parameters which minimize error for a fixed spike-rate.

3.2.2 Derivation of Linearized Model and Optimal Parameters

The neural source coder attempts to encode a non-negative function $s(t)$ defined over the interval $[0, T]$. The time between the ith and $(i+1)$th spike is the ith interspike interval, Δ_{t_i}. The metabolic energy constraint is modeled as a constraint on the spike rate R. The parameters A and γ of the neural encoder should then be chosen to minimize

$$\min_{A,\gamma} \frac{1}{T} \int_0^T (s(t) - r(t))^2 dt \qquad (3.32)$$
$$\text{subject to } N_{spike}/T \leq R$$

where N_{spike} is the number of spikes used to encode the signal. Intuitively, the constraint should be tight as all available energy should be used in encoding the signal with minimal error. For arbitrary signals $s(t)$, it is difficult to optimize the parameters of the encoder, as the spikes lead to discontinuities in the encoding error. Asymptotic bounds on the reconstruction error and optimal parameter values are derived in the limit of high spike-firing rates.

Consider encoding a real-valued function, $s(t)$, with the encoding model given by Eqs. 3.21 and 3.22. The reconstruction filter is

$$h(t) = A \exp(-t/\tau) \qquad (3.33)$$

with a known τ. The first step is to analyze the encoding error $e(t) = s(t) - r(t)$ between two spike times corresponding to Δ_{t_i}. This leads to an asymptotic result on the interspike interval and the integral of the squared encoding error. It is then possible to derive optimal values of the encoder parameters A^* and γ^*. Assume that the real-valued, twice-differentiable function $s(t)$ is defined over $[0, T]$ with $s(t) > 0$. Also assumed is $s(t) \gg A - \gamma$, which is consistent with encoding a continuous signal at a high spike-rate. Finally, it is assumed that $s'(t) > -(s(t) + A - \gamma)/\tau$. Without this assumption, the signal could decay too rapidly to generate more spikes. The first result bounds the error function $e(t)$ between two successive spike-times. Without loss of generality, we assume the time of the first spike of the interval is at time zero.

Lemma 1. *Given the adaptive-threshold neural encoder and input signal $s(t)$ defined above, there exists a value $\Delta_t > 0$ for any $\epsilon > 0$ such that $e(t) =$*

$s(t) - r(t)$ between the two spike times $t_1 = 0$ and $t_2 = \Delta t$ is approximated by $\hat{e}(t) = (s'(0) + \frac{s(0)+A-\gamma}{\tau})t - (A - \gamma)$ with absolute error of at most ϵ.

Proof. The first-order Taylor series expansions of $s(t)$ and $r(t)$ for $t > 0$ are given by $s(t) = s(0)+s'(0)t+g_1(t)$ and $r(t) = r(0)+r'(0)t+g_2(t)$, where $s'(0)$ and $r'(0)$ are the first (right) derivatives of $s(t)$ and $r(t)$. The error residuals, $g_1(t), g_2(t) \propto t^2$, are given by the mean-value form of Taylor's theorem. The reconstruction function derivative is

$$r'(0) = -\frac{s(0) + A - \gamma}{\tau} \tag{3.34}$$

and $r(0) = s(0) + (A - \gamma)$. Combining these two approximations gives

$$e(t) = s(t) - r(t) \tag{3.35}$$

$$e(t) = s'(0)t + g_1(t) - A + \gamma + \frac{s(0) + A - \gamma}{\tau}t - g_2(t) \tag{3.36}$$

$$e(t) = (s'(0) + \frac{s(0) + A - \gamma}{\tau})t - (A - \gamma) + g(t) \tag{3.37}$$

where $g(t) \propto t^2$. Since $\Delta_t > t \in (0, \Delta t)$, $|g(t)|$ is less than or equal to $|g(\Delta_t)|$. Then for any $\epsilon > 0$, Δ_t can be selected such that $|g(\Delta_t)| < \epsilon$, which implies that $|e(t) - \hat{e}(t)| < \epsilon$. □

Using the results from Lemma 1 and the assumption that $s(t) \gg A - \gamma$, one can derive the following result on Δ_t.

Lemma 2. *Given the adaptive threshold neural encoder and $s(t)$ described above, there exists a $\Delta_t > 0$ such that Δ_t is approximated by $\hat{\Delta}_t = \frac{A}{s'(0)+s(0)/\tau}$ with absolute error of at most ϵ.*

Proof. Equation 3.37 of Theorem 1, evaluated at the time of the next spike, when $e(\Delta_t) = \gamma$, gives

$$\gamma = (s'(0) + \frac{s(0) + A - \gamma}{\tau})\Delta_t - (A - \gamma) + g(\Delta_t) \tag{3.38}$$

$$\Delta_t = \frac{A}{s'(0) + (s(0) + A - \gamma)/\tau} - \kappa g(\Delta_t) \tag{3.39}$$

where $\kappa = 1/(s'(0) + (s(0) + A - \gamma)/\tau)$. Applying the assumptions that

$s(0) \gg A - \gamma$, the interspike interval is given by

$$\Delta_t = \frac{A}{s'(0) + s(0)/\tau} - \kappa g(\Delta_t) \tag{3.40}$$

By selecting Δ_t small enough that $|\kappa g(\Delta_t)| < \epsilon$, $|\hat{\Delta}_t - \Delta_t|$ is at most ϵ. □

Building on Lemmas 1 and 2, the next result gives an expression for the average squared error between two successive spike times.

Theorem 1. *Given the signal $s(t)$, the adaptive threshold neural encoding model, and the expressions of $\hat{e}(t)$ and $\hat{\Delta}_t$ from Lemmas 1 and 2, the average reconstruction error over the interval 0 to $\hat{\Delta}_t$ is given by $\frac{1}{\hat{\Delta}_t}\int_0^{\hat{\Delta}_t}(\hat{e}(t))^2 dt = \frac{A^2}{3} - \gamma A + \gamma^2$.*

Proof. Applying the form of $\hat{e}(t)$ from Lemma 1 and the assumption that $s(t) \gg A - \gamma$, the average reconstruction error over the interval $[0, \hat{\Delta}_t)$ can be written as

$$\begin{aligned}\frac{1}{\hat{\Delta}_t}\int_0^{\hat{\Delta}_t}(\hat{e}(t))^2 dt &= \frac{1}{\hat{\Delta}_t}\int_0^{\hat{\Delta}_t}((s'(0) + s(0)/\tau)t - (A-\gamma))^2 dt \\ &= \frac{1}{\hat{\Delta}_t}\Bigg(\frac{(s'(0) + s(0)/\tau)^2}{3}\hat{\Delta}_t^3 \\ &\quad - (A-\gamma)(s'(0) + s(0)/\tau)\hat{\Delta}_t^2 + (A-\gamma)^2\hat{\Delta}_t\Bigg)\end{aligned} \tag{3.41}$$

Substituting the result of Lemma 2 for the interspike interval yields

$$\frac{1}{\hat{\Delta}_t}\int_0^{\hat{\Delta}_t}(\hat{e}(t))^2 dt = \frac{A^2}{3} - \gamma A + \gamma^2 \tag{3.42}$$

□

Using this result, it is possible to derive the optimal values of A and γ for the energy-constrained encoder problem.

Theorem 2. *Given the adaptive-threshold neural encoder, $s(t)$ as defined above, and the expressions for $\hat{e}(t)$ and $\hat{\Delta}_t$, the value of A which satisfies an average spike-rate constraint R is given by*

$$A^* = \frac{\frac{1}{T}\int_0^T s'(t)dt + \frac{1}{T\tau}\int_0^T s(t)dt}{R} \tag{3.43}$$

with absolute error less than $\epsilon > 0$ for a large enough N_{spike}.

Proof. The expression for $\hat{\Delta}_t$ from Lemma 2 for any spike time t_i can be rewritten as $A = (s'(t_i) + s(t_i)/\tau)\hat{\Delta}_{t_i}$. To satisfy the rate constraint $R = N_{spike}/T$, there must be N_{spike} spikes in total. Summing the total amplitude increase from N_{spike} over the interval T and multiplying both sides by $\frac{1}{T}$ yields

$$\frac{1}{T}\sum_{i=1}^{N_{spike}} A = \frac{1}{T}\sum_{i=1}^{N_{spike}} (s'(t_i) + s(t_i)/\tau)\hat{\Delta}_{t_i} \tag{3.44}$$

$$RA = \frac{1}{T}\sum_{i=1}^{N_{spike}} (s'(t_i) + s(t_i)/\tau)\hat{\Delta}_{t_i} \tag{3.45}$$

The spike times define a partition of the interval $[0, T]$ with partition norm $\max_i \hat{\Delta}_{t_i}$. The terms $\sum_{i=1}^{N_{spike}} s'(t_i)\hat{\Delta}_{t_i}$ and $\sum_{i=1}^{N_{spike}} s(t_i)\hat{\Delta}_{t_i}$ are the Riemann sums of the functions $s'(t)$ and $s(t)$ with respect to the partition. As N_{spike} increases, the norm of the partition decreases. These sums therefore approximate their respective integrals for any error $\epsilon_1, \epsilon_2 > 0$ for some partition with small enough norm. Requiring that $\epsilon_1 + \epsilon_2 \leq R\epsilon$, replacing the sums with the corresponding Riemann integrals yields

$$A^* = \frac{\frac{1}{T}\int_{t=0}^{T} s'(t) + \frac{1}{T\tau}\int_{t=0}^{T} s(t))}{R} \tag{3.46}$$

with absolute error $|A - A^*|$ of at most ϵ. □

This result gives the parameter A^* which satisfies a given rate constraint. As the spike-rate constraint changes, the parameter A^* is adjusted to achieve the constraint. The final result gives the threshold value γ which minimizes the average squared reconstruction error.

Theorem 3. *Given an adaptive-threshold neural encoding model, an input function $s(t)$, and the results of Lemmas 1 and 2, the value of γ which minimizes the average squared reconstruction error is given by $\gamma^* = A/2$.*

Proof. As the parameter A is set to satisfy the constraint on spike rate, only the parameter γ needs to be chosen to minimize the objective function of Problem 3.32. As the asymptotic form of the average squared error over the interval $[0, \Delta_t]$ does not depend on the signal level $s(t)$, the overall average

squared error can simply be minimized by choosing γ to minimize the averaged squared error given by Theorem 1. This is quadratic in γ and yields a unique minimum.

$$\min_{\gamma} A^2/3 - A\gamma + \gamma^2 \tag{3.47}$$

Taking the derivative with respect to gamma yields $\gamma^* = A/2$. □

The parameter values γ^* and A^* optimize Problem 3.32, providing the best parameters for energy-constrained neural encoding with an adaptive threshold model for large enough firing rates.

3.3 Discussion

This chapter has introduced two alternative approaches to deriving the optimal source-coding neuron in the limit of high spike-rates. In both methods, it is necessary to assume that the variation in the input signal between two spikes can be approximated by a simple model. This approach allows for analytic analysis of the nonlinear system.

The first approach assumed a piece-wise constant input which resulted in a threshold that varied with the stimulus level. This implies slow variation between spikes, and can be thought of as an approximation of a time-varying signal with a piece-wise constant signal. For most signals, this approximation will hold with increasing accuracy as the time between spikes decreases. Given the first-order reconstruction filter, the optimal strategy is to track the encoding error and fire a spike when a stimulus-dependent threshold is reached. This threshold varies from $A/\sqrt{12}$ to $A/2$, with the upper limit achieved in the limit of large signals. Interestingly, a dependence between the cell membrane voltage and spike initiation threshold has been noted in vivo [35]. This could be related to the concept of a stimulus-dependent threshold for optimal encoding, although this needs to be explored in more detail.

An alternative approach is based around linearizion of the input signal and reconstruction through a first-order Taylor series approximation. In the limit of high spike-rates, this linearization holds with arbitrarily small error. The resulting error is linear and is minimized for a fixed firing threshold $\gamma = A/2$. Therefore, in the limit of high firing rates, an optimal neural coder will track

the encoding error and fire spikes when the error hits a fixed threshold. This model predicts an encoding error dependent on the signal, signal derivative, and encoding parameters. The error is always bounded between $A/2$ and $-A/2$.

Given the lack of direct experimental evidence, it is unclear exactly what criterion should be used to determine minimum error. Although the squared-error criterion (related to the L^2-norm) is a common error model, it is not necessarily optimized by neural systems. Interestingly, the results of this chapter hold for other L^p norms as well. Using the L^1 norm, one can integrate the absolute value of the error $s(t) - r(t)$. In the linearized case, the optimal γ is also $A/2$. This solution also minimizes the L^∞ norm, which is the maximum absolute value of the error. If γ is not equal to $A/2$ at the time of spiking, the absolute error before or after the spike will be greater than $A/2$, resulting in an increased L^∞ norm. Appendix A derives an optimal firing level of $\gamma = A/2$ for the L^p norms with $p \geq 1$. The results of the linearized analysis therefore apply to any L^p norm, although other objective functions are still possible.

Both approaches show that an optimal neural encoder must incorporate a reconstruction term to calculate error, as shown in Fig. 1.1. Although the form of the threshold γ varies, both approaches determine firing times based on the encoding error. This thesis extends existing models of adaptive threshold models [14, 13] and predictive coding in neurons [58] by deriving the form of the optimal encoder in the asymptotic limit of high firing rates. The neural source coder will, in the limit of high spike-rates, time spikes to minimize error given a constraint on the number of spikes fired. A critical step, however, when studying neural coding, is to compare the predictions of the neural source coder to data from experiments. This is the focus of Chapter 4.

CHAPTER 4

COMPARISON TO EXPERIMENTAL DATA

The neural source coder shows that, theoretically, a neuron could achieve minimum-error, energy-constrained encoding using a feedback mechanism to track reconstruction error. Based on the reconstruction error, the threshold γ is used to time spikes such that minimum error is achieved for a given spike rate. This encoding process is similar to existing models with adaptive thresholds [14, 13], but these models may not time spikes optimally. To begin validating the idea that neurons may time spikes to achieve minimum-error, energy-constrained encoding, it is necessary to compare the predictions of the source-coding neuron to data recorded from experimental neurons.

Here, the energy-constrained optimal encoding model is tested against experimental spike-times recorded from two datasets. The first is *in vivo* extracellular recordings of spike times from primary sensory afferents in the electrosense system of a weakly electric fish. The second dataset consists of an *in vitro* intracellular recording of a pyramidal, neocortical neuron of a rat. To provide a baseline comparison, the energy-constrained, optimal neural encoder is compared against a standard LIF neuron model and a LIF model with Dynamic Threshold and a resetting input (LIF-DT, see [27]). The ubiquity and computational simplicity of the LIF model make it an appealing choice for comparison despite its well-known limitations. Due to the close relationship between the proposed optimal encoding strategy and the class of dynamic threshold models, a comparison between the proposed approach and the LIF-DT model is very relevant.

There is a close match between the predicted and experimental spike-times in these two very different neurons. This suggests that the proposed optimal encoding strategy may indeed capture something fundamental about the mechanism of spike generation. This goes beyond existing dynamic threshold models by providing a new perspective on the joint encoding and decoding of neural signals. These results suggest that a neuron may attempt to carefully

time its spikes such that the signal can be reconstructed with minimum error, making the best use of a limited number of spikes.

4.1 Materials and Methods

Experimental work on weakly electric fish was carried out at the University of Illinois at Urbana-Champaign, USA, with approval from the university IACUC and was kindly made available by Mark Nelson and Rama Ratnam. The pyramidal cell dataset used here is from the rat, and was collected by Thomas Berger and Richard Naud in the laboratory of Henry Markram at École Polytechnique Federale de Lausanne (EPFL), Switzerland. The EPFL data are available in the public domain through the International Neuroinformatics Coordinating Facility (INCF) 2009 Spike Time Prediction Challenge [36].

4.1.1 Electrophysiology in the Weakly Electric Fish

Surgical and electrophysiological recording procedures in the weakly electric fish follow those reported by Nelson et al. [63]. The fish used in the study are of unknown sex. Briefly, adult brown ghost knife fish (*Apteronotus leptorhynchus*, 12-17 cm long), a species of gymnotiform fish, were lightly anesthetized by immersion in 100 ppm tricaine methane-sulfonate (MS-222, Sigma) for 2 minutes, and then immobilized with a 3 μl intramuscular injection of 10% gallamine triethiodide (Flaxedil, Sigma). The fish was restrained in a holding tank containing water and actively ventilated via a mouth tube. A surgical incision was made on the skin just posterior to the operculum to expose the posterior branch of the anterior lateral line nerve (pALLN). The nerve fiber from a P-type (probability coding) primary electrosensory afferent was isolated and its action potentials were recorded using glass micropipettes filled with 3M KCl solution. Spike times and their associated spike waveforms were sampled and stored for offline analysis (at 60 μs resolution). The ongoing electric-organ discharge (EOD) generated by the fish was monitored with a pair of carbon electrodes placed near the head and tail of the fish. Stimulation was provided by modulating the EOD with a single-cycle raised cosine of 100 ms duration and delivered across the whole body using two

carbon rods placed on opposite sides of the fish along the anterior-posterior axis. The stimulus amplitude was calibrated with respect to the transdermal potential, measured between a recording electrode close to the skin on the lateral trunk of the fish and a reference electrode inserted under the skin on the dorsal surface. A 1 mV root mean-square (RMS) voltage increase was defined as the reference (0 dBV). Stimulus intensities ranged from 0 dBV to -60 dBV attenuation in 5 dB steps with 20 stimulus repetitions at each amplitude. Stimulus waveforms time-locked to the neural data were stored for offline analysis.

4.1.2 Intracellular Recording of Rat Pyramidal Neurons

The 2009 INCF Spike Time Prediction Competition provides datasets with the challenge to reproduce the spike times using a computational model [36]. Stimulus data are also provided, although the competition did not require that the stimuli be reconstructed from the given spike activity. The dataset from Challenge A (one of four challenges) is considered here, and is available in the public domain along with a complete description of the methods from the organizers (http://www.incf.org/community/competitions/archive/spike-time-prediction/2009/challenge-a). Briefly, the data were obtained from *in vitro* current-clamp recordings in the soma of L5 pyramidal cells in the primary somatosensory cortex of the rat. The sex of the rat was not made known. The voltage data were filtered (2.4 kHz bandwidth Bessel filter) and sampled at 100 μs resolution. Recordings of the somatic membrane potential were obtained in response to 60 seconds of injected current. The stimulus was repeated for a total of 13 trials. The stimulus and the first 39 seconds of the response from each trial were made public, whereas the remaining 21 seconds of the response remained private and was reserved for testing by the organizers of the competition. The stimulus consisted of the following sequence: four step current inputs with a duration of 2 s with an inter-stimulus duration of 2 s, a white noise sequence of 2 second duration, and six simulated spike trains generated by an inhomogeneous Poisson process convolved with exponential decays of different time constants and summed together for a duration of 42.5 s. The intensities were chosen randomly over 300 to 500 ms blocks to elicit firing rates between 5 and 10 Hz. From the voltage recordings, spike

times were found using a threshold of 0 mV. This study used the first 39 seconds of the publicly available current-clamp stimulus and the spike times extracted from the 13 trials.

4.1.3 LIF and LIF-DT Neural Models

To provide a baseline of comparison for the proposed encoding model, the spike-time predictions of the model are compared with both experimental spike-times and two common neural models. The first is the classical leaky integrate-and-fire (LIF) model, which is a standard and ubiquitous model. Although it is known that the LIF model does not capture many spiking phenomena observed in real neurons, it is very common and computationally simple. For this comparison, the model is defined by

$$\tau_m \frac{dV(t)}{dt} = -V(t) + RI(t) \tag{4.1}$$

where R is the membrane resistance, τ_m is the membrane time-constant, $I(t)$ is the input current, and $V(t)$ is the predicted membrane voltage.

Spikes are fired when the membrane potential V(t) exceeds a threshold θ. When a spike is fired, the membrane potential is reset to zero. The constant-threshold model can be extended to the dynamic-threshold case [27, 31]. In this case, the threshold is defined as a time-varying function

$$\theta(t) = h(t) * \big(\sum_i \delta(t - t_i) \big) \tag{4.2}$$

with $h(t) = A \exp(-t/\tau)$. This gives an exponentially decaying threshold. Spikes are fired when $s(t) - \theta(t) = 0$. This is very close to the firing rule for the proposed encoder, but with a fixed value of γ.

This work tests the LIF-DT model with resetting. In this case, when $s(t) - \theta(t) = 0$, the membrane voltage is reset to 0 and the threshold is increased. Although very similar to the proposed encoder, this additional nonlinearity can result in unpredictable behavior.

4.1.4 Coincidence Measure

A measure of closeness between two spike trains is required to compare simulated predictions and experimental data. The coincidence factor [64] compares two spike trains by counting the number of spikes which occur within a window of Δ seconds of a spike from the other spike train. Coincidence is then defined between an experimental spike-train (data) and a predicted spike-train (model) as

$$\Gamma = \frac{N_{\text{coin}} - E[N_{\text{coin}}]}{N_{\text{data}} + N_{\text{model}}} \frac{2}{1 - 2\nu\Delta} \tag{4.3}$$

where N_{coin} is the number of coincident spikes, $E[N_{\text{coin}}]$ is the expected number of coincident spikes if the model was a homogeneous Poisson process with the same spike rate, N_{data} is the number of experimental spikes and N_{model} is the number of spikes from the model. The second term normalizes the result, where ν is the spike rate of the model.

The result is normalized so 1 indicates a perfect match between every spike. A coincidence of 0 means there are no more coincidences then expected by a spike train with a Poisson process. For the weakly electric fish dataset, the coincidence window is half an EOD period. For the INCF competition, a coincidence window of 4 ms was used.

4.1.5 Reconstruction Error

Reconstruction error was calculated from the RMS value of the error normalized by the RMS value of the stimulus, and reported as dBV RMS (relative to the stimulus)

$$10 \log_{10} \frac{(\int_0^T (s(t) - r(t))^2 dt)^{1/2}}{(\int_0^T s(t)^2 dt)^{1/2}} \tag{4.4}$$

The normalization allows reconstruction error to be compared across multiple input stimuli.

4.1.6 Parameter Selection

To simulate results with the optimal encoding model, the Eqs. 3.13, 3.2, and 3.20 were applied to ensure optimal encoding.

However, there were still additional degrees of freedom to be resolved. Equation 3.2 does not fully define A and τ, leaving an unaccounted-for degree of freedom. Additionally, the datasets required extra parameters described below. To set these parameters, a sweep of the relevant space was conducted and the parameter values which resulted in the best coincidence with the experimental spikes were chosen. For both datasets, the model parameters were fit against a single trial.

For the LIF and LIF-DT models, there are no optimal parameter values. For these models, all parameters were adjusted to obtain maximum coincidence with the experimental spike-train.

For the P-type spike-trains, the stimulus (modulated EOD waveform) was recorded at the skin of the fish. It was filtered with a bandpass filter centered at the EOD frequency with a bandwidth of approximately 50 Hz. This preserved the EOD waveform and amplitude modulations while eliminating artifacts in the recorded stimulus. Stimuli were measured at the skin of the fish with respect to a subdermal reference electrode placed on the dorsal side of the fish.

These are most likely not the true potential differences across the receptor due to the directional tuning of electroreceptors [65]. They were rescaled with respect to the baseline EOD to correct for stimulus discrepancies using a parameter a_{eod}. This affects the absolute value of the stimulus peak amplitude but preserves the differences between the stimuli (in dBV). For the optimal coder the scale factor which optimized coincidence was 4.95 (stimulus level: -20 dBV), 6.28 (stimulus level: -10 dBV) and 4.55 (stimulus level: 0 dBV). Where applicable, the parameter values used to simulate the data were $\tau = 34.5$ ms and $A = 2.05 \times 10^{-4}$ V (-20 dBV), $\tau = 22$ ms and $A = 3.42 \times 10^{-4}$ V (-10 dBV), and $\tau = 24.5$ ms and $A = 3.22 \times 10^{-4}$ V (0 dBV). For each stimulus level, the parameters were chosen to maximize coincidence with the P-type spike-train from one randomly selected trial (out of twenty). The same parameters were used to generate spike times for the remaining 19 trials. The parameters are similar across stimulus strength, with the small differences resulting from the small changes in the average

baseline firing rate as measured in the pre- and post-stimulus periods.

The LIF model was tuned using the threshold parameter and the time-constant of the input filter. For simplicity, the input filter resistance R was fixed at 1. The threshold level could then be adjusted to achieve the desired firing rate. The half-wave-rectified EOD waveform was used as input to the neuron. The EOD scale factor which maximized coincidence was 5.1 (-20 dBV), 4.9 (-10 dBV) and 4.2 (0 dBV). Where applicable, the parameter values used to generate LIF spike-trains and PSTHs were $\tau_m = 50$ ms and $\theta = 3.28 \times 10^{-5}$ V (-20 dBV), $\tau = 114$ ms and $\theta = 1.44 \times 10^{-5}$ V (-10 dBV), and $\tau_m = 98$ ms and $\theta = 1.62 \times 10^{-5}$ V (0 dBV). As with the optimal coder, the LIF parameters were selected to maximize coincidence with the P-type spike-train from one randomly selected trial (out of twenty). The same parameters were used to generate spike times for the remaining 19 trials. The LIF and LIF-DT models do not have a built-in decoder. To generate decoded waveforms, it is necessary to choose a reconstruction filter for both of these models.

To compare the LIF model with the optimal encoder, a first-order reconstruction filter was used to reconstruct the signal from the LIF spike-trains. The filter parameters were chosen to minimize the average reconstruction error between the EOD envelope and the LIF spike-trains. The optimum reconstruction filter parameters were determined through simulations, and the reconstructions depicted used the following parameters: $\tau = 27$ ms and $A = 2.58 \times 10^{-4}$ V (-20 dBV), $\tau = 11$ ms and $A = 6.01 \times 10^{-4}$ V (-10 dBV), and $\tau = 6.5$ ms and $A = 1.1 \times 10^{-}3$ V (0 dBV). P-type afferents can fire a maximum of one spike per EOD cycle, so the optimal encoder and the LIF neuron were limited to firing at most once per EOD cycle.

To tune the LIF-DT model, a similar procedure to the LIF model was used. The input filter resistance was again assumed to be 1. The membrane time constant τ_m, adaptation time-constant τ, and adaptation height A were adjusted to achieve the baseline firing rate and maximize the coincidence with the P-type spike-train from a random trial. The same EOD scale factors were used as for the proposed neural encoding model. The half-wave-rectified EOD waveform was used as input. The optimal parameters were $A = 7 \times 10^{-}5$ V, $\tau = 35$ ms, $\tau_m = 2$ ms (-20 dBV), $A = 6.4 \times 10^{-5}$ V, $\tau = 44$ ms, $\tau_m = 1$ ms (-10 dBV), and $A = 6.4 \times 10^{-5}$ V, $\tau = 44$ ms, and $\tau_m = 1$ ms (0 dBV). Like the LIF model, the LIF-DT model has no notion of a

decoded waveform. We therefore had to determine a low-pass reconstruction filter which minimized the average reconstruction error for the LIF-DT spike-trains. The reconstruction parameters were $A = 2.1 \times 10^{-5}$ V and $\tau = 36$ ms (-20 dBV), $A = 2.6 \times 10^{-4}$ V and $\tau = 28.5$ ms (-10 dBV), and $A = 3.9 \times 10^{-4}$ V and $\tau = 20$ ms (0 dBV). The LIF-DT model was constrained to fire at most one spike per EOD cycle. The parameters of the LIF-DT model differ significantly from the parameters of the LIF model due to the two interacting discontinuities which determine spiking behavior. The first discontinuity is the jump in the adaptive threshold and the second is the reset of the input voltage.

To fit the spike times from the INCF competition, the current waveform was first filtered with a first-order low-pass filter with a gain of 10^6 and a time-constant of τ_m. The filter gain served to convert the input signal from hundreds of picoamps into the millivolt range. The three methods were used to predict the precise spike times for one trial with parameters being adjusted to match spike times with highest coincidence factor Γ. For the optimal neural source encoder, these parameters were: $A = 1.5$ mV, $\tau = 224$ ms, and $\tau_m = 20.3$ ms. For the LIF model, the parameters were $\tau_m = 225$ ms and $\theta = 1.24$ mV. The parameters minimizing reconstruction error for the LIF model were $A = 2.2$ mV and $\tau = 150$ ms. For the LIF-DT model, the values were $\tau_m = 13$ ms, $\tau = 165$ ms, and $A = 2.7$ mV. The parameters minimizing reconstruction error for the LIF-DT model were $A = 1.6$ mV and $\tau = 187$ ms. For all models when simulating the INCF dataset, a 1 ms absolute refractory period was enforced.

Reconstructions of the experimental spike-trains were created by finding the parameters A and τ which minimized the reconstruction error when the spike trains were convolved with a filter $h(t) = A \exp(-t/\tau)$. For the weakly electric fish dataset, the optimal parameters were $A = 0.17$ mV and $\tau = 45$ ms (-20 dBV), $A = 0.29$ mV and $\tau = 26.8$ ms (-10 dBV), and $A = 0.4$ mV and $\tau = 20$ ms (0 dBV). For the INCF dataset, the parameters which minimized reconstruction error for the experimental spike-train were $A = 2$ mV and $\tau = 157$ ms.

4.2 Results

The proposed optimal encoding scheme predicts spike times, which can be validated experimentally by comparing them to experimental data. Further, for a given spike rate (energy constraint), the internal decoder provides a reconstruction which has lower error than other reconstructions. These predictions will be compared to spike-timing data obtained from a peripheral sensory neuron in the electrosensory system of weakly electric fish (*in vivo*) and from a cortical pyramidal neuron in the somatosensory system of the rat (*in vitro*). They will also be compared to spike trains predicted by a classical leaky-integrate and fire (LIF) neuron and a LIF neuron with a dynamic threshold (LIF-DT).

4.2.1 Encoding by Weakly Electric Fish Primary Sensory Neurons Using Stimulus-Dependent γ

Generally, the predicted spike-times from the optimal encoding model follow the same pattern of spiking as the data from the P-type neuron. Figure 4.1A, B show the stimulus (black trace, A: -10 dBV and B: 0 dBV intensities) and spike response (black spikes) of a primary P-type electrosensory afferent from the weakly electric fish, the optimum reconstruction (red trace) and spike response (red spikes) of the neural coder, the response of a leaky-integrate-and fire (LIF) neuron (blue spikes), and the response of an LIF-DT neuron (magenta spikes). The energy constraint of the optimal coder was the baseline spike rate of the afferent (237 spikes/s). For each of 20 trials, the initial condition of the optimal decoder was set so that the time to first spike of the encoder was the same as the time to first spike of the P-type unit.

At the -10 dBV amplitude (Fig. 4.1A) the peak firing rate is well below saturation, and there is good agreement with the experimental spike-times as seen from a comparison of the P-type and encoder spike-trains (top). The Fig. 4.1A insets magnify the time period around the stimulus onset (inset a) and offset (inset b). At the onset of the stimulus, as intensity increases, the optimal encoder predicts that the neuron will rapidly fire spikes to encode the changing stimulus level with minimal error. In the model, this is due to a rapid build-up in the error $s(t)-r(t)$ resulting in a shortening of the recovery

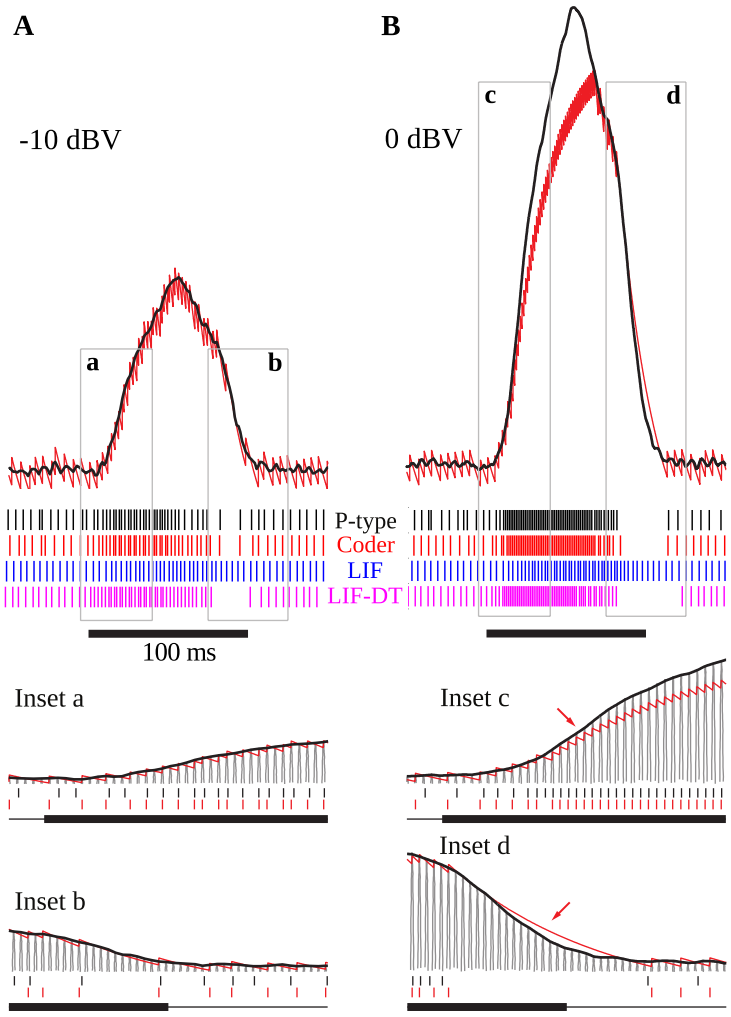

Figure 4.1: Stimulus coding in an example P-type afferent from a weakly electric fish. The experimental results are compared with the proposed optimal neural encoder, a leaky integrate-and-fire-neuron (LIF), and a LIF neuron with dynamic-threshold (LIF-DT) at two different stimulus intensities: (A) -10 dBV, and (B) 0 dBV. The stimulus, recorded at the skin of the fish (top, black trace), is a 100 ms modulation of the electric organ discharge (EOD) waveform of the fish. The decoder output (optimal reconstruction of the envelope modulation) is overlaid (red trace). Spike trains are shown below the stimulus, P-type (black), optimum encoder (red), LIF (blue), LIF-DT (magenta). Reconstruction from LIF and LIF-DT neurons are not shown. Onset and offset periods (insets a-d) are magnified (lower panels) to show details of experimental versus predicted spike-timing. The EOD (carrier) waveform is also shown with stimulus and reconstruction. The 0 dBV stimulus causes saturation in firing rate during the rise (arrow, inset c) and peak of the stimulus, and suppression of firing during the latter part of the decay (arrow, inset d).

period of the decoder following a spike (red trace). When the stimulus decays (inset b), the error is sub-threshold $s(t) - r(t) < \gamma$, and the decoded signal goes into a free decay thereby lengthening the ISI. This is seen more clearly in inset b where the ISI between spikes 3 and 4 is longer for both coder (red spikes) and experimental P-type spikes (black spikes). Whenever the error grows slowly, the time for the error to reach the threshold will be longer, and so the time interval between spikes increases.

Large stimuli with large slopes at the onset and offset can generate rates which drive a neuron into saturation (peak firing rate) and suppression, serve to illustrate other aspects of the optimal coder (Fig. 4.1B, 0 dBV). Following the onset, the stimulus grows so rapidly that the decoder is unable to reduce the reconstruction error, and therefore fires at the maximal rate, reaching saturation well before the peak of the stimulus (inset c, red arrow). Thereafter, the source encoder and the afferent both fire at their peak rate. The reconstruction falls just short of the stimulus at the peak (red trace in Fig. 4.1B).

On the decaying slope of the stimulus (inset d) the stimulus falls off rapidly, and its rate of decay is faster than the decay rate of the filter impulse response (inset d, time-interval around red arrow). At this point, the neural coder (and the afferent) cease to fire. The most accurate way to represent an extremely sharp onset (high attack rate) is to fire at high rates. Conversely, the most accurate way to represent a rapid offset (high decay rate) is to completely cease firing. Thus, the source encoder provides an explanation for the rapid changes in discharge timing at the onset and offset of stimuli; namely, spikes are placed only where they are needed. This is a major consequence of the energy constraint and a feature of optimal coding.

The optimal neural encoding model predicts the number of spikes and timing fairly accurately. The coincidence factors Γ averaged over 20 trials were 0.2 ± 0.06 (-10 dBV) and 0.49 ± 0.04 (0 dBV). These are conservative estimates because we used a small coincidence window Δ of one-half the EOD period (0.6 ms). While the features in the timing of P-type spikes are captured by the optimal coder, the LIF neuron encodes stimulus amplitude in its firing rate and does not predict timing as accurately. For the LIF model, the coincidence values of 0.12 ± 0.04 (-10 dBV) and 0.19 ± 0.04 (0 dBV) are smaller than coincidence values for the optimal coder. The LIF neuron does not reproduce the suppression in firing observed in the afferent

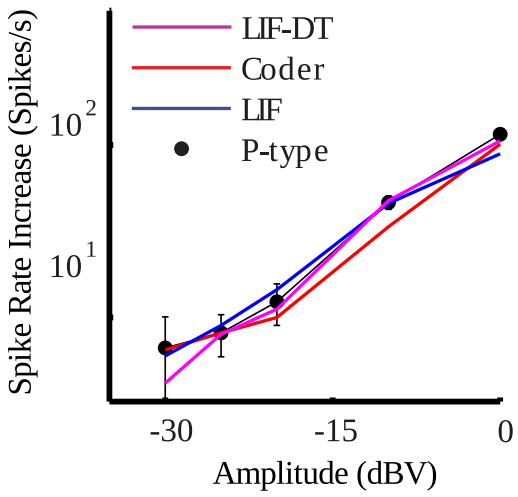

Figure 4.2: Change in spike rate as a function of stimulus intensity in response to modulations of the EOD waveform. Shown are the change in spike-rates for the P-type afferent (filled black circles), optimal neural encoder (red), LIF model (blue), and LIF-DT model (magenta). The change in spike rate is calculated as the difference between the average spike-rate elicited by the stimulus in the window shown in Fig. 4.1 and the baseline firing rate, averaged over 20 trials. All models tested are capable of predicting the change in spike-rate. If encoding were strictly following a rate-code, this information would be sufficient to encode the signal.

and encoder spike-trains. The LIF-DT model has a higher coincidence factor than the LIF model, 0.16 ± 0.09 (-10 dBV), 0.42 ± 0.05 (0 dBV). Using a Mann-Whitney U-test for the 0 dBV stimuli, we reject the null hypothesis that the mean coincidences are the same between the deterministic optimal coder and LIF-DT model ($p < 0.01$). For the LIF-DT model and optimal encoder at the -10 dBV stimulation level, the difference in mean coincidence was not found to be significant. The mean coincidence for the optimal coder is significantly higher than the mean coincidence for the LIF neuron at both the 0 dBV and -10 dBV stimulus levels ($p < 0.01$).

Interestingly, despite the poorer performance of the LIF neuron, all models are capable of capturing a change in the aggregate spike-rates. The spike rates as a function of stimulus intensity were estimated for the spike trains. Figure 4.2 shows the rate-intensity curve in logarithmic coordinates. Spike rate is depicted as an increase in average firing rate within the stimulus window over the baseline discharge rate. The P-type firing rates are obtained from experimental data and shown as points (filled black circles). The spike

rates are in good agreement with one another over a wide range of stimulus amplitudes. All four neuronal models convey information about the mean signal amplitude in the average firing rate in nearly identical ways, even though LIF neuron spike-timing is in disagreement with the P-type afferent, the optimal coder, and the LIF-DT neuron. This suggests that matching the average rate alone is not sufficient to achieve optimal encoding.

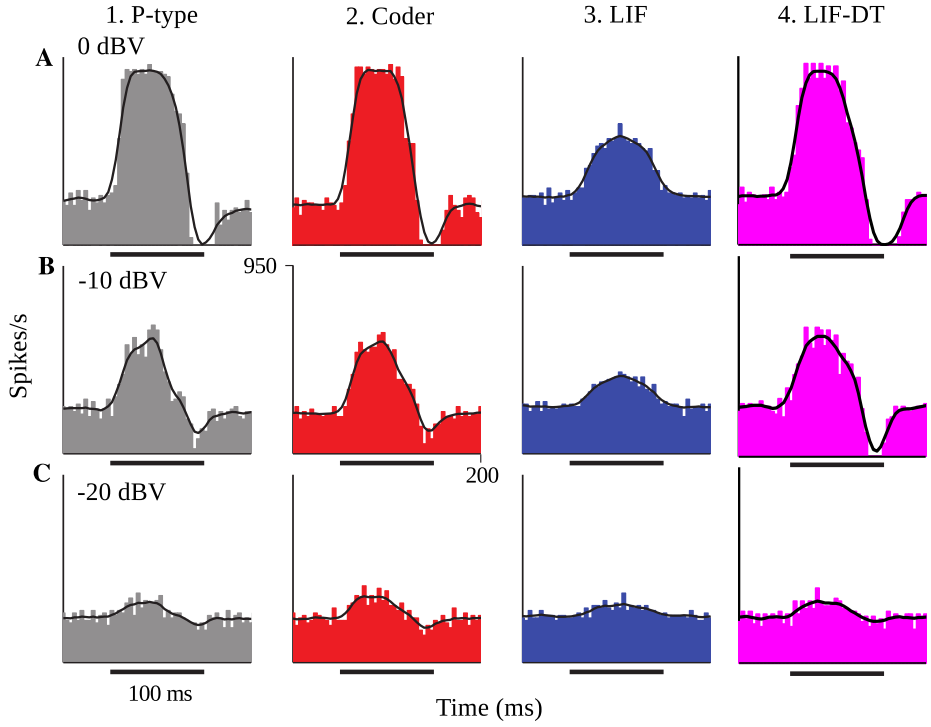

Figure 4.3: Peri-stimulus time histograms (PSTHs) obtained in response to stimuli shown in Fig. 4.1. The columns from left to right are for the P-type responses, the spike trains predicted by the optimal neural encoder, the spike trains predicted by a LIF model, and the spike trains predicted by a LIF-DT model. The rows show responses to stimuli of amplitudes 0 dBV (A), -10 dBV (B), and -20 dBV (C). Each PSTH was determined from 20 trials (4 ms bins). To highlight the change in spike rate, a smoothed estimate was produced using a sliding window of length 16 ms (black traces). The experimental PSTH shows strong adaptation in the spike rate which is not proportional to the stimulus. The PSTH of the spikes simulated by the optimal encoder closely approximate the time-varying spike-rate seen in the P-type responses. The spikes from the LIF model predict a spike rate which is proportional to the input signal. The LIF-DT model does predict adaptation, but does not match the experimental data as closely as the proposed encoder.

The fluctuations in spike rate can be studied more closely using the Peri-

Stimulus Time Histogram (PSTH). Figure 4.3 reports PSTHs over 20 trials at three intensities: Figures 4.3A (0 dBV), 4.3B (-10 dBV), and 4.3C (-20 dBV) for P-type afferent (gray, column 1), optimal coder (red, column 2), LIF neuron (blue, column 3), and LIF-DT neuron (magenta, column 4). The smoothed histogram is also shown as the black trace. The P-type afferent, optimal coder, and LIF-DT neurons have similar PSTHs and demonstrate response saturation (Figs. 4.3A1, 4.3A2) and varying degrees of response suppression at stimulus offset (all intensities). It should be noted that the P-type PSTHs and the optimal coder PSTHs are not directly proportional to the stimulus, unlike the LIF PSTH. Broadly, a comparison of the optimal coder PSTHs (column 2) with experimental data (column 1) supports the assertion that the optimal coding principle captures spike timing features accurately.

The LIF neuron, LIF-DT neuron, and experimental data do not inherently have a reconstructed signal. To reconstruct these spike trains, a first-order filter was found with values of A and τ that minimized reconstruction error between the stimulus envelope and the reconstructed waveform. Figure 4.4 depicts reconstructions for the spike trains at three different stimulus intensities (rows A-C), for optimal-coder-generated spike trains (red, column 1) LIF neuron spike-trains (blue, column 2), and LIF-DT neuron spike-trains (magenta, column 3). As expected, errors are lower for the reconstructions using the optimal coder. Predicted reconstruction errors from the optimal encoder model were significantly lower than both the LIF and LIF-DT neurons (Mann-Whitney U-test, $p < 0.01$). However, fidelity of coding is only one issue. The optimal coder reconstruction also preserves amplitude and timing features of the stimulus, unlike the LIF reconstructions which suffer amplitude distortions and temporal distortions such as lengthening (smearing) of estimated stimulus duration. The quality of reconstructions from the LIF-DT neuron are in between those of the optimal coder and the LIF reconstructions, with noticeable distortion at higher signal amplitudes. The LIF-DT neuron preserves spike-timing information much like the optimal coder (see Fig. 4.1). These results suggest that information in spike timing is necessary to recover stimulus features without distortion and without appreciable time-delay.

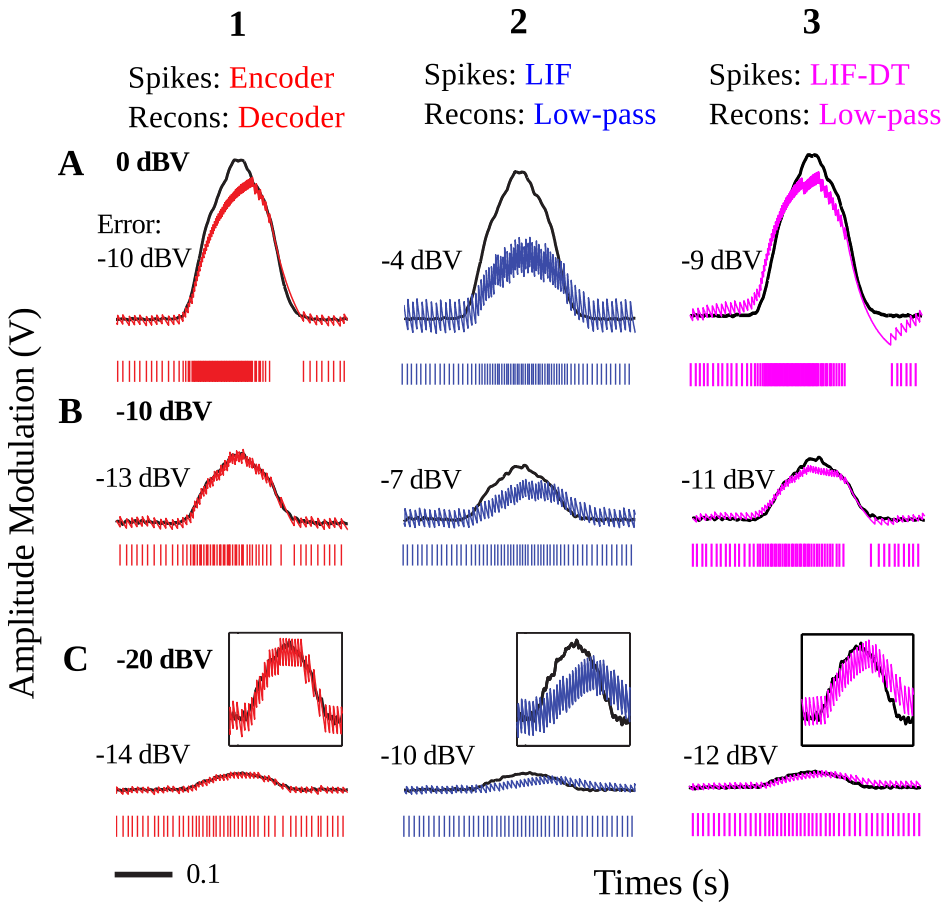

Figure 4.4: Examples of reconstructed stimuli from the optimal encoder, a LIF neuron model, and a LIF-DT neuron model. The spike trains were reconstructed using low-pass filters for three different stimulus levels: (A) 0 dBV, (B) -10 dBV, (C) -20 dBV. The experimental data are from a P-type afferent. The panels depict the stimulus (black trace) and the reconstructed stimulus (encoder: red, LIF: blue, LIF-DT: magenta) from one of 20 trials. For reference, the spike train is shown below the stimulus. For the -20 dBV stimulus, insets provide a magnified view of the stimulus and reconstruction. Reconstruction error in dBV (relative to the stimulus) is reported in each panel, with more negative values indicating smaller error. For the LIF and LIF-DT neuron models, a reconstruction filter was optimized to provide the lowest possible average reconstruction error. The reconstructions from the optimal encoder track the stimulus onset and offset without noticeable delays, and track the stimulus amplitude. However, the LIF reconstructions suffer amplitude distortion. The quality of LIF-DT reconstructions lie between those of the optimal decoder and the LIF neuron, with noticeable distortion at the highest signal amplitudes. This is due to the fact that the LIF-DT spikes are not timed to minimize reconstruction error.

4.2.2 Encoding by a Cortical Sensory Neuron Using Stimulus-Dependent γ

Figure 4.5 shows *in vitro* data from a cortical pyramidal neuron in response to injected current (frozen noise, top black trace; raster plot of 13 trials), the optimal coder response (red spikes), matched LIF neuron (blue spikes), and matched LIF-DT neuron (magenta spikes). The total duration is 21.5 s. Note that we filtered the stimulus (low-pass, with cut-off of 50 Hz). Parameters are reported in Section 4.1. Experimental spike data from Trial 1 (red arrow) were used to tune the optimal coder and LIF neuron with a matched spike rate (energy constraint). Insets B and C, arbitrarily selected (duration 1.5 s, and 1 s, respectively), are expanded and shown in Figs. 4.5B, 4.5C. In general, the optimal coder predicts spike-timing with good accuracy, with mean $\Gamma = 0.38 \pm 0.02$ compared to the 13 experimental trials. Predictability was good for those spikes where inter-trial timing is reliable, but there is greater ambiguity when spike timing is less reliable. The model also tends to generate too many spikes in responses to changes in the input signal. The LIF spike train exhibited poorer coincidence with $\Gamma = 0.12 \pm 0.02$, although it appears to broadly match the cortical and coder spike trains (Fig. 4.5A, blue spikes). However, when seen on an expanded scale it can be seen that there is poor coincidence reflected in the smaller value of Γ. The LIF-DT neuron also shows comparable performance with the optimal coder, with $\Gamma = 0.38 \pm 0.04$. The coincidence for the optimal coder was significantly higher than the LIF model but not the LIF-DT model (Mann-Whitney U-test, $p < 0.01$). This result suggests that dynamic threshold models can closely model the experimental spike times with and without resetting.

Optimum reconstructions using the best filter parameters are shown in Fig. 4.6 for the experimental, optimal encoder, LIF, and LIF-DT spike-trains. The stimulus trace (black) is overlaid with the reconstructions of the stimulus (optimal coder, red; LIF neuron, blue; LIF-DT Neuron, magenta). Figure 4.6A covers the entire stimulus duration (reconstruction errors are specified above the trace), and Fig. 4.6B shows an expanded view of the inset. Also included in Panel B is the cortical spike-train (bottom). In Fig. 4.6B, it can be seen that the LIF neuron demonstrates considerable lag when reconstructing sharp transients (e.g., arrows a and b) whereas the optimum coder reconstruction matches the onset transients with almost no lag (Fig. 4.6B,

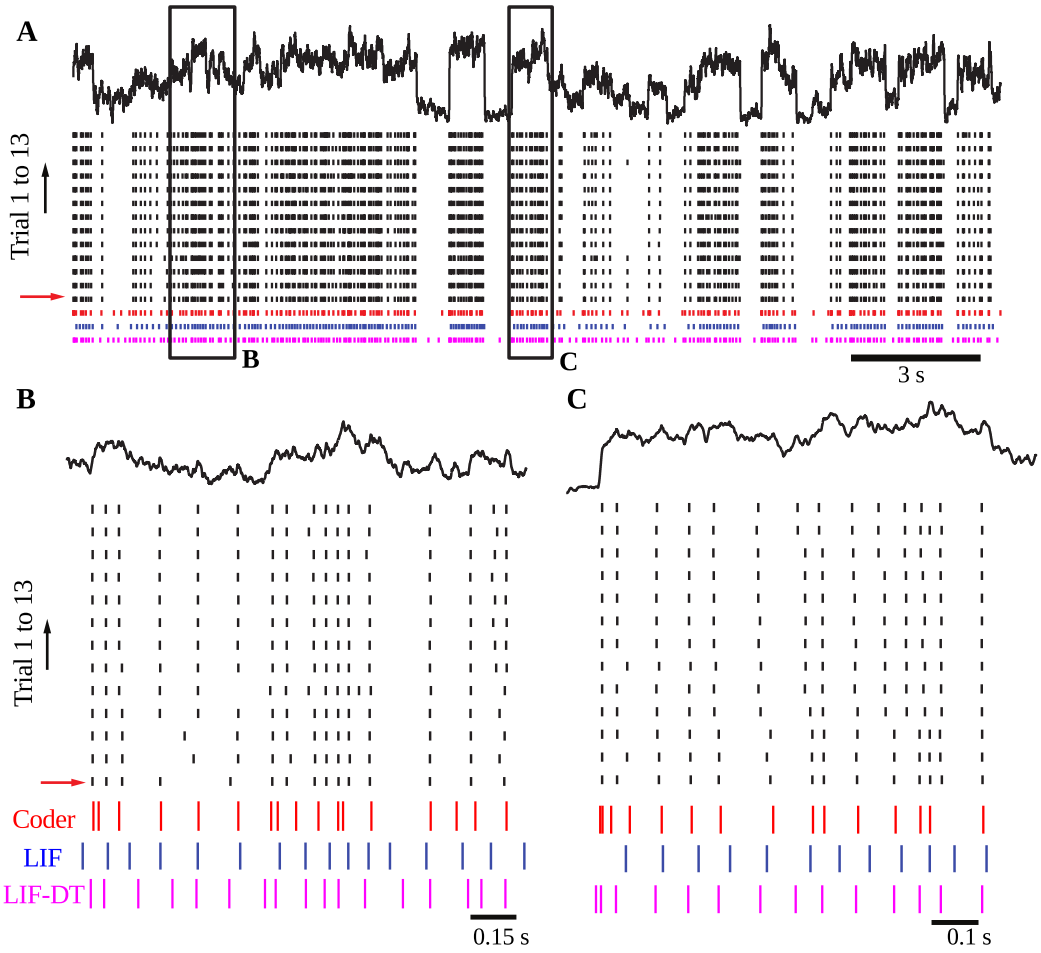

Figure 4.5: Comparison of experimental and simulated spike-times for a cortical pyramidal neuron from the INCF Spike Time Prediction Challenge dataset. Spikes shown are from the cortical pyramidal neuron, optimal coder, LIF-DT and LIF neuron in response to frozen noise. Panel A shows the current-injection stimulus trace (black), raster plots of cortical response to 13 trials (black), predicted coder spike train (red), predicted LIF spike train (blue), and predicted LIF-DT spike train (magenta) over the entire duration of 21.5 s. The model parameters were adjusted to maximize coincidence with trial 1 (red arrow). The optimal neural encoder and the two LIF models' spike times are deterministic, so only one trial can be generated for the given input stimulus. Panels B and C show expanded views of the input and spike times for the two insets (arbitrarily selected) shown in A. The optimal coder makes prediction of spike-times that are in good but not complete agreement with the experimental data, particularly at the onset of sudden changes. The LIF-DT model has slightly worse coincidence, but also makes very good predictions. The LIF spike-times have poor coincidence.

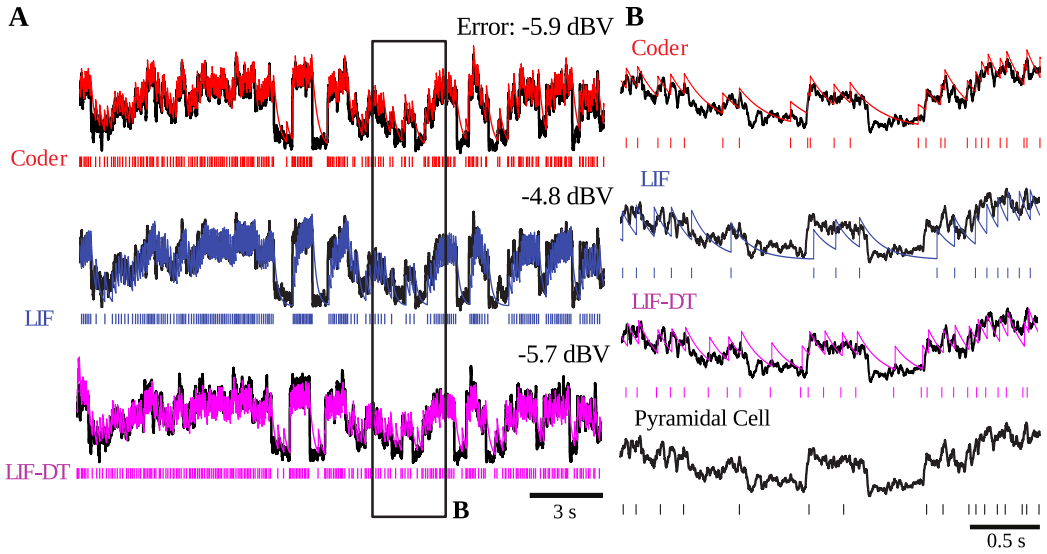

Figure 4.6: Example stimulus reconstructions for the cortical pyramidal neuron dataset. Reconstructions are shown from the optimal coder, a LIF neuron model, and a LIF-DT neuron model. Spike trains were reconstructed using a low-pass reconstruction filter. Experimental data from the cortical pyramidal neuron are depicted in Fig. 4.5. Panel A shows the stimulus (black trace), reconstructed stimulus from the encoder (top, red), LIF neuron (middle, blue), and LIF-DT neuron (bottom, magenta). Reconstruction errors in dBV (relative to the stimulus) are reported for each trace, with more negative values indicating smaller error. Panel B shows an inset of A with a magnified view of the stimulus and reconstructions. For comparison, stimulus and cortical neuron spikes are also shown. The optimal decoder and LIF-DT neuron reconstructions track the stimulus onset and offset without noticeable delays, and match the stimulus amplitude. Due to the low spike-rate and variable input signal, reconstruction errors are larger than the weakly electric fish dataset.

top trace). The LIF model here responds slowly due to the long integration time-constant. The LIF-DT neuron also shows spikes fired when the input stimulus is small. The LIF-DT model does not properly predict subthreshold variations without an additional free parameter. When used for coding error, the dynamic threshold has the advantage that it can follow temporal changes in the input signal more quickly and with greater fidelity. This is a direct consequence of the optimal coding mechanism, and the energy-fidelity trade-off.

4.2.3 Encoding Using Linear Approximation

In addition to testing the stimulus-dependent form of γ, it is also of interest to explore the predictions of the source coding neuron using the linearized form of the error and the fixed threshold of $\gamma = A/2$. This form of the encoder is also used to predict a spike rate versus error curve, analogous to the rate-distortion curve in lossy source coding.

The responses of primary electrosensory neurons of the weakly electric fish were modeled by a neural source coder with the optimal parameters from the linearized model. The source-coding neuron was also applied to the response of a pyramidal neuron from the somatosensory cortex of the rat. Several parameters were unknown, including the value of τ and the rescaling factor. For these parameters, the values which maximized coincidence were applied. Unlike the stimulus-dependent threshold, however, the parameters A and γ were determined using Theorems 2 and 3 from Chapter 3.

To provide a baseline for comparison, a brute-force approach was used to generate A and γ for a range of spike rates (R) by searching over the parameter space. For the weakly electric fish neuron, the best time-constant was $\tau = 22$ ms, and for the cortical neuron, the time-constant was $\tau = 43$ ms. The encoding MSE of the experimental spike-trains was estimated by calculating the error between the input signal and the convolution of the experimental spike-trains with the filter $g(t) = A_e \exp(-t/\tau)$. The same value of τ was used for the experimental reconstruction as the energy-constrained neural encoding simulation.

Figures 4.7 and 4.8 show the results of applying the energy-constrained neural encoder to twenty trials of EOD modulations from the weakly electric fish with a -10 dBV amplitude. Figure 4.7A shows an example encoding for the value of R closest to the experimental data. The histograms of the spike times over twenty trials, shown in Fig. 4.7B, show a close match between the simulated encoding and the experimental data. The decoded signal closely follows the input signal envelope. Figure 4.8 shows the spike rate and distortion trade-off curve using both the brute-force approach and Theorems 2 and 3. Error is reported in dBV relative to the stimulus amplitude, and the spike rate is reported in spikes per second. The parameter values A and γ appear to converge to the brute-force parameters for high spike-rates. The point corresponding to the experimentally recorded neuron is also shown.

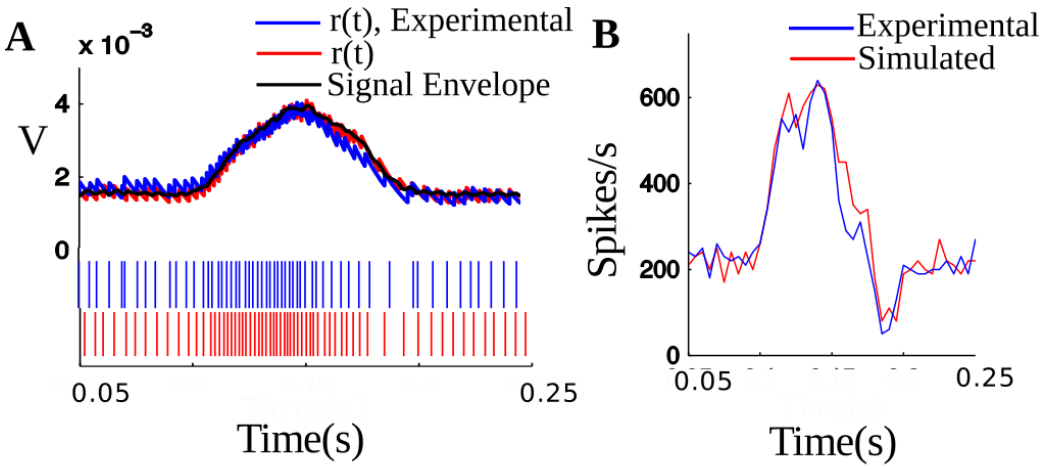

Figure 4.7: Results of applying the optimal energy-constrained neural encoder to recordings from a weakly electric fish. Panel A and B show the results of applying the optimized encoding model to twenty modulations of the EOD waveform. A segment of the encoded spikes and reconstructed signal for the simulation closest to the experimental spike-rate is shown in panel A, with blue lines indicating experimentally recorded spike-times and red lines indicating simulated spike-times. The encoder generally follows the experimental spike-times. This is made more quantitative in Panel B, which shows close agreement between the histograms of spike times computed over twenty trials using 5 ms bins.

The curve predicted by the optimal values is quite close to the brute-force approach over a wide range of spike rates. This promising result implies that the derived parameters apply over a wide range of spike rates.

Figures 4.9 and 4.10 show the application of the neural source coder to the current-clamp stimulation of a cortical neuron. Examining the simulated encoding with the closest spike rate to the experimental neurons, one can see that the reconstructed signal broadly follows the injected current waveform. The experimental spike-times show a similar pattern. Figure 4.10 also shows the spike rate versus distortion trade-off for the simulated encoder. The experimental data, in this case, are very close to the simulated curve. Despite the fact that this dataset uses an input signal which violates many of the assumptions of the derivation, the predictions seem to match experimental data well and are quite close to the optimal parameters found by brute-force search.

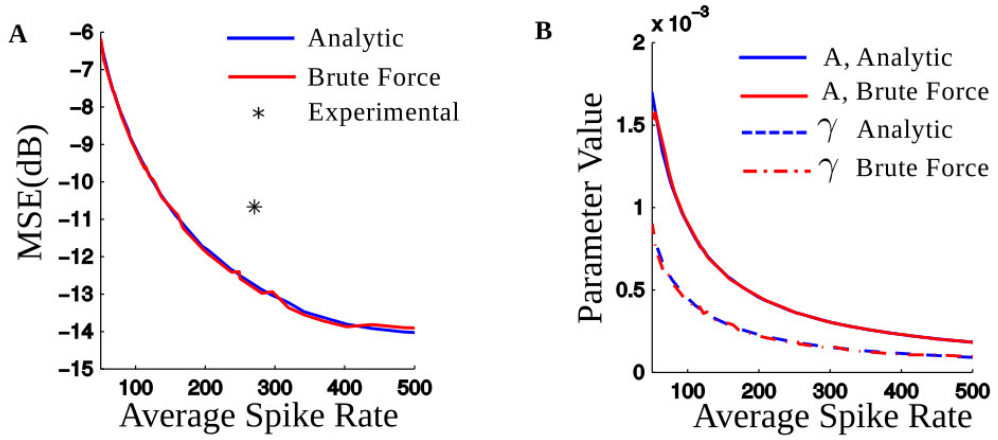

Figure 4.8: Optimal parameters from applying the optimal energy-constrained neural encoder to the weakly electric fish dataset. Panel A shows the MSE (in dB relative to $s(t)$) versus energy (measured by the spike-rate) trade-off curve. The point representing the experimentally recorded neuron is also shown. Panel B shows a close match using Theorems 2 and 3 and a brute-force parameter search to determine A and γ. Although the optimal parameters are derived only for a high spike-rate, the parameters appear to be near-optimal over a wide range of spikes. The experimental neuron exhibits an error-energy trade-off which is close to the optimal curve.

4.3 Discussion

This chapter compared a neural model which results in reconstructions with minimal error for a given spike rate to data recorded experimentally. The motivation for the source-coding neuron rests on the following assumptions: (1) A neuron is subject to an energy constraint in the form of a limit on the average spike-rate. (2) A neuron must transmit information with the highest possible fidelity for a given average spike-rate. (3) The encoding neuron has some idea about the process of decoding. The first two assumptions are not new, as discussed in Chapter 2. Energy-efficient coding by neurons is a topic of wide interest in the neuroscience community [10, 6] and the information theory community [12, 55] as is coding fidelity, which has been examined from information theoretic and statistical signal processing perspectives. However, little was known about the trade-off between energy and reconstruction error, which has been explored in detail in this chapter.

The comparison with experimental data in two very different systems, P-type neurons in a weakly electric fish and neocortical neurons in a rat, re-

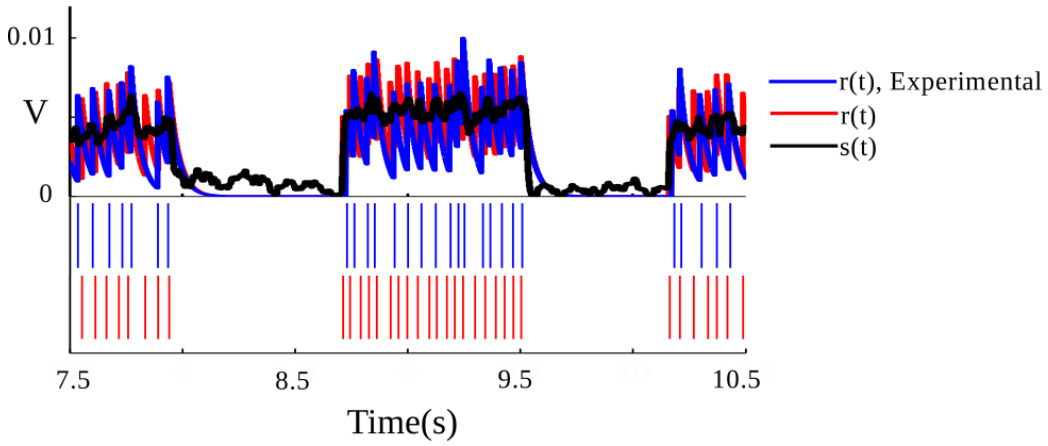

Figure 4.9: Results of applying the optimal energy-constrained neural encoder to a single trial of the current injection dataset, with total length of 21.5 seconds. A segment of the encoded spikes and reconstructed signal for the simulation closest to the experimental spike-rate is shown. The blue lines indicate experimentally recorded spike-times and red lines indicate simulated spike-times. The encoder generally follows the pattern of experimental spike-times.

sulted in close predictions of spike times which were at least as good or better than the LIF-DT model. The optimal encoder also generates reconstructed waveforms, whereas the other models require a separate reconstruction filter to be defined. Again, the reconstructions predicted by the optimal encoder model were at least as good or better than those generated from the LIF-DT model. The agreement between the predicted and experimental data in these two very different systems suggests there may be a common shared mechanism for spike generation which can be modeled as an optimal neural encoding scheme.

It is particularly interesting that this approach appears to model a cortical neuron under current injection. This neuron has a much lower spike rate and a rapidly fluctuating input, which does not satisfy the assumptions under which a solution was derived. Moreover, it is not clear *in vivo* how to model an input signal to a cortical neuron. It is also not clear that these neurons should simply relay input signals. These questions will require further experimental investigation. The current-injection dataset, however, simplifies this problem by providing a single, controlled input signal to this neuron. Despite the low spike-rate, the experimental response seems consistent with the idea of optimal encoding by cortical neurons.

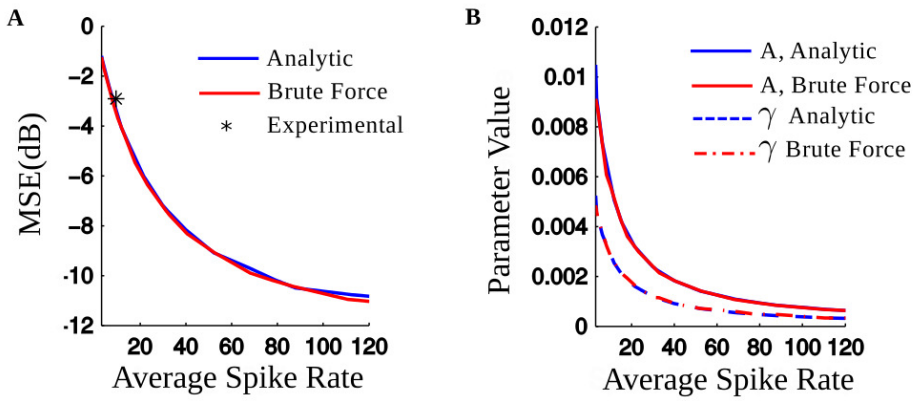

Figure 4.10: Optimal parameters from applying the optimal energy-constrained neural encoder to the neocortical neuron dataset. Panel A shows the MSE (in dB relative to $s(t)$) versus energy (measured by the spike-rate) trade-off curve. The point representing the experimentally recorded neuron is also shown. Panel B shows the parameters using Theorems 2 and 3 and the parameters from a brute-force search to determine A and γ. Even in a dataset with a low spike-rate, the parameters appear to give near-optimal performance. The experimental neuron exhibits an error-energy trade-off which is close to the optimal curve.

The approximate solution of Problem 3.1 relies on an assumption of high spike-rate. A more general approach will be needed to ensure the encoding is optimal for rapidly varying or stochastic input signals. This derivation also differs from previous approaches in that it predicts a value of γ which is dependent on the signal. Spike firing therefore depends not only on the reconstructed signal $r(t)$ but also γ. Previous dynamic-threshold models without resets fire spikes when $s(t) - r(t) = 0$ [13, 14]. The firing level γ in the optimal encoder is dependent on the value of the input signal $s(t)$, although this dependence is fairly small for high spike-rates (between $A/\sqrt{(12)}$ and $A/2$). In many cases the threshold can be approximated by $\gamma = A/2$. There is evidence suggesting that the firing threshold may be dependent on the signal level. Recently for example, Fontaine et al. [35] showed that spike thresholds can vary with the level of the membrane voltage. While their model assumes fast adaptation (of the order of 1 ms), and is based on Na-channel inactivation, the dynamic threshold time-constants for the data considered here cover much larger timescales, from tens to hundred milliseconds. These may be mediated by a voltage-dependent conductance, such as the M-current which is known to contribute to increased refractoriness on short to long time-scales

[30].

This work considers a dynamic threshold at an abstract level by lumping all the currents into a simple adaptation model (a low-pass element). The approach does not specifically model neural geometry using a multi-compartmental approach nor does it specifically model ionic currents. The advantage of this approach is an analytically tractable model, but it does not explicitly model biophysical mechanisms. Biophysically realistic currents can be incorporated into the threshold dynamics, which is a possible extension of this work. Benda and Herz [20] incorporate M-current, AHP currents, and slowly recovering Na currents, while Jolivet et al. [34] consider a full-conductance model that incorporates an adapting potassium conductance. Liu and Wang [31] and Benda et al. [32] provide a comparison of models with dynamic (adapting) threshold and biophysically realistic currents, concluding that behavior is similar under many conditions. Chacron et al. [27, 28] suggest that the low-pass dynamics built into their dynamic threshold model may be mediated by Kv3.1 channels, but their model did not specifically incorporate Kv3.1 dynamics. In summary, there is a diversity of approaches in the study of dynamic or adapting thresholds, ranging from the abstract to the biophysically realistic. This work should lead to research into biophysically realistic refinements to the proposed optimal coder.

There are several critical unanswered questions in this work. First is the question of biological mechanisms. One possibility is that a neuron is capable of estimating the encoding error $s(t) - r(t)$ and adjusting its firing level γ. This process must be under metabolic control to allow for long-term adaptation to changes in firing-rate. There are candidate mechanisms that satisfy these criteria. For instance, the KCNQ/Kv7 (M-current) family of channels [30] may be likely candidates. They are a regulator of neuronal excitability, and are coupled to metabolic processes via the membrane phospholipid PI(4,5)P2 [66]. The M-current channels are present in the axonal initial segment where spike initiation takes place [67]. These factors make them suitable initial candidates for further investigation.

The optimal neural encoder model suggests that an individual neuron is capable of tracking encoding error, possibly as a subthreshold membrane voltage. It is important to understand how this approach can expand to populations of neurons. The notion of an externally generated error signal is commonly used in predictive coding models of the auditory system [68] and

in hierarchical prediction in the visual system [69, 70]. These predictive coding models differ from the proposed approach in several key ways. The predicted input is generated by higher-level brain structures at the network-level and provides descending information to generate a reference signal against ascending sensory information. The proposed neural encoder, however, is conceptually different and does not rely on a descending reference signal from higher brain structures. Incorporating this error mechanism into models of neural networks may improve understanding of low-error, low-energy encoding of signals by neuronal populations.

Using the parameters derived from the linearized form of the error, the optimization process results in an energy versus distortion trade-off curve rather than the traditional bit-rate versus distortion curve (rate-distortion function). Conceptually, this is an interesting observation that suggests that neurons are tuned for different trade-offs of energy expenditure and encoding error. In this comparison, the P-type afferent has a high spike-rate and comparatively low error. The cortical neuron has a low spike-rate but higher error.

In the limit of high spike-rates, it is possible to derive expressions for the minimal encoding error, the filter amplitude, and the spike-firing threshold. The optimal spike-times predicted by the optimal encoder are in close agreement with experimentally determined spike-times. The asymptotic results appear to hold over a wide range of spike rates as determined by a brute-force search of the parameter space. The predicted energy versus distortion curves are within 2 dB of the energy and distortion trade-off observed for experimental neurons. This is encouraging, as it suggests that the results from studying the linearized form of the error closely predict experimental data. This provides a simpler model for analysis than the stimulus-dependent threshold, while still capturing critical features of experimental data.

Overall, using the stimulus-dependent threshold or the linearized error approximation, the proposed optimal neural encoding scheme predicts spike times which are promisingly close to those from neurons recorded from two very different species and structures. This suggests that there may be a shared mechanism of spike generation which times spikes to carefully minimize encoding error subject to a long-term energy constraint. Much work is left to be done to experimentally validate this model and investigate the biological plausibility of such an approach.

CHAPTER 5

INSTANTANEOUS RATE-CODING BY AN OPTIMAL, ENERGY-CONSTRAINED NEURAL ENCODER

The previous chapters have introduced an optimal, energy-constrained neural coder, but it is unclear how this principle relates to the current understanding of encoding by single neurons. Broadly, the two most common approaches to understanding encoding by individual neurons advocate either for rate coding or temporal coding [37, 71, 72]. Rate codes assume that information is represented in the average spike-rate over some counting window. For example, a higher stimulus intensity would result in a higher average spike-rate. This is an idea dating back at least to Adrian [73]. Rate codes are robust to variability in spike timing, which has led many to believe that rate codes may serve as a fundamental coding strategy in neural systems [74]. On the other hand, it has long been noted that rate coding is not necessarily efficient at transmitting information. Temporal codes, which postulate that the precise timing of spikes carry information, have the potential to transmit more information in the same window of time [75]. For example, the time-to-first-spike can be used to reliably distinguish between stimulus intensities with only a single spike [76, 72]. In the auditory system of non-human primates, it has been shown that spike trains with millisecond precision carry more information about the stimulus than spike trains with coarser resolution [77]. In simulation, it can also be shown that the precise pattern of spiking carries more information than expected by a rate code [78]. There is still considerable debate on whether temporal codes or rate codes best describe the neural coding scheme.

Prior work has attempted to bridge the gap between these two, sometimes conflicting, approaches to understanding neural encoding. As the width of the temporal window decreases, the information entropy of a spike train increases [79]. Rate codes with decreasing averaging windows approach an instantaneous spike-rate code, which can be estimated as the inverse of the sequence of interspike intervals [80]. The instantaneous rate can also be in-

terpreted as the probability of observing a spike at a particular time, and thus, can be estimated experimentally as a rescaling of the Peri-Stimulus Time Histogram (PSTH). Dayan and Abbott [81] argue that observations of a slowly varying instantaneous rate is consistent with a rate-coding hypothesis, and a more rapidly modulated instantaneous rate suggests temporal coding. Experimentally, it has been shown in the cricket auditory system that the instantaneous spike-rate over a small window provides a better estimate of responses to repetitive stimuli than the average spike-rate [82] and that the interspike intervals of short bursts of action potentials code modulation intensity in the electrosensory lobe of a weakly electric fish [83].

This chapter seeks to reconcile some of these widely differing views. The optimal source-coding neuron [84] is connected with the views of rate and temporal coding. In the limit of high firing rates, an instantaneous-rate coder is derived which minimizes reconstruction error subject to a constraint on energy expenditure. The instantaneous rate depends on the input signal, input signal derivative, and the reconstruction filter. The predictions of the instantaneous-rate coder are compared to data from the two systems studied in Chapter 4, namely the peripheral sensory neuron of a weakly electric fish and the the response of a neocortical neuron of a rat. The results indicate that estimates of the experimental spike-rate correspond closely to the predicted instantaneous rate, modeling spike-rate adaptation. Instantaneous rate coding also predicts the time-to-first-spike (a simple temporal code) and average spike-rate in the neocortical neuron. These results suggest that the optimal source-coding neuron shows some key aspects of both rate and temporal coding.

5.1 An Instantaneous-Rate Coder for Minimum-Error, Energy-Constrained Neural Coding

This chapter considers the encoding (generation of spikes) and decoding (estimation of the input signal from spikes) of a non-negative, twice-differentiable input signal $s(t)$. The coded spike-train is composed as a sequence of spikes at times t_i. For a given neuron, spike waveforms are essentially identical and are simply represented as a sum of impulses, $\sum_i \delta(t-t_i)$ [4]. The decoding process maps $\sum_i \delta(t-t_i)$ to $r(t)$, an estimate of the input signal $s(t)$. In this thesis,

the signal is recovered by filtering the spike train with a fixed, linear reconstruction filter specified by the impulse response $h(t), t \geq 0$. This approach is consistent with the reconstruction of dynamic signals by spike-triggered average filters [8] or stimulus reconstruction filters [38, 4]. A simple reconstruction filter is given by the impulse response $h(t) = A \exp(-t/\tau), t \geq 0$. This filter form is based on the classic idea of a pre-synaptic and post-synaptic neuron, where the post-synaptic potential can by modeled by filtering the sum of impulses with a low-pass filter representing the post-synaptic membrane [7]. The decaying exponential corresponds to a RC circuit model of the cell membrane, which is commonly used to model the passive dynamics of a cell membrane, for example in Hodgkin-Huxley models [9]. The reconstructed signal is then given by $r(t) = h(t) * (\sum_i \delta(t - t_i)) = \sum_i h(t - t_i)$.

This thesis has hypothesized that a neuron encodes an input signal with minimal reconstruction error given a constraint on the available energy. In neurons, a major source of energy consumption over a period of time (T) is the number of spikes fired [5, 11]. Energy expenditure in a neuron can be largely factored into generating post-synaptic potentials, maintaining baseline potentials, generating and propagating action potentials, and releasing and recycling vesicles. For a fixed input signal, energy expenditure can be divided into costs which do not depend on the number of action potentials, and those which are proportional to the number of action potentials. From the perspective of an encoding model, it is therefore possible to model energy expenditure per unit time as $E = b + kR$. Here E is the expended energy rate, b is the baseline cost, k is the cost per spike, and R is the spike rate. An optimal neural encoding strategy should therefore minimize reconstruction error such that an average spike-rate is maintained. In the proposed model, spikes are fired when the error reaches a threshold level γ. This leads to the following constrained optimization problem

$$\begin{aligned} &\min_{A,\tau,\gamma} \frac{1}{T} \int_0^T (s(t) - r(t))^2 dt \\ &\text{subject to } R \leq (E - b)/k \end{aligned} \tag{5.1}$$

In this problem, the parameter A is the value of the filter $h(t)$ at time 0, the parameter τ is the time-constant of $h(t)$, and γ is the variable threshold level. Chapter 3 shows the derivation of an optimal strategy to solve this prob-

lem for the case of slowly varying signals which are approximately constant between spikes [84]. In this case, an optimal strategy is to track the reconstruction error $e(t) = s(t) - r(t)$ and to fire a spike when $e(t_i) = \gamma(s(t), r(t))$, where γ is a stimulus-dependent firing threshold available in closed form. This leads to a code which times spikes to minimize error. In the limit of large signals relative to the decoding filter parameter A, this rule reduces to $\gamma = A/2$.

This chapter proposes an alternative method for generating spike times which are, in the limit of high spike-rates, equivalent to the neural source-coding model. Given the parameters A and τ it is possible to derive an instantaneous rate function. This instantaneous rate is then encoded as spikes with an integrate-and-fire model. For high rates, the optimal neural source coder and instantaneous rate coder have identical interspike-intervals. Since the intervals are identical for high firing rates, the instantaneous rate coder is an alternative approach to minimize reconstruction error subject to a constraint on the expended energy. Thus, in the limit of high spike-rates, the spike-timing code introduced in Chapter 3 and the instantaneous rate code are two different ways of describing the same code.

5.1.1 Instantaneous-Rate Coding

For the case of a single-pole low-pass reconstruction filter given by $h(t) = A\exp(-t/\tau), t \geq 0$ and the asymptotic firing rule $s(t) - r(t) = A/2$, it is possible to derive an analytic expression for the instantaneous firing rate, defined as the inverse of the interspike interval, given the values of A and τ.

Assuming a high enough spike rate, the decoded signal $r(t) = \sum_i h(t - t_i)$ and input signal $s(t)$ can be approximated, with small error, by their first-order Taylor series expansions at time t_i

$$r(t_i + t) = r(t_i) + r'(t_i)t \tag{5.2}$$

$$s(t_i + t) = s(t_i) + s'(t_i)t \tag{5.3}$$

where $r'(t_i)$ is the first right derivative. Taking t_i to be the firing time of spike i, one can assume that $r(t_{i+}) = s(t_i) + A/2$, if a spike was fired following the asymptotic spike-firing rule. An example of $s(t)$ and $r(t)$ are shown in Fig. 3.2. The linearization of $r(t)$ is also shown. At time t_i, the first right

derivative of the reconstruction is

$$r'(t_i) = -(s(t_i) + A/2)/\tau \tag{5.4}$$

Assuming that $s(t_i) >> A/2$, this can be approximated as

$$r'(t_i) \approx -s(t_i)/\tau \tag{5.5}$$

Given these approximations, it is possible to calculate the time between the spikes.

$$\begin{aligned} s(t_i) + s'(t_i)(t_{i+1} - t_i) - A/2 = \\ r(t_{i+}) + r'(t_i)(t_{i+1} - t_i) = \\ s(t_i) + A/2 - (s(t_i)/\tau)(t_{i+1} - t_i) \end{aligned} \tag{5.6}$$

Rearranging Eq. 5.6 to solve for the time between spikes gives

$$(t_{i+1} - t_i) = \frac{A}{(s'(t_i) + s(t_i)/\tau)} \tag{5.7}$$

Inverting the expression for $(t_{i+1} - t_i)$ gives the instantaneous spike-rate, $i(t)$

$$i(t) = \frac{s(t)/\tau + s'(t)}{A} \tag{5.8}$$

The relationship of the instantaneous rate to the energy constraint in Eq. 5.1 is apparent if we consider a constant signal $\bar{S} = s(t)$. Then the rate is constant and given by

$$i(t) = \frac{\bar{S}}{A\tau} = R \tag{5.9}$$

This expression agrees with the results from Chapter 3 for the optimal neural source coder, where the rate generated by a constant stimulus was estimated from the average output level of the reconstruction filter. The instantaneous rate function $i(t)$ given by Eq. 5.8 captures the spike rate in the limit of high firing rates, when $h(t)$ can be approximated linearly with low error. The rate function depends on the input signal, the derivative of the input signal, and the filter parameters A and τ.

The expression for the instantaneous rate suggests a new method to gener-

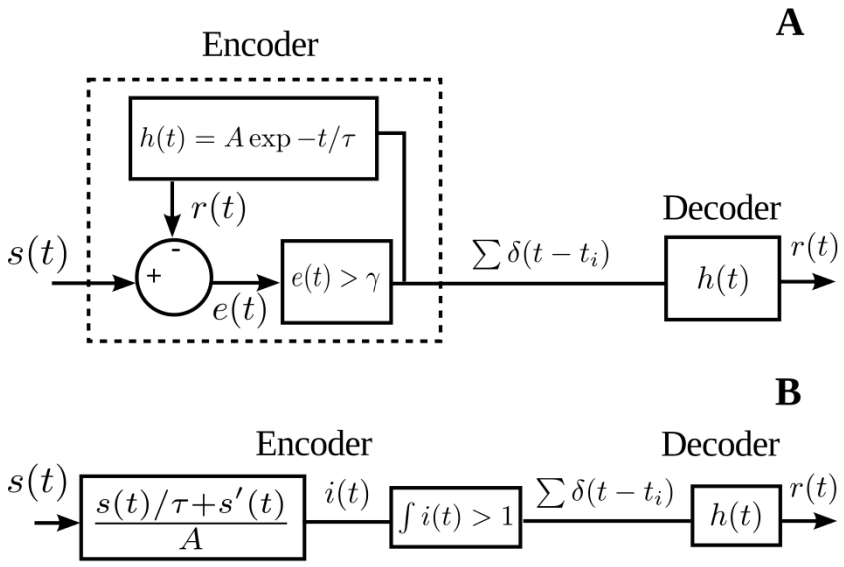

Figure 5.1: Comparison of two neural encoding models. Panel A shows the schematic of the optimal neural source coder. The encoder is implemented using a dynamic threshold with a decoding filter impulse response of $h(t) = A \exp(-t/\tau), t \geq 0$. The dynamic threshold encoder generates an internal error signal which is compared to a threshold firing rule. When the threshold is exceeded, a spike is fired. The decoder filters these spikes to generate the reconstructed signal. In the limit of high firing rates, this strategy achieves minimal error subject to a constraint on the spike rate. Panel B shows an alternative interpretation of optimal, energy-constrained encoding which is also valid at high spike-rates. In this case, an instantaneous rate $i(t)$ is computed from the signal $s(t)$. Spikes are then fired proportionally to this function using an integrate-and-fire model. In the limit of high firing rates, the instantaneous-rate approach generates a spike train with interspike intervals identical to the encoder in A. Therefore, in the limit of high firing rates, this approach is an equivalent solution to Eq. 5.1.

ate a spike train which achieves the minimum (asymptotically in the limit of high spike-rates) of Eq. 5.1. First, generate the instantaneous rate function $i(t)$ from $s(t)$ using Eq. 5.8. Next, fire spikes proportionally to $i(t)$ using a simple integrate and fire model. Given a spike at time t_i, the next spike will be fired after an interval Δ_t defined by

$$\int_{t_i}^{(t_i+\Delta_t)} i(t)dt = 1 \tag{5.10}$$

When a spike is fired, the output of the integrator is reset to 0. This model is

compared to the optimal neural source coder proposed previously [84] in Fig. 5.1. The neural source coder computes the error between the reconstruction $r(t)$ and input signal $s(t)$ to generate a spike train which is the solution of Eq. 5.1 in the limit of high spike-rates. For high spike-rates, we show both coders produce spike sequences with identical interspike intervals.

In the limit of high spike-rates, the asymptotic expression for the interspike intervals of the optimal neural source coder shown in Fig. 5.1A is [85]

$$\Delta_t = \frac{A}{(s'(t_i) + s(t_i)/\tau)} \tag{5.11}$$

For the spike-firing rule defined in Eq. 5.10, the interspike interval, at high firing rates, can be approximated as

$$\begin{aligned} \int_{t_i}^{(t_i+\Delta_t)} i(t)dt &\approx (t_i + \Delta_t - t_i)i(t_i) = 1 \\ \Delta_t = \frac{1}{i(t_i)} &= \frac{A}{(s'(t_i) + s(t_i)/\tau)} \end{aligned} \tag{5.12}$$

The instantaneous rate is Δ^{-1}. Since both methods produce spike-sequences with the same interspike intervals, in the limit of high spike-rates, the instantaneous rate coder is also an asymptotically optimal solution to Eq. 5.1. This derivation holds for high firing rates because $h(t)$ can be approximated as linear in this limit. The solution to the optimization problem can be viewed either as the optimal neural source coder, which computes reconstruction error internally, or an instantaneous rate coder defined by the signal, the signal derivative, and the filter parameters.

5.2 Methods

Responses of the proposed instantaneous rate coding model and a standard rate-coding model were generated for three sets of data: a simulated input with known functions for the signal and signal derivative, the responses of a P-type primary electrosensory afferent of a weakly electric fish, and the responses to current injection from a rat somatosensory cortical neuron in an *in vitro* preparation [36]. The data for the second and third datasets were discussed previously in Chapter 4. This chapter studies the predictions of the

instantaneous rate coder against these experimental data in order to better understand how minimum-error, energy-constrained encoding is related to rate and temporal coding.

Figure 5.2 shows the simulated function, which was modeled as two sigmoid functions with known slope parameters. The first sigmoid simulated a sudden positive change. By subtracting the second sigmoid from the first, a smaller negative step was simulated. The simulated function provided an example with known signal and signal derivative terms to test the instantaneous rate coding. Responses were simulated at a sampling rate of 5000 Hz for a duration of one second.

5.2.1 Parameter Selection

To generate the instantaneous rate code, it is first necessary to determine the parameters A and τ, as well as the dataset-specific parameters. Previously [84], the parameters of the optimal neural source coder shown in Fig. 5.1A were determined to maximize the spike-time coincidence factor between the model spike-times and the experimental spike-times. The coincidence factor [64] compares two spike trains by counting the number of spikes which occur within a window of Δ seconds of a spike from the other spike train. The coincidence is then defined between an experimental spike-train (data) and a predicted spike-train (model) as

$$\Gamma = \frac{N_{\text{coinc}} - E[N_{\text{coinc}}]}{N_{\text{data}} + N_{\text{model}}} \frac{2}{1 - 2\nu\Delta} \tag{5.13}$$

where N_{coinc} is the number of coincident spikes, $E[N_{\text{coinc}}]$ is the expected number of coincident spikes if the model was a homogeneous Poisson process with the same spike rate as the model spike train, N_{data} is the number of experimental spikes, and N_{model} is the number of spikes from the model. The second term normalizes the result, where ν is the spike rate of the model.

In this thesis, the optimal parameters derived in Chapter 3 were also used to generate the instantaneous rate code. Briefly, spike-time coincidence was optimized by sweeping over τ and the stimulus-specific parameters. The neural source coder (Fig. 5.1A) with $\gamma = A/2$ was simulated for this parameter set. For each value of τ and the stimulus parameters, the following two steps were performed.

1. Select A so that the average spike-rate constraint is satisfied.

2. Use the optimal value of γ to generate an encoded spike-train using the optimal source coder. Compute the coincidence between the encoded spike-train and one experimental trial.

The parameter values which resulted in the highest coincidence were also used as the parameters for the proposed instantaneous rate coder.

For the experimental data from the P-type afferent of a weakly electric fish, the raw waveform was filtered with a second-order band-pass filter with a 3 dB bandwidth of approximately 50 Hz, centered at the EOD frequency. The values of A, τ, and a_{EOD} were found for the stimulus levels (0 dBV through -30 dBV) in order to maximize the coincidence averaged over all stimulus levels. The value of a_{EOD} was 5.30. The values of τ and A were 24.0 ms and 2.92×10^{-4} V. The same parameters were used for all 20 trials at all stimulus levels.

For the current-clamp injection data, the current waveform was first filtered with a first-order low-pass filter with unity gain and a time-constant of τ_m. The parameter values were chosen to maximize average coincidence with the spike-times in response to the three positive DC steps included in the data. The optimal parameters were $\tau_m = 26.3$ ms, $\tau = 75$ ms, and $A = 487.4$. Note that for this dataset, A is defined in nA, which is the units of the experimental stimulus. The variable A could be converted to a voltage by assuming an appropriate membrane resistance value.

5.2.2 Instantaneous-Rate Coding

For each set of data, the instantaneous-rate function was calculated using the reconstruction filter parameters, input function, and input function derivative following Eq. 5.8. For the simulated data, the input function was assumed to be the simulated waveform. For the weakly electric fish data, the input signal was taken to be the envelope of the EOD waveform after the band-pass filter. For the INCF data, the input signal was assumed to be the current-injection waveform after low-pass filtering. For the simulated data and the DC step stimuli in the current-clamp injection data, the signal derivative was computed analytically. For the modulations of the EOD

waveform, the input signal derivative was found by filtering the input signal with an eleventh-order differentiating filter, implemented digitally with a frequency cut-off of $\pi/2$. These signals were used to calculate the theoretical instantaneous-rate function following Eq. 5.8. Using the instantaneous-rate function, spikes were generated using Eq. 5.10. The integrator output was initialized to 0 for the weakly electric fish data. For rat cortical neuron data, the integrator output was initialized to 0.5. This is because the input signal value starts at 0. The error only needs to accumulate to a level of $A/2$ before the first spike should be fired.

A rate-coding strategy was also implemented using a simple integrate-and-fire model, which fires spikes proportionally to the signal level. For each set of data, the input signal was rescaled by the mean firing rate derived from the experimental data, f_{exp}, divided by the mean input signal level, $\bar{S}$. Given a spike at time t_i, the next spike is fired after an interval Δ_t such that

$$\int_{t_i}^{t_i+\Delta_t} \frac{f_{\text{exp}}}{\bar{S}} s(t)dt = 1 \tag{5.14}$$

When a spike is fired, the output of the integrator is set to 0. Spikes were reconstructed by filtering with the impulse response $h(t) = A\exp(-t/\tau), t \geq 0$, using the values of A and τ described above. To generate the spike trains, the initial value of the integrator was set identically to the instantaneous-rate coder.

The error between the reconstructed waveforms and stimuli was computed using the RMS value of the error divided by the RMS value of the stimulus, reported in dB as

$$10\log_{10}\frac{(\int_0^T (s(t)-r(t))^2 dt)^{1/2}}{(\int_0^T s(t)^2 dt))^{1/2}} \tag{5.15}$$

This metric allows for better comparison across stimulus levels.

5.3 Results

The proposed instantaneous-rate coder and a standard rate coder were applied to study the simulated dataset, different modulation levels of the EOD waveform of a weakly electric fish, and current-clamp injection in the INCF

data. The reconstructed waveforms and spike times were compared to the experimental stimuli and spike times.

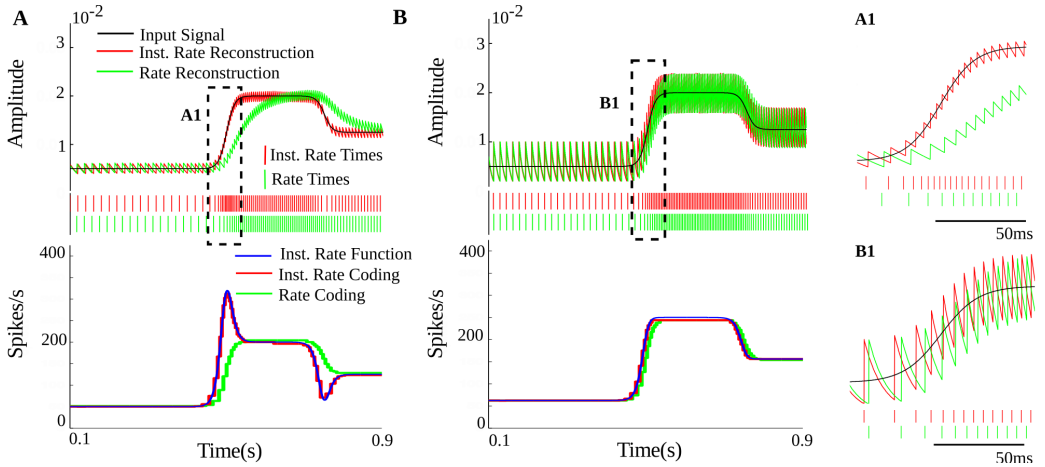

Figure 5.2: Encoding of a simulated waveform consisting of a sigmoid function centered at 500 ms added to a second sigmoid function centered at 750 ms, with a negative amplitude. This waveform had sudden changes but well-defined derivatives. The waveform was used as the input for the proposed instantaneous rate coder and a rate coder (integrate and fire model). Panel A shows the reconstructed waveforms and resulting rate functions for $A = 0.002$ and $\tau = 50$ ms. The instantaneous rate code reconstruction tracks the input signal, providing minimum-error encoding. The rate code produces significant distortion. The theoretical instantaneous rate (Eq. 5.8, calculated using the sigmoid functions and their derivatives) and the rate of the instantaneous rate coder (estimated from the simulated spike-times, generated using the encoder specified by Eq. 5.10) show nearly identical spike rates, as expected. Both methods show spike-rate adaptation in response to the signal at the onset and offset of the waveform. The inset A1 shows a small section of the simulation which emphasizes the spike-rate adaptation at the onset. The rate-code predicts a spike rate which is proportional to the signal, resulting in worse reconstruction error. Panel B shows the response of the instantaneous rate coder using the parameters $A = 0.008$ and $\tau = 10$ ms. Different parameter values change the instantaneous rate function predicted by Eq. 5.8. In this case, the term proportional to the signal $s(t)$ is much larger than the term proportional to the signal derivative. This results in an optimal instantaneous rate function which is closer to the rate-coding approach. The inset B1 shows the onset of the signal, where the instantaneous-rate code is much closer to the rate code. Depending on the situation, the optimal instantaneous rate coder can show strong spike-rate adaptation or rate encoding.

First, the instantaneous-rate coder was applied to a simulated waveform,

consisting of two sigmoid functions, using the parameters (A) $A = 0.002$ and $\tau = 50$ ms, (B) $A = 0.008$ and $\tau = 10$ ms. For the simulated dataset, the stimulus level has arbitrary units, and the values of A are reported without a unit. Figures 5.2A and B show the reconstructed waveforms and spike rates for these two sets of parameter values. The spike rates were estimated using the inverse of the interspike interval. Panel a shows the case where A is smaller and τ is larger. These parameters emphasize the derivative term in Eq. 5.8. This leads to an increase in firing rates when the signal derivative is positive and a decrease in firing when the derivative is negative. The instantaneous-rate function predicts a constant rate whenever the signal is not changing (when the derivative is zero). This behavior is similar to spike-rate adaptation observed in many primary sensory neurons [86]. The rate coder, on the other hand, predicts a spike rate which is exactly proportional to the stimulus. Firing spikes proportionally to the signal leads to large errors in the reconstruction. Panel b shows the encoding for a larger value of A and a smaller value of τ. In this case, the term of Eq. 5.8 which is proportional to the signal dominates the rate. The instantaneous rate is close to the rate coder. The instantaneous-rate coder predicts observed encoding behaviors, such as spike-rate adaptation and rate coding.

The proposed instantaneous-rate coder and rate coder were applied to the weakly electric fish data to generate reconstructions of the signal envelope. Figure 5.3 shows reconstructed waveforms, Peri-Stimulus Time Histograms (PSTHs), and spike-time rasters for the instantaneous-rate coder and rate coder. The instantaneous-rate coder (red) closely follows the instantaneous-rate function for the -10 dBV and -20 dBV steps and matches the experimental PSTH (black, Fig. 5.3B). The rate coder (green) fires spikes proportionally to the signal envelope. This pattern of spiking does not follow the pattern seen in the experimental spikes. The reconstructed waveforms for the instantaneous rate code closely follow the signal envelopes for all three stimulus levels. The reconstructions of the rate code produce significant distortions in the signal envelope. The reconstruction lags the change in the input signal, resulting in higher error. Mean reconstruction errors (RMS) for the instantaneous-rate code and rate code were: -12.8 dB and -4.0 dB (0 dBV), -13.4 dB and -7.0 dB (-10 dBV), -12.7 dB and -10.2 dB (-20 dBV). These differences were all found to be significant using a Wilcoxon rank-sum test (20 trials, $p < 10^{-6}$).

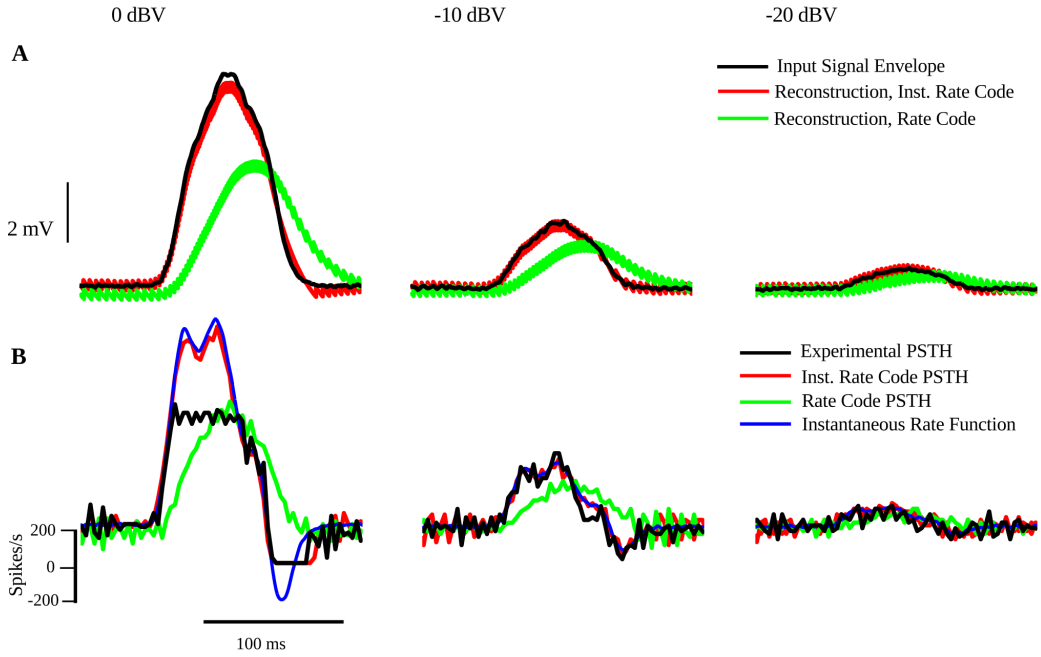

Figure 5.3: Instantaneous-rate coding and rate coding in response to AM modulation of the EOD waveform of a weakly electric fish. The predictions of the instantaneous rate code are shown in red, the predictions of the rate code in green, the experimental data are shown in black, and the instantaneous rate function (Eq. 5.8) in blue. The fish was stimulated with three amplitudes of EOD waveform modulations (row A, black traces) of duration 100 ms. Row a shows the reconstructed waveform for the instantaneous-rate code (red) and rate code (green). For the three stimulation levels, the reconstructed signal of the instantaneous-rate code closely follows the signal envelope. The reconstruction of the rate code shows significant lag in reconstructing the signal, leading to higher error. Row B shows the Peri-Stimulus Time Histograms (PSTHs) for the experimental spikes, the instantaneous-rate-coded spikes and rate-coded spikes, calculated over 20 trials, along with the theoretical instantaneous-rate function from Eq. 5.8. For the -10 dBV and -20 dBV cases, the PSTH of the experimental spike-times, the PSTH of the instantaneous-rate-coded spikes, and instantaneous-rate function coincide very closely. In the 0 dBV case, it is clear that the experimental spikes are driven into saturation when firing once per EOD cycle. The instantaneous-rate function predicts a rate which is not realizable by the experimental neuron. In the case of -10 dBV and -20 dBV stimulation, however, the instantaneous-rate function is a very close match to the experimentally observed PSTH, suggesting that the instantaneous-rate coder closely models the spike times recorded from the P-type afferent.

An interesting phenomenon can be observed in the responses to the 0 dBV stimulus in Fig. 5.3B. Due to the rapid change in the input stimulus, the theoretically calculated instantaneous rate function predicts spike rates that exceed the maximum and minimum possible spike rate for real neurons. In weakly electric fish, P-type afferents fire no faster than once per EOD cycle and can fire no slower than zero spikes per second. The instantaneous-rate function for the 0 dBV stimulus predicts a spike rate that is too large at the onset of the stimulus. As the stimulus falls off, the theoretical function predicts a negative spike-rate. The instantaneous-rate coder also predicts rates above the maximum allowable rate, but cannot fire with a negative spike-rate. Further constraints would be required to ensure the instantaneous rate function predicts spike rates which are physically realizable.

It is important to note that over the entire window of 0.3 s shown, both rate coding models predict a stimulus-dependent change in the spike rate. Figure 5.4 shows the spike rate for the rate coder, instantaneous-rate coder, and experimental data. The rates are all quite close except at the 0 dBV stimulus level, when the neuron is driven into saturation. In this case, the instantaneous-rate coder predicts a rate which is too large. The increase in spike rate with stimulus intensity is typically expected of a rate code. In this sense, the instantaneous-rate code is consistent with observations of rate-coding in different sensory neurons, unless the neuron is driven into saturation. The instantaneous-rate code, however, also follows the spike rate at shorter time scales and leads to lower reconstruction error, as seen in Fig. 5.3.

5.3.1 Response of a Cortical Neuron to Current-Clamp Stimulation

The proposed instantaneous-rate coder and rate coder were used to predict spike times in response to DC current-clamp injections. Figure 5.5 shows the response of the instantaneous-rate coder, rate coder, and experimental neuron to three levels of DC stimulation. The reconstructed waveforms, spike-time rasters, and spike rates are shown. The spike rates are estimated using the inverse of the interspike interval. For the DC stimulation, the experimental data show an initial increase in spike rate which returns to

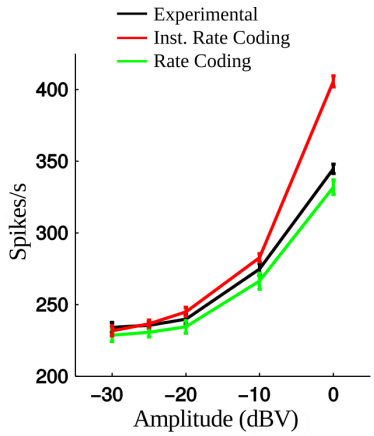

Figure 5.4: Shown here are the spike rates for the experimental (black), instantaneous-rate encoded (red) and rate encoded spikes (green), averaged over a 0.3 s window. These are plotted as a function of five stimulus levels ranging from −30 dBV to 0 dBV. Error bars indicate the standard deviation over 20 trials. Both the instantaneous rate coder and the rate coder show a long-term average spike-rate close to the experimental data, except for the 0 dBV case. As seen in Fig. 5.3, the instantaneous rate code does not show the saturation seen experimentally, leading to a higher spike-rate. The spike rate varies with stimulus intensity. This suggests a possible rate-coding scheme, at least when the signal is not saturated. However, as seen in Fig. 5.3, the adaptation in the instantaneous spike-rate over shorter time windows leads to lower reconstruction error.

a constant level. This is also apparent in the instantaneous-rate function. The spikes are timed to code the sudden change in the signal level then maintain this new level. The instantaneous rate coder predicts this behavior at the two larger stimulus levels. The rate coder does not predict the initial increase in spike rate. Because the initial spike rate is not high, the change is not coded with low error by the rate coder, as seen in the reconstructed waveforms. The reconstruction errors for the instantaneous-rate coder and rate coder were: −3.2 dB and −2.4 dB (Level 1), −5.8 dB and −5.3 dB (Level 2), −7.1 dB and −6.7 dB (Level 3). For this data, a single deterministic waveform was encoded with deterministic models, so a significance test was not appropriate. At the lowest signal level, the predicted instantaneous rate is somewhat higher than the experimental spike-rate. This is likely due to the derivation of the instantaneous rate using a linearization of the reconstructed waveform. At very low spike-rates, the exponential decay is not well modeled as a linear function.

Figure 5.6 shows two interesting properties of both the experimental data and the instantaneous rate coder. Averaged over the full two seconds of stimulation, the instantaneous-rate coded, rate coded, and experimental spike-trains all show a level-dependent change in firing rate, or rate-coding. Also interesting is the level-dependent change in the time-to-first-spike due to the interplay of the low-pass filtered input signal and the instantaneous-rate function. The time-to-first-spike is determined by the increase in the signal derivative at the onset of the step. Larger steps have a steeper derivative and a faster first spike. The rate code predicts long first-spike times. The times-to-first-spike are often interpreted as a simple temporal code [76]. The theory of minimum-error, energy-constrained neural encoding is consistent with both experimental observations, suggesting that the instantaneous-rate function can help explain some aspects of both rate coding and temporal coding.

5.4 Discussion

The proposed instantaneous-rate coder provides a method for firing spikes with ISIs determined by the instantaneous-rate function in Eq. 5.8. This strategy is an alternative method, in the limit of high spike-rates, for generating spike trains with intervals which match the previously proposed optimal neural source coder [84]. Although the generated spike trains are asymptotically equal, these two methods give different insights about minimum-error, energy-constrained encoding. The optimal instantaneous rate is actually a function of the stimulus, stimulus derivative, and reconstruction filter parameters. Note that in the datasets considered here, such as the cortical neuron, the spike rate is often not high. Nevertheless, the instantaneous-rate coder generates spike trains which show many features of the experimental data.

Comparing the modeled spike-times with the experimental data from a P-type afferent of a weakly electric fish (Fig. 5.3) and DC current injection (Fig. 5.5) of a rat cortical neuron, the instantaneous-rate coder closely predicts the experimental spike-rates. The pattern of spiking observed experimentally is consistent with the proposed instantaneous-rate function. For these stimuli, the instantaneous-rate-encoding model makes much more accurate predictions than a rate-coding model which is proportional to the input stimulus.

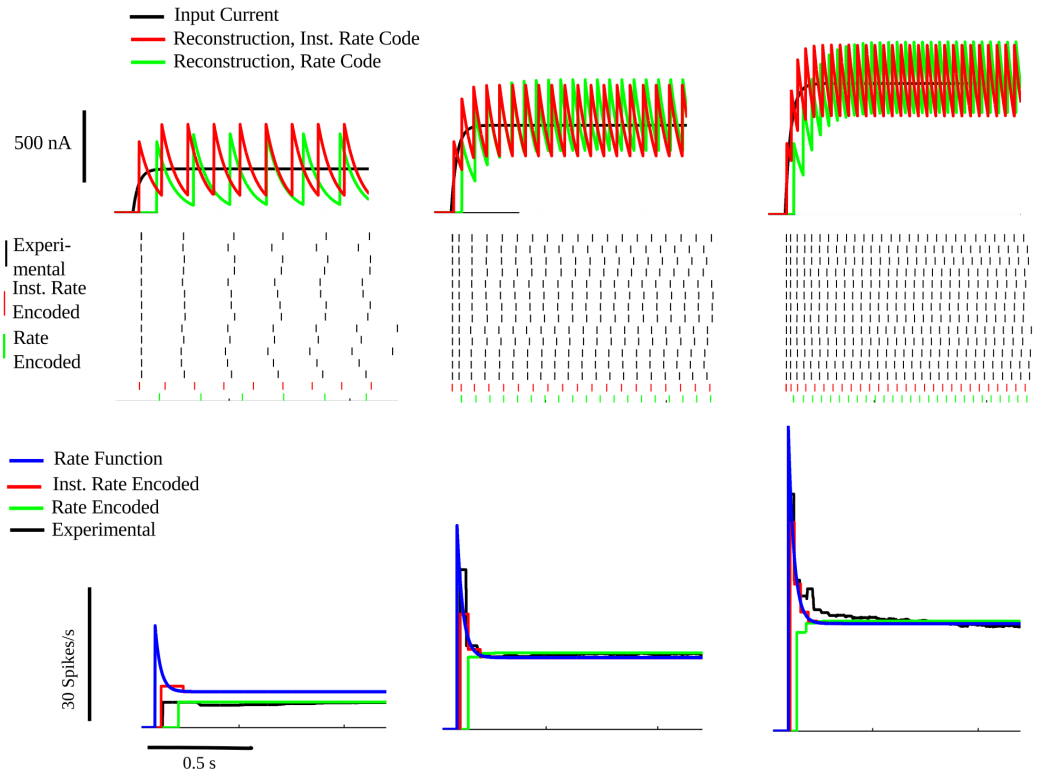

Figure 5.5: Instantaneous-rate encoding and rate encoding of three amplitudes of DC step stimulation of a cortical neuron *in vitro* using a current-clamp configuration. The figure shows the input steps (top row, black trace), which are filtered with a first-order low-pass filter. The step is coarsely represented by the reconstructed signal of the instantaneous-rate coder (red). The rate coder reconstruction (green) results in higher reconstruction error due to the lag in tracking the onset of the signal. The second row shows the spike times from 13 experimental trials along with the instantaneous-rate-coded and rate-coded spike-trains. The third row shows the theoretical instantaneous-rate function from Eq. 5.8, the rate function of the experimental spikes (estimated using the inverse of the interspike interval), the rate function of the instantaneous-rate-coded spikes and the rate function of the rate-coded spikes. For the two larger stimuli, the experimental data, instantaneous-rate-coded spikes, and theoretical instantaneous-rate function are in close agreement. All three show a sharp increase in spike rate, followed by a decay to a new baseline level. At the lowest stimulus level, the instantaneous-rate function predicts a spike rate which is higher than the experimental rate. This may be due to the linearizations and assumptions made in deriving Eq. 5.8, which do not hold for long interspike intervals.

The rate-coding approach produces poor reconstructions as well.

For cases where the spike-rate is not saturated, Fig. 5.3B shows that the

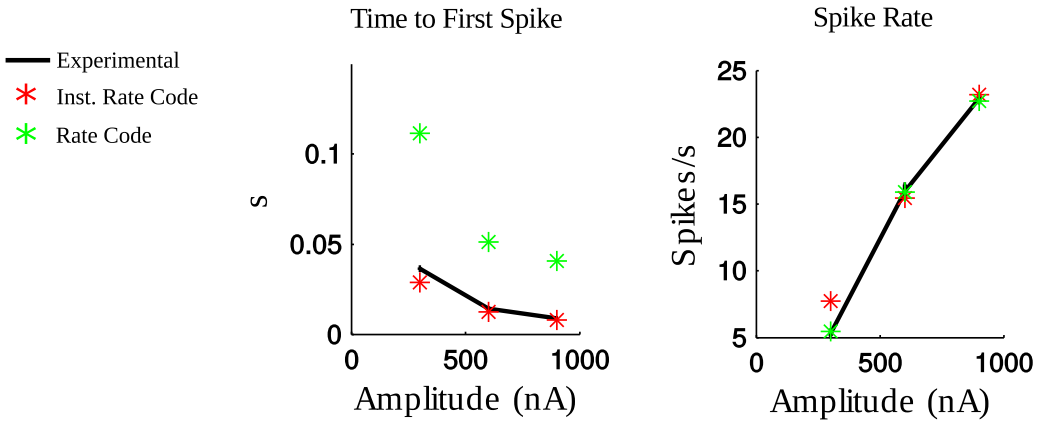

Figure 5.6: Time-to-first-spike and spike rate of instantaneous-rate encoding and rate encoding of three amplitudes of DC step stimulation of a cortical neuron *in vitro* using a current-clamp configuration. This shows that the instantaneous rate coder exhibits some characteristics of both a rate and a temporal code. The time-to-first-spike and the average rate (calculated over 2 seconds) both match the experimentally observed spikes. Although the rate-coded spikes match the experimental spike-rate, they do not show the same time-to-first-spike. Optimal encoding with an instantaneous rate coder can model some aspects of both temporal and rate codes.

instantaneous rate function can be used as an estimator for the PSTH. Here, the PSTH is scaled by the bin size and the number of trials to produce units of spikes/s. After rescaling, the PSTH corresponds closely to the predicted instantaneous rate. This suggests an interpretation of experimental PSTHs from primary sensory neurons as a measure of the instantaneous rate. The high spike-rates observed in the primary neuron may be due to the requirement of encoding sensory signals in the periphery with high fidelity.

The neural source coder is closely related to prior work on predictive coding in spiking networks [58]. This study also proposed an optimization problem which balanced fidelity against spiking activity (as a surrogate for energy), where the goal was to encode the state variables of a dynamical system in the activity of a population of spiking neurons. This population was meant to simulate cortical networks. Assuming a fixed threshold, a neural model similar to the neural source coder was derived and studied in simulated populations of cortical neurons. This current analysis builds upon prior work by predicting a stimulus-specific instantaneous spike-rate which, in the limit of high spike-rates, produces a spike train which minimizes reconstruction error for a given energy constraint.

The predicted instantaneous-rate function is determined by two terms– one proportional to the signal level and one proportional to the signal derivative. For a constant or slowly varying signal, the instantaneous rate is proportional to the signal level. This is essentially rate coding. For more rapidly fluctuating signals, the signal derivative plays a role in determining the spike rate, typically leading to high spike-rates for a brief period when the signal level changes. This spike-rate adaptation leads to spikes which are closely timed to changes in the signal. Instantaneous rates which are slowly varying favor a rate-encoding hypothesis, whereas rapidly varying instantaneous rates are thought to imply temporal codes [81]. The responses of the instantaneous rate coder to the DC step inputs (Fig. 5.6), match both the average spike-rate and time-to-first-spike. Due to the adaptation in the instantaneous spike-rate, the resulting code shows some properties of both rate and temporal coding. Previously, coding strategies have been developed which show aspects of both rate and temporal coding depending on the regime being tested [87]. It has also been shown that neural models can be tuned on a continuum to act as coincidence detectors or integrators [88]. Populations of neural models can be tuned between synchronous firing (a kind of temporal code) and rate coding, depending on the model parameters [89]. These results show that an instantaneous-rate code can operate in different regimes of a single underlying mechanism.

One important aspect of neural encoding which was not explicitly explored in our study was correlations between ISIs. Negative correlations between adjacent ISIs have been observed in a wide range of neurons [90], and have been implicated as particularly important for encoding in P-type sensory afferents [91, 92]. Previous studies of neural models which generate negative serial correlation coefficients have been shown to improve information transmission [27] and detection of weak sensory signals [93]. More recent work has shown that a neural model with adaptation currents results in negatively correlated ISIs and uncorrelated adaptation current levels, leading to improved information transmission with low decoder complexity [94]. The neural source coder is mathematically similar to some adaptive threshold models [27, 14]. As these adaptive threshold models produce negatively correlated ISIs, the neural source coder will likely result in similar ISI correlations. The results show that the instantaneous-rate coder generates the same ISI sequence as the neural source coder in the limit of high spike-rates; there-

fore, the instantaneous rate coder should also produce negatively correlated ISIs.

Although the proposed instantaneous-rate coder shows some aspects of both rate and temporal encoding, it is important to note that the temporal coding observed is due to the adaptation in spike rate caused by the term proportional to the signal derivative. The instantaneous rate is sensitive to changes in the signal, which results in precise spike-times when the signal level changes rapidly. In general, temporal coding is often poorly defined and refers to different observed phenomena which are not necessarily related to spike-rate adaptation. Many experimental observations of temporal encoding, such as encoding in spike-time correlations or phase-locking, are not addressed here. Further work will be needed to explore the proposed instantaneous rate coder (and the optimal neural source coder) in these contexts.

The instantaneous-rate coder replicates many aspects of the experimental data, but the generation of an instantaneous-rate function is not necessarily a biophysically plausible mechanism for implementing minimum-error, energy-constrained encoding. However, the instantaneous-rate coder generates spike-intervals which are equivalent to the source coding neuron shown in Fig. 5.1A. Benda and Herz [20] showed that M-currents, AHP-type currents, and slow recovery from inactivation of fast sodium channels can introduce spike-frequency adaptation in computational models. The value of the instantaneous-rate coder is not as a possible biophysical mechanism, but rather as a tool for understanding neural encoding. Further work will be required to understand the biophysical mechanisms underlying the trade-off between encoding error and energy consumption.

Minimum-error, energy-constrained neural encoding by individual neurons can be achieved by a rate coder of an instantaneous-rate function which depends on the input signal, signal derivative, and the reconstruction filter parameters. In the limit of high spike-rates, this approach generates interspike intervals which are identical to the interspike intervals generated by an optimal source-coding neuron. Promisingly, the instantaneous-rate function closely models the spike rates recorded experimentally from a P-type afferent of a weakly electric fish and reproduces the observed PSTHs. The instantaneous-rate coder also predicts the average spike-rate and time-to-first-spike of a cortical neuron's response *in vitro* to DC step inputs. This result suggests that the instantaneous-rate coder can capture some aspects of

both rate-coding and temporal coding at different levels of the sensory pathway. Certain experimental observations of rate and temporal coding may in fact arise from an underlying mechanism of optimal neural encoding subject to an energy constraint.

CHAPTER 6

A STOCHASTIC THRESHOLD PREDICTS INTERVAL STATISTICS AND IMPROVED POPULATION CODING

Neurons are often thought to be noisy information-processing units, but many studies have explored the possible benefits of noise in neural systems. In some systems, added noise can improve performance, an effect known as noise-enhanced processing (closely related to stochastic resonance and dithering in quantizers). The neural source coder presented in this thesis predicts spike times which minimize reconstruction error; up to this point these spikes are generated by a deterministic firing rule. This chapter extends this model to stochastic spike-firing by introducing a noisy threshold. Comparing the predictions of this model to spike trains recorded from 53 P-type afferents of weakly electric fish, the model can predict anti-correlated spike times and higher-order interval statistics. Common stochastic spiking models, such as renewal or Poisson models, do not show this behavior. Further simulations show that additive threshold noise can improve encoding performance in a neural population without interconnections. Estimated error is approximately 8 dB lower for a population of eight neural source coders than populations with renewal or Poisson statistics. The model was also used to predict spike times of a cortical neuron subject to current injection. In this case, the source-coding neuron predicts reliable spike times in response to frozen-noise stimulation, but progressively decorrelated spike trains in response to DC step stimulation. A neural source coder with noisy threshold accurately predicts the statistics observed in real neurons and suggests a mechanism to lower encoding error in populations of sensory neurons.

The previous chapters have introduced a deterministic neural coding model, the neural source coder, where the model is constrained to maintain an average firing rate while minimizing error. The encoder tracks the coding error $s(t) - r(t)$ and fires a spike whenever the error reaches a deterministic, stimulus-dependent firing threshold $\gamma(s, t)$. The firing threshold $\gamma(s, t)$ is optimal in the limit of high firing-rates, which achieves the energy-fidelity

trade-off. This type of coding is analogous to lossy source coding in digital systems, where the coding error is minimized for a fixed bit rate [95]. So far in this thesis, the source-coding neuron has been deterministic. This chapter provides its stochastic extension.

Physiological neurons exhibit variability in their spike times even when stimulated repeatedly with a deterministic stimulus [96, 97]. On the other hand, the neural source coder, as originally developed in Chapter 3, has a deterministic spike-firing threshold. Repeated stimulation with a deterministic stimulus will generate identical spike times. These spikes are timed so as to minimize coding error. Thus, for the same stimulus and constraint on the spike-rate R, any other set of spike times will lead to an increase in coding error. This chapter therefore extends the original model and determines the role of timing jitter in a source-coding neuron, and whether it has any benefits when representing sensory signals.

The key assumption is that noise is added to the threshold. To make the stochastic neural source coder realistic, the ISI statistics are constrained to follow the statistics of the experimental neurons against which the source-coding neuron is being tested. While the most common assumption is that neuronal spike-times follow a Poisson process [98], this chapter considers non-renewal statistics, in particular anti-correlated ISIs [91]. Several reasons motivate this choice. A dynamic or adaptive threshold was originally proposed as a mechanism that gave rise to ISI anti-correlations [25]. Anti-correlations stabilize the mean spike-firing rate and have been presumed to serve the ethologically important function of weak-signal detection [27, 91], particularly in sequential or real-time tasks [99, 93]. While sensory neurons in several model systems are known to exhibit such correlations (see [93, 90]), the P-type primary electroreceptor afferent demonstrates some of the strongest known anti-correlations [91] and has been successfully modeled using a dynamic threshold [14, 27, 28]. The proposed source-coding neuron was developed from observations of P-type spike-trains [84], albeit deterministically. It is therefore reasonable to expect that a stochastic extension of the source-coding neuron will also exhibit anti-correlations. Thus, it is of interest to ask how these correlations can be introduced into a spike train, and determine their effects on coding at the single neuron and population levels.

When studying neuronal noise, a classical view is that neurons are sim-

ply inherently noisy due to the underlying biophysics, and that neuronal networks function despite these noisy mechanisms [100]. Over the last 20 years, however, many studies have investigated the enhancement of neurons and neural networks by the addition of noise. The idea of noise-enhanced processing, or stochastic facilitation, is related to the concept of dithering in quantization [101], and is often termed stochastic resonance [102, 103, 104]. Additive threshold noise has been shown to enhance processing in both single-neuron models [105] and populations of neuron models [106, 107, 108]. In particular, additive noise in a population of neuron models improves the signal-to-noise ratio of reconstructed waveforms when using a simple summing architecture [106]. Experimental evidence for stochastic facilitation in neuronal systems has been observed in a range of systems such as cutaneous mammalian mechanoreceptors [106] and cricket sensory systems [109]. There is substantial evidence, both computational and experimental, that noise in neural systems serves to enhance coding and processing of sensory signals.

This work extends the source-coding neuron with the addition of a stochastic threshold. Spike-train statistics are controlled by the parameters of the noise, the encoding model, and the input signal. The hypothesis is that while the addition of stochastic spike-firing will only increase encoding error for single neurons, it could lead to greatly reduced encoding error in a population of neurons. The source-coding neuron with stochastic threshold is used to simulate responses to the baseline stimulus and amplitude modulations in the electrosense system of weakly electric fish. The higher-order interval statistics and correlations between intervals are well modeled by the source-coding neuron with noisy threshold. Simulations of small populations of source-coding neurons show a clear noise-enhancement of encoding error. The source-coding neuron also demonstrates similar patterns of spike-time reliability as observed experimentally [110]. The addition of a stochastic threshold to the source-coding neuron predicts the statistics of experimental spike-trains and reduced encoding error in populations of stochastic units.

6.1 Stochastic Threshold

The neural encoding model in sensory neurons should map an experimental stimulus $s(t)$ to a sequence of spike times, $t_1, t_2, \ldots, t_n$. The input stimulus

is non-negative and defined over the interval $[0, T]$. Since the spike train is defined by its times, it is possible to represent the encoded signal as a sum of Dirac delta functions, $\sum_i \delta(t - t_i)$. The reconstruction filter is defined by the impulse response $h(t)$, and the reconstructed waveform is defined as $r(t) = h(t) * (\sum_i \delta(t - t_i))$. The impulse response is given by $h(t) = A \exp(-t/\tau)$, where A is the initial height of the impulse response and τ is the membrane time-constant. Spikes are fired when $s(t) - r(t) = \gamma(s(t))$, where

$$\gamma(s(t)) = A\frac{(1 + 2s(t)/A) - \sqrt{1 + 4(s(t)/A)^2}}{2} \tag{6.1}$$

In the limit of large signal levels ($s(t) >> A$), the threshold asymptotically reaches a constant $\gamma = A/2$. The asymptotic limit of $\gamma = A/2$ is a good approximation for most cases, and is used in this chapter. It is known that changes in firing threshold between successive firings are small as seen from current-voltage phase plots (for example [35]). This observation is supported by the source-coding model which predicts that optimality can be achieved with small signal-dependent shifts in the firing threshold. For the rest of this chapter, the asymptotic limit of γ is used.

This firing rule, however, is deterministic and will not generate variable responses to repeated stimuli [97]. The source-coding neuron can be augmented with a stochastic firing rule to generate variable spike-times, possibly at the cost of increased encoding error. In this chapter, stochastic spike-firing is introduced using an additive threshold noise $\nu(t)$, representing the probabilistic opening and closing of voltage-gated sodium channels. In the stochastic model, spikes are fired when

$$s(t) - r(t) \geq \gamma(t) + \nu(t) \tag{6.2}$$

Threshold noise can be generated by filtering a white-noise process to create a bandlimited output. In continuous time, this noise source is an Ornstein-Uhlenbeck process [111]. In a discrete-time simulation, with sampling period T_s and $t = nT_s$, a Gaussian white noise process σw_n can be filtered to generate a process with a desired bandwidth, B. The resulting process is defined by

$$\nu_n = \rho\nu_{n-1} + \sigma w_n \tag{6.3}$$

The bandwidth in Hertz of the resulting noise is given by

$$B = \frac{1}{2\pi T_s} \cos^{-1}\left(\frac{2\rho - \frac{1}{2}(1+\rho^2)}{\rho}\right) \tag{6.4}$$

The resulting stochastic source-coding neuron is shown in Fig. 6.1. The optimal neural source coder computes the reconstruction of the spike train and computes the encoding error. This error is compared to a threshold $\gamma(t) + \nu(t)$, and a spike is generated if the error exceeds this threshold. The noise process is described by the bandwidth B in Hertz and the white-noise variance σ. In this work, the white noise is assumed to be Gaussian. The neural source encoder is defined by the parameters A and τ of the reconstruction filter.

In certain cases, the statistical properties of the P-type afferents could not be described adequately using the low-pass filtered Gaussian noise defined above. For these afferents, a form of $\nu(t)$ with a band-pass power spectral density was required. In discrete time, this was generated using an autoregressive moving-average model applied to a Gaussian white-noise process σw_n

$$\nu_n = \sum_{i=1}^{N} \rho_i \nu_{n-i} + \sum_{j=0}^{M} \theta_j \sigma w_{n-j} \tag{6.5}$$

where the coefficients ρ_i and θ_j were designed as a third-order, Type-II Chebyshev band-pass filter using the Matlab Filter Design toolbox (The Mathworks, Natick, MA). The pass band of the filter was defined by a center frequency f_c and a bandwidth B.

6.1.1 Electrophysiological Methods

Similarly to Chapters 4 and 5, data from two model systems were used to test the stochastic source-coding neuron: (1) *in vivo* extracellular recordings of spike trains from the P-type primary electrosensory afferent of the weakly electric fish *Apteronotus leptorhynchus*, and (2) *in vitro* intracellular recordings from a neocortical pyramidal neuron in the rat somatosensory cortex.

In the weakly electric fish, responses of 52 units to baseline EOD activity were recorded along with the response of one additional unit to baseline

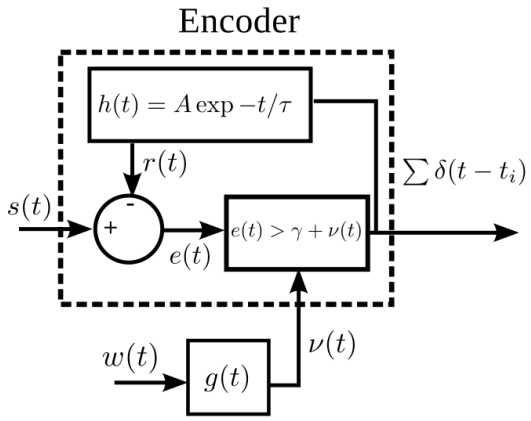

Figure 6.1: A block diagram of the neural source coder with noisy spike-firing rule $\gamma(t)$. The reconstruction filter is $h(t) = A\exp(-t/\tau), t \geq 0$. To encode the signal as a spike train, the reconstructed waveform $r(t)$ is computed and used to determine the error $e(t)$. The error is compared to a firing threshold $\gamma(t)$ in order to generate spikes. The threshold is modified by an additive, bandlimited noise process $\nu(t)$. This noisy firing threshold results in random spiking behavior in response to repeated, deterministic experimental stimuli. The model is defined by the parameters A, τ, the bandwidth of the input process B, and the variance of the noise process σ.

activity and stimulation by modulations by a raised-cosine waveform of different stimulus intensities. Stimulation was provided by a pair of carbon electrodes placed perpendicularly to the lateral line on either side of the fish.

The responses of a regular-spiking L5 pyramidal cell from the rat somatosensory neocortex recoded *in vitro* is also tested in this chapter. This dataset was made publicly available by the 2009 INCF Spike Time Prediction Competition [36]. The stimuli consisted of four DC steps (one negative and three positive) and frozen-noise stimulation. The frozen-noise stimulation was generated by filtering a nonhomogenous Poisson process and repeated for all 13 trials.

6.1.2 Spike-Train Statistics and Reconstruction Error

Experimentally recorded spike-trains were compared against the spike trains generated by the source-coding neuron with a noisy threshold. The spike trains were treated as point processes, and the statistical properties of the ISIs were determined [112]. The analysis presented here is drawn largely from previous in-depth studies of the statistics of baseline spike-trains and

interval sequences [91].

For a sequence of N spikes, the ISIs are defined as the differences between each spike time and the succeeding spike time.

$$\Delta_i = t_{i+1} - t_i, 1 \leq i \leq N-1 \tag{6.6}$$

The spike train can also be studied using interval sequences of higher-orders [91]. An order-k sequence consists of the differences in time between a spike and the k-th following spike.

$$\Delta_{k,i} = t_{ki+1} - t_{k(i-1)+1}, 1 \leq i \leq (N-1)/k \tag{6.7}$$

The distribution of Δ_i is the ISI distribution and is typically estimated from a normalized histogram of the experimentally recorded ISIs. The ISI distribution characterizes the first-order interval statistics, but experimental spike-trains show interesting structure in their higher-order statistics as well [91].

To study the relationship between ISIs, the joint histogram of the ISIs (Δ_i, Δ_{i+1}) can be computed. In the joint histogram, one ISI and its successive ISI are paired together. This histogram estimates the probability of observing an ISI of particular length followed by an ISI of another length. The plotted joint histogram is also referred to as an ISI return plot, and the joint histogram is used to visualize the relationship between ISIs.

The higher-order interval distributions were characterized using their variance and Coefficient of Variation (CV). The CV is a dimensionless quantity relating the variance of a distribution to its mean. For the kth-order interval distribution, the coefficient of variation is defined as

$$CV_k = \frac{\mathrm{var}(\Delta_{k,i})^{1/2}}{E[\Delta_{k,i}]} \tag{6.8}$$

The relationship between successive ISIs was determined using the Serial Correlation Coefficient (SCC) of the ISI sequence. The SCC ρ_l at lag l was computed as

$$\rho_l = \frac{\sum_{i=1}^{N-1}(\Delta_i - E[\Delta_i])(\Delta_{i+l} - E[\Delta_i])}{(\sum_{i=1}^{N-1}(\Delta_i - E[\Delta_i])^2 \sum_{i=1}^{N-1}(\Delta_{i+l} - E[\Delta_i])^2)^{1/2}} \tag{6.9}$$

where the ISI sequence was of length N. SCC values range from 1 to -1.

Reconstruction error was calculated using the RMS value of the error. This was normalized by the value of the stimulus, which allows for better comparisons for different stimuli.

$$10 \log_{10} \frac{(\int_0^T (s(t) - r(t))^2 dt)^{1/2}}{(\int_0^T s(t)^2 dt)^{1/2}} \tag{6.10}$$

6.1.3 Poisson and Renewal Spike-Trains

To provide a baseline comparison to the spike trains generated by the source-coding neuron with noisy threshold, two additional methods were used to simulate spike trains. The first method was to generate spike trains following a homogeneous Poisson process. For a Poisson process the ISI, Δ, is exponentially distributed with an intensity parameter $\lambda = R$, giving the probability density function

$$f(\Delta) = R \exp(-R\Delta), \Delta \geq 0 \tag{6.11}$$

To generate the Poisson process, the following procedure was used for each simulated unit. First the experimental spike-rate was calculated and used as the parameter R. Then, starting at time $t = 0$, An interval Δ was generated using the exponential distribution. The simulation time was incremented to $t = t + \Delta$. The process was continued until $t + \Delta > T$, where T was the length of the experimental data.

A renewal process is an interval process where intervals are identically and independently distributed. To generate renewal spike-trains, the experimental ISI histogram was first calculated, using bins of one-tenth of an EOD cycle. This was normalized to estimate the distribution of the ISIs from the experimental data. The intervals were assumed to be identically and independently distributed following this experimentally derived distribution. To generate simulated spike-trains with renewal statistics, a simulation was first started at time $t = 0$. An interval Δ was drawn (with replacement) from the experimentally derived distribution. The simulation time was then updated to $t = t + \Delta$. This process continued until $t + \Delta > T$, where T is the length of the experimental data. The sequence of intervals then followed a renewal

process with interval distribution identical to the experimental data.

6.1.4 Parameter Fitting

To compare the predictions of the source-coding neuron with noisy firing threshold to the experimental data, a method to select A, τ, the noise bandwidth, and σ was required. First, the parameter A was constrained to ensure the baseline firing rate was met [84]. The average reconstruction level resulting from a single spike is $A\tau$, so for a baseline stimulus level of b and a baseline rate of R, A should be constrained to be

$$A = \frac{b}{\tau R} \tag{6.12}$$

This leaves three degrees of freedom, τ, noise bandwidth B, and σ, which were adjusted to best match the joint ISI histogram (Δ_i, Δ_{i+1}). A parameter search was conducted over τ, the noise bandwidth, and σ. For each set of parameter values, a simulated spike-train was generated. The joint ISI histogram was computed for this spike train, binned into whole numbers of EOD cycles. The squared error between the simulated and experimental joint ISI histograms was computed. The parameter set with the lowest error was selected for that unit. Each experimentally recorded unit had a different set of parameter values.

For the single P-type afferent which was also stimulated with raised cosine modulations of the EOD, a single scaling parameter, a_{EOD}, was needed. This is due to the unknown orientation of the electrode relative to the stimulated electrosensory receptors, which influences the strength of the response [65]. The parameter was used to scale any deviation from the baseline EOD level. This parameter was determined after A and τ. For the 20 trials, the experimental spike-trains were first filtered through the reconstruction filter $A\exp(-t/\tau)$ to create an estimate of the signal envelope $\hat{s}(t)$. The value of a_{EOD} was used to rescale $\hat{s}(t)$. The value of a_{EOD} which minimized the mean squared error between the rescaled $\hat{s}(t)$ and $s(t)$, averaged over the 20 trials, was selected.

In order to generate simulated spike-trains to compare with the data recorded *in vitro* from the neocortical rat neurons, an additional parameter was required. In the experiment, the electrode and intracellular fluid of

the cell body likely low-pass filtered the injected-current waveform. For simulation purposes, the input current waveform provided with the dataset was first filtered using a first-order low-pass filter with time constant τ_m. For the source-coding neuron, the parameters A, τ_m, τ, noise bandwidth, and σ must be chosen. Given τ_m, the parameter A was estimated using the time-to-first-spike for each of the three positive DC stimuli in the dataset. The value of A was estimated from each DC level and the results averaged together. For a given DC step, the value for A is calculated as

$$A = 2I(1 - \exp(-t_1/\tau_m)) \tag{6.13}$$

where I is the height of the DC step and t_1 is the first-spike time. To determine the remaining free parameters, a search was conducted over τ_m, τ, B, and σ. The spike times were computed for all three stimulus levels and the frozen-noise stimulus. The spike times were filtered with a Hann window of length 20 ms to estimate the instantaneous rate. The average squared error between the simulated and experimental instantaneous spike-rate was calculated. The parameter set with the lowest squared error was chosen.

6.2 Results

The stochastic source-coding neuron, Poisson process model, and renewal model were used to predict spike times from 53 experimentally recorded P-type afferents and a cortical pyramidal neuron. Statistics and reconstructed waveforms were computed for each spike train.

Figure 6.2 shows a comparison of the spike-train statistics of the experimental P-type (black), source coding (red), Poisson (blue), and renewal (green) spike-trains. Although the EOD waveform (Fig. 6.2A, top, black, high-frequency oscillations at 878 Hz) was supplied as input to the source coder, the reconstructed signal $r(t)$ (red) tracks the envelope of the EOD and not the rapidly varying carrier. Spike trains are shown below the EOD trace with at most one spike per EOD cycle, in the positive phase. Thus the ISI distributions are peaked at multiples of the EOD period (Fig. 6.2B) in all cases except for the Poisson neuron, where the distribution is exponential. The most probable ISIs are about 4-5 EOD periods long (Figs.

6.2B1, 6.2B2, 6.2B4) whereas the mean ISIs are identical in all four cases. By design, the renewal ISI distribution is identical to the P-type ISI distribution. There is some similarity between the ISI distribution from the source coding neuron and the P-type ISI distribution, but it is not a perfect match. The renewal and Poisson processes demonstrate independent and uncorrelated ISIs, i.e., $P(\Delta_i, \Delta_{i+1}) = P(\Delta_i)P(\Delta_{i+1})$. This is reflected in their joint distributions depicted in Figs. 6.2C3, 6.2C4. However, the ISIs in the experimental data are correlated (Fig. 6.2C1) and demonstrate long-short anti-correlations (see [91]). The source-coding neuron closely matches this long-short anti-correlation pattern (Fig. 6.2C2). The serial correlation coefficients for the ISI sequence are another way of showing the dependencies in the intervals (Fig. 6.2D). The P-type and source-coding neuron show strong negative correlations at the first lag (around -0.5) whereas the renewal and Poisson models are uncorrelated over all lags, $l \geq 1$. The source-coding neuron manages to accurately capture the P-type ISI correlations, and thus the spike trains from these two neurons have similar correlation structure. An analysis of the statistics of higher-order interval distributions, in particular the variance-growth curves (Fig. 6.2E) and CV-growth curves (Fig. 6.2F) further demonstrate that the source-coding neuron matches the non-renewal P-type statistics at least up to interval orders of about 100, i.e., several hundred milliseconds (see also [91] for a detailed analysis of P-type afferents). Renewal processes have a variance that grows proportionally with k (as seen in Fig. 6.2E). However, anti-correlated interspike intervals demonstrate a much slower growth in variance, with the P-type neuron showing almost constant variance initially (up to about $k = 100$) and increasing thereafter [91]. This increase is likely due to additive measurement noise and long-term adaptation processes not modeled in the source-coding neuron. This can be seen in Figs. 6.2E and 6.2F as well. However, the source coding neuron demonstrates variance that is identically constant across all orders k. Thus, the source-coding neuron closely matches the non-renewal statistical properties of the P-type neuron.

The statistics of the P-type afferents varied considerably over the 53 units studied. Almost all units showed a strong negative correlation between succeeding ISIs ($\rho_1 < 0$ and none showed a positive correlation). The variable ρ_1 is the serial correlation coefficient at lag $k = 1$. Three typical classes of statistics are observed as shown in Fig. 6.3.

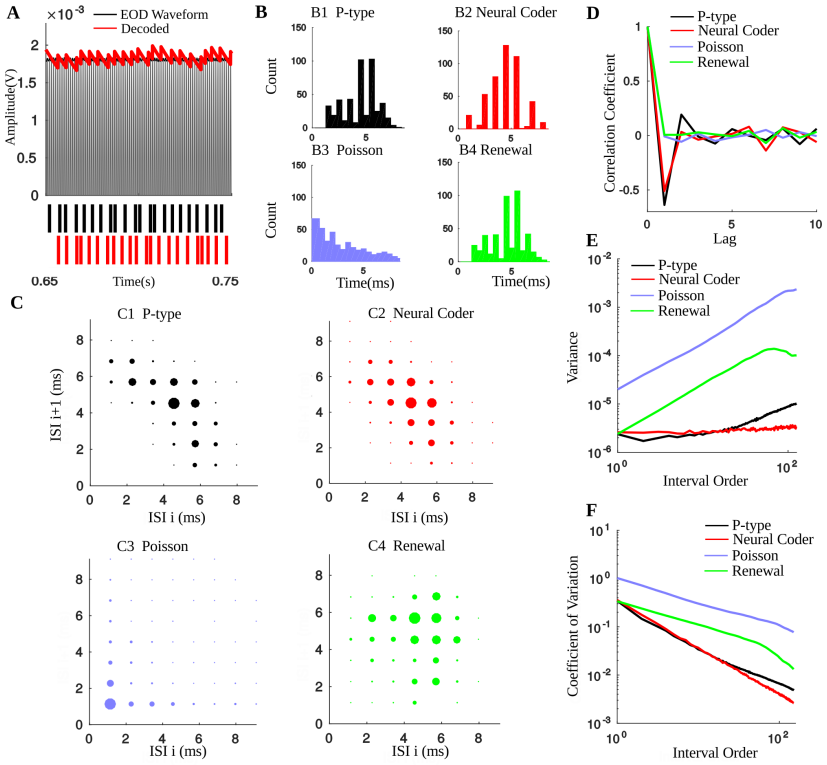

Figure 6.2: Comparison of statistics of an experimental spike-train and model neuron spike-trains. The colors are black (P-type data), red (source-coding neuron), green (renewal model), blue (Poisson model). Panel A shows an example of a baseline EOD waveform (black oscillating trace) and reconstruction (red trace) from the source-coding neuron. Note that the envelope, rather than the EOD waveform, is being encoded by the source-coding neuron. Bottom traces show the spikes. Panel B shows the ISI distributions from 2 s of data. The renewal model, by design, matches the experimental ISI exactly. Panel C shows the ISI joint distributions $P(\Delta_i, \Delta_{i+1})$. The size of the circles is proportional to the probability. The experimental ISIs demonstrate long-short intervals, i.e., anti-correlations (see also [91]). Critically, source-coding neurons also demonstrate anti-correlations, but the renewal and Poisson neurons do not. Panel D gives the serial correlation coefficients (ordinate) as a function of interval lag (abscissa). The long-short anti-correlations are evident from the marked negative correlation at lag = 1. The renewal and Poisson spike-trains have uncorrelated ISIs. Panel E plots the growth of variance as function of interval order. Renewal and Poisson neurons show a linear growth in variance, whereas the source coding neuron has nearly constant variance. P-type spike trains are similar to the spike-train from the source-coding neuron for interval orders up to about 100. Panel F shows the CV as a function of interval order.

1. ρ_1 of almost exactly -0.5, followed by coefficients ρ_k which are nearly zero for $k \geq 2$. These afferents have a joint ISI distribution resembling Fig. 6.3A1, and serial correlation coefficients as shown in Fig. 6.3A3. These afferent statistics can be readily captured using a low-pass filtered noise source in the firing rule, Eq. 6.1 (joint ISI distribution shown in Fig. 6.3A2, and matching correlation coefficient in Fig. 6.3A3).

2. $-0.5 < \rho_1 < 0$, followed by negative coefficients ρ_k, $k \geq 2$ at higher lags, gradually decreasing to zero. These afferents have a joint ISI distribution resembling Fig. 6.3B1, and serial correlation coefficients as shown in Fig. 6.3B3. These afferent statistics can also be captured using a low-pass filtered noise source in the firing rule, Eq. 6.1 (joint ISI distribution shown in Fig. 6.3B2, and matching correlation coefficient in Fig. 6.3B3).

3. $-1 < \rho_1 < -0.5$, followed by alternating positive and negative ρ_k, $k \geq 2$, gradually diminishing to zero. In the joint ISI distributions, these units often display two clusters of ISI pairs as seen in Fig. 6.3C1. Two successive ISIs with the same value, regardless of length, are highly improbable. This leads to strongly anti-correlated ISI sequences (Fig. 6.3C3). For this type of afferent a low-pass filtered noise source in the firing rule fails to capture the joint ISI distribution. However, when a band-pass filtered noise source is added to the firing rule, instead of a low-pass filtered noise source, then the joint ISI distribution (Fig. 6.3C2); serial coefficients (Fig. 6.3C3) are accurately captured. The noise process is determined by a center frequency f_c , a bandwidth B, and a power σ and generated as described in Section 6.1.1. Using these parameters it is possible to fit units which have two clusters of ISI pairs and $\rho_1 < -0.5$. Alternatively, it is possible that there is a modulation in the baseline EOD waveform. If the baseline EOD waveform was modulated with a depth of approximately 5% and much lower frequency than the EOD waveform, it is possible to also produce a similar ISI return pattern.

The neural source coding model is also able to replicate the power spectral density observed in experimental spike-trains. These spike trains exhibit a high-pass characteristic, as shown in Fig. 6.4. In contrast, the renewal

process and LIF neuron have much flatter spectra. It has been suggested that power spectra with a high-pass characteristic are related to the signal-processing concept of noise shaping [113]. Noise shaping can improve the resulting signal-to-noise ratio of a quantizer. The high-pass spectra is also closely related to the anti-correlated intervals observed in Fig. 6.3. Prior work has shown that a spike train with a high-pass power spectrum could have higher coherence with a stimulus than a spike train with a flat spectra [114].

Over the 52 units with baseline activity, the interval order statistics observed for a single unit in Fig. 6.2 have been shown to hold over the entire population [91]. Interval order statistics were averaged over the 52 units with baseline activity, including the variance, CV, and Fano factor. These are shown in Fig. 6.5. Averaged over the entire population, the neural coder shows very similar statistics as the experimental data for the first 10 to 100 intervals. The variance increases sub-linearly and the Fano factor decreases with order. The renewal and Poisson models both increase linearly in variance and show a flat Fano factor. Interestingly, the neural coder population statistics diverge from the experimental population for long interval orders which approach 100.

In summary, Figs. 6.2-6.5 demonstrate that the source-coding neuron accurately captures the statistical properties of P-type afferents up to approximately 50-100 ISIs. Beyond this time-scale, the P-type units deviate from the behavior predicted by the source coding neuron.

To investigate the possible role and benefits of stochastic spike-firing in the electrosensory system of weakly electric fish, populations of various sizes were simulated using the source-coding neuron with noisy threshold, Poisson, and renewal spike-trains. Figure 6.6 shows the results of these simulations for the experimentally recorded baseline activity also shown in Fig. 6.2. For each plot, the simulation was repeated 100 times and the mean result presented in order to generate smooth curves. First, a population of eight identical source-coding neurons were simulated. This population size is approximately equal to the number of afferents which innervate neurons in the Electrosensory Lateral line Lobe (ELL) [115]. Population reconstruction was conducted by averaging the outputs of the units together. The goal was to reconstruct the quiescent EOD envelope, which is a DC-level signal (see Fig. 6.2A). Figure 6.6A1 and Fig. 6.6A2 show the results of this simulation as the noise

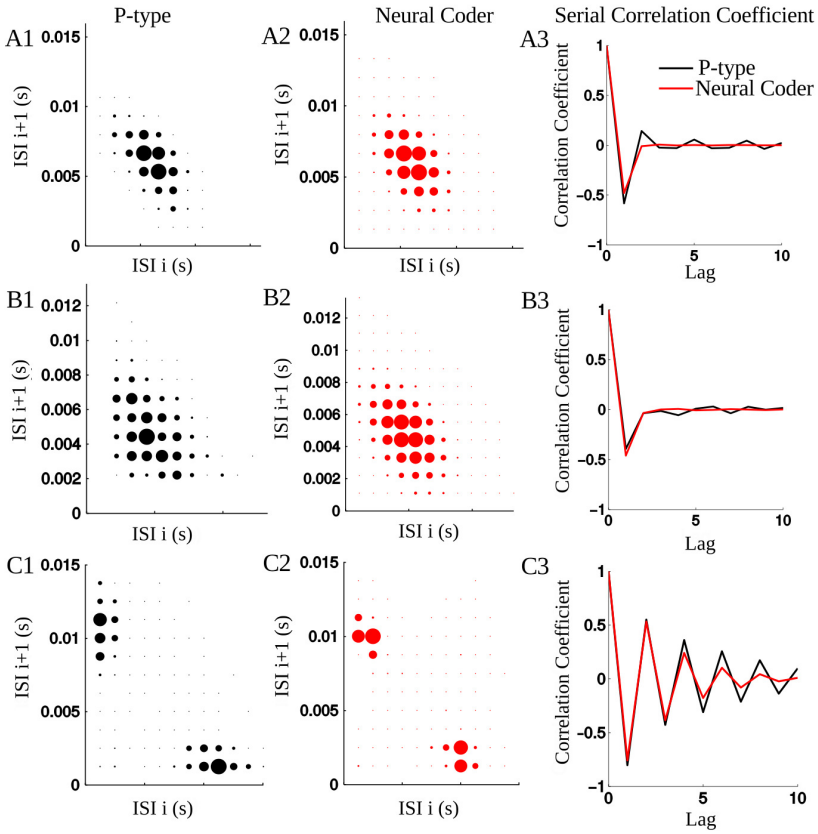

Figure 6.3: Three serial correlation patterns typically observed in P-type afferent spike-trains whose joint ISI distributions are shown in Panels A1, B1, and C1. The P-type neuron in Panel A1 has $\rho_1 \approx -0.5$ and all other ρ_k are approximately zero (see Panel A3). The P-type neuron in Panel A2 has $-0.5 < \rho_1 < 0$ followed by negative ρ_k, $k \geq 2$ which gradually decrease to zero (see panel B3). The P-type neuron in Panel C1 (and D1) has $-1 < \rho_1 < -0.5$, followed by alternating positive and negative ρ_k, gradually diminishing to zero (see Panel C3). For the examples shown in Panels A1 and B1, the source-coding neuron is able to reproduce the joint ISI distributions (Panels A2 and B2) and the serial correlations (Panels A3 and B3) using a low-pass filtered noise source in the firing rule. However, a low-pass-filtered noise source cannot reproduce a $\rho_1 < -0.5$. If a band-pass-filtered threshold noise process is introduced in the source-coding neuron then the joint ISI distribution is accurately reproduced (Panel C2) along with $\rho_1 < -0.5$ and the alternating positive-negative correlations (Panel C3).

threshold standard deviation, σ, and bandwidth are varied. Reconstruction error reaches a clear minimum as a function of the variance of the threshold noise process (Fig. 6.6A1). Thus, there is a noise enhancement, or stochastic facilitation, where reconstruction error is large for small and large values

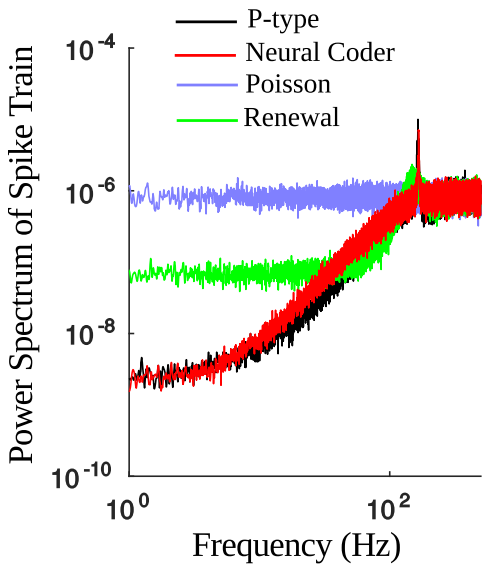

Figure 6.4: The power spectral densities of the raw spike-trains for the simulated neural models and experimental data shown in Fig. 6.3A. A spike train generated by a Poisson process shows a power spectrum which is flat across frequencies. The renewal model shows a slight increase at higher frequencies. The neural source-coding neuron and experimental spike-train show a high-pass characteristic, which is related to the anti-correlated structure of the ISIs.

of noise power but is greatly reduced at intermediate values. There are no gains in encoding error for a single stochastic neuron. In fact, for a single source-coding neuron, the deterministic firing rule minimizes reconstruction error for a given stimulus [84], and the addition of noise to the threshold only increases the reconstruction error. Figure 6.6A2 shows that as the bandwidth is varied, a large range of bandwidths produces low error in the population. Using the value of variance which resulted in minimum error in Fig. 6.6A1, populations of source-coding, Poisson, and renewal neurons were simulated for various population sizes (Fig. 6.6B1). The Poisson and renewal spike-trains were reconstructed using a first-order low-pass filter with identical parameters to the source-coding neuron. All methods showed a decrease in reconstruction error with the number of units averaged, but the source-coding neuron showed the lowest reconstruction error at all population sizes. For the Poisson neuron, the improvement in encoding error is consistent with the $1/N$ fall-off expected from averaging (dotted black line). The improvement in error for each unit added is shown in Fig. 6.6B2. All three models show that improvement shows diminishing returns after approximately 10 units,

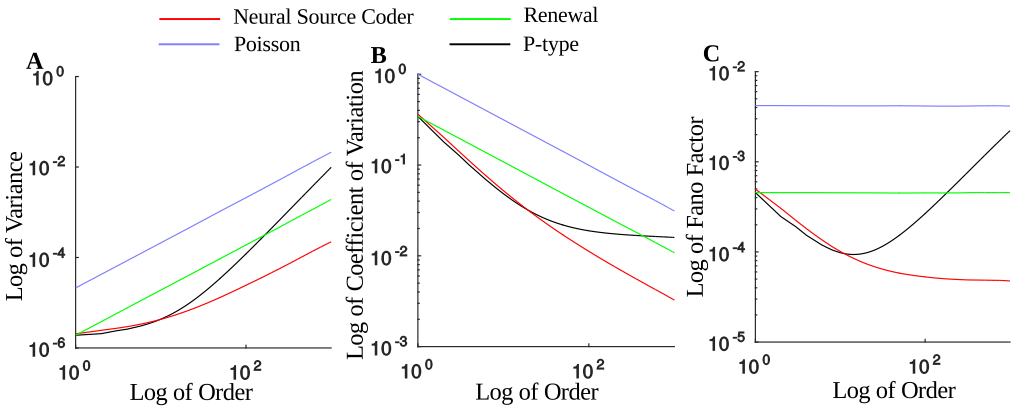

Figure 6.5: Interval order statistics, averaged over the population of 52 units with only baseline activity. Panel A shows the variance versus interval order. Panel B plots the CV versus interval order. Panel C shows the Fano factor versus interval order. For all three metrics, the population average of the neural coding model matches the experimental neurons for the first 10-100 intervals, then diverges. The P-type afferent shows more regular statistics than expected from a Poisson or renewal process. Spike trains with these statistics may lead to optimal detection performance [91]. Standard Poisson and renewal models do not show the same pattern of statistics seen in the population average.

on the order of the number of units averaged by ELL neurons [115]. These simulations suggest that the negative correlations between ISIs observed in experimental neurons may play a key role in encoding signals in populations with minimal error.

While Fig. 6.6 depicts population reconstructions for a DC-level (quiescent) EOD envelope, it is very relevant to ask whether populations of identical source-coding neurons can also reduce encoding error in response to weak modulations of the EOD waveform. Such modulations can be induced by small prey and can cause transient changes in the firing activity of P-type electroreceptors [116]. Thus, a quick and accurate detection of modulations is of ethological importance [91, 93]. The average reconstructed waveform from a population of eight simulated neural source coders are shown in Fig. 6.7A1. In Fig. 6.7A2, a population of eight Poisson neurons with variable rate were simulated and used to reconstruct the signal. The Poisson spike-trains used a rate proportional to the signal level. The source-coding neuron population tracks the changes in the waveform with lower error than the Poisson population. The spike-rate histograms in Figs. 6.7B1 and 6.7B2

show that the highest rates for the source-coding neuron occur at the onset of stimulation. The population of eight source-coding neurons was simulated 100 times to produce average errors for different values of noise standard deviation, σ, shown in Fig. 6.7C. There is also a clear stochastic facilitation, or noise enhancement, for the population, but a noisy threshold only increases error for a single neuron. Populations of Poisson neurons and neural source coders were then simulated for different population sizes, and the simulations repeated 100 times to produce smooth estimates. Figure 6.7D1 shows that the reconstruction error is still improved by averaging over multiple units, although the decrease is smaller than in the baseline case seen in Fig. 6.6. The error from the neural coder population is much lower than the Poisson population. This improvement in error is somewhat slower than the $1/N$ improvement expected from averaging. Figure 6.7D2 shows the improvement in error provided by each unit. Again, the neural source coder population shows diminishing returns after a population size of 10 units. As with the DC stimulus, a population of neural source coders with noisy thresholds results in low encoding error for small modulations in the EOD waveform. Encoding these modulations with low error is of great ethological relevance.

Another important aspect of stochastic spike-firing which has been observed experimentally is the reliability of spike times in response to different stimuli [110]. For instance, it has been observed that cortical neurons recorded *in vitro* in response to current injections exhibit decreasing correlation over time in response to DC stimulation (low trial-to-trial reliability), but these neurons show high trial-to-trial correlation (high reliability) in response to repeated presentation of frozen-noise stimulation (repeated presentations of the same realization of a random process). Figure 6.8 explores the spike-time reliability predicted by the source-coding neuron with noisy threshold for the parameter values which best matched the PSTH of the cortical neuron, computed over 13 trials. Figure 6.8A shows the stimulus current (black) and reconstructed waveform (red) for the DC step stimulus (left) and noise stimulus (right). In the DC case, the reconstructed waveform tracks the stimulus level. For the noise stimulus, the reconstruction broadly follows the current, but with higher error due to the low spike-rate. Figure 6.8B shows the raster plots in response to DC stimulation (left) and noise stimulus (right). In the DC case, for both the experimentally recorded spike-trains and the neural-source-coded spike-trains, spikes are produced with high probability at the

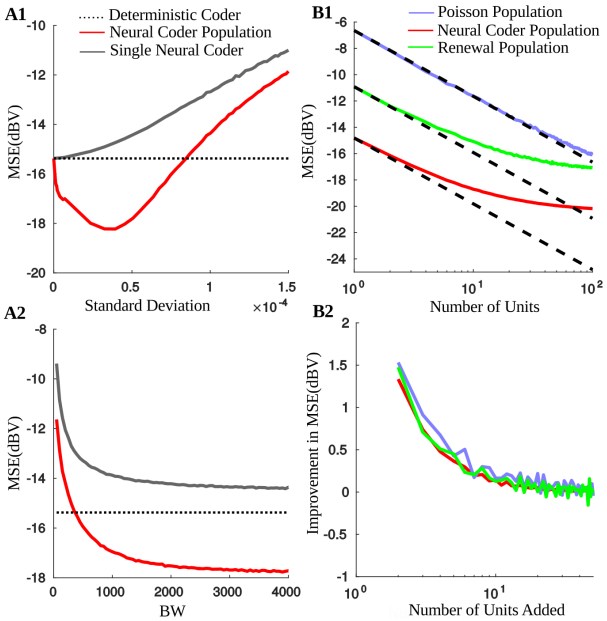

Figure 6.6: Encoding of a quiescent EOD waveform by a population of simulated neural source coders. A baseline stimulus was encoded with a deterministic source-coding neuron, a population of source-coding neurons with noisy thresholds, a population of renewal process neurons and population of Poisson neurons. Panel A1 shows the change in population encoding error as a function of the standard deviation of the noise. There is a noise enhancement for the population of noisy neurons. Adding a noise process with nonzero power results in lower reconstruction error than a deterministically generated spike-train. The single stochastic neuron does not show this benefit. Panel A2 plots the variation in population encoding error with bandwidth of the noisy threshold. In the population, error is low for a wide range of bandwidths above 1 kHz. Panel B1 plots the encoding error as a function of the number of units averaged together. For the neural encoder with stochastic threshold, the value of variance which minimized error in A1 was used. The dotted black lines indicate the improvement expected from averaging independent observations ($1/N$). The error decreases with the number of units averaged, and the encoding error is lower than spike trains with Poisson or renewal statistics. This suggests that the neural source coder with noisy threshold can lead to improved encoding in populations of sensory neurons using a simple population averaging approach. Panel B2 show the improvement in error per unit added to the population. For all three models, the improvement per unit small after approximately 10 units.

onset of the stimulus. As time progresses, the spikes become increasingly decorrelated trial-to-trial. Thus there is a stimulus-induced correlation at

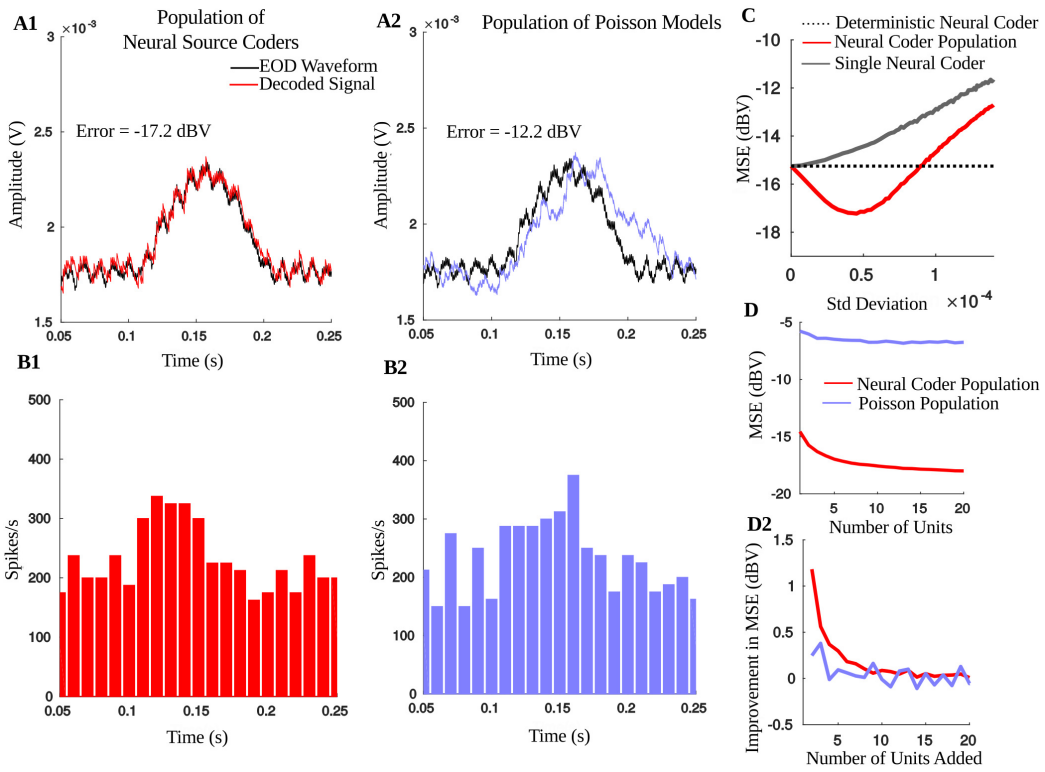

Figure 6.7: Responses to stimulation with 100 ms raised-cosine modulations in the EOD waveform in a weakly electric fish. Populations of eight neural source coder and Poisson neurons were simulated for each of the 20 experimental trials. The Poisson spike-trains were simulated with a rate proportional to the stimulus level. Panel A shows the stimulus envelope (black) and the reconstructed waveform from a population of eight neural source coders (red) and Poisson neurons (blue) for a single trial. The source coding neurons follow the stimulus closely, but the Poisson population reconstruction shows significant error. Panel B shows the spike-rate histograms of the two populations of eight neurons shown in Panel A. The neural source coder (red) shows the highest rate on the rising slope of the envelope, indicating spike-rate adaptation. Panel C plots the MSE as a function of noise standard deviation for a population of eight neurons, showing that the population of source-coding neurons shows a stochastic-facilitation effect not seen in a single neural coder. Panel D1 shows the MSE as a function of the number of units in a simulated population. There is a decrease in error of several dB for the neural source coder. The Poisson model has higher reconstruction error. Panel D2 plots the improvement in dB from adding a model neuron to the population. Adding Poisson units to the Poisson population does not lower error as much as adding units to the source-coding neuron population.

the onset of the stimulus which decorrelates over time. This decorrelation, as argued for the P-type afferents in Fig. 6.6, may play an important role in population encoding. For the frozen-noise stimulus, however, the spikes occur with high trial-to-trial correlation. This behavior is also predicted by the noisy source-coding model. The sudden changes and variation in the input signal drive spiking at specific times with very high probability. This results in spike trains which are very similar trial-to-trial. This is further shown by Fig. 6.8C, which shows the normalized, smoothed, PSTHs corresponding to the raster plots. In the DC case, the PSTH is peaked immediately following stimulation, then falls with time. The PSTHs for the noise stimulus, however, do not show this same progression in time. Figure 6.8D shows that the spike-time variance, over the 13 trials, increases with the spike number for the DC stimulus. Interestingly, the variance of the experimental data continues to grow more quickly than for the source-coding neuron. In the case of the noise stimulus, the variance does not grow with time. Instead, there are peaks in the variance, corresponding to missing spikes. The neural source coder with noisy threshold can predict both the repeatability of the spike-times in response to frozen-noise stimulation and the decorrelation of spikes over time in response to the DC stimulation.

6.3 Discussion

The neural source coder with stochastic threshold is capable of reproducing a range of observations observed in experimentally recorded spike-trains. By introducing stochastic spiking, small populations of neurons could be averaged together to reduce encoding error. In the original derivation of the neural source-coding model [84], however, the spike-firing rule is deterministic. Given a deterministic stimulus, the model predicts the deterministic spike-times which minimize reconstruction error. In the source-coding neuron, adding threshold noise to a single-neuron model does not improve encoding fidelity or the ability to predict spike times. This result is in contrast to some previous studies which show stochastic resonance effects in single-neuron models [105]. Different nonlinear systems will respond differently to noise, and these previous studies did not investigate an optimal strategy for timing spikes using the neural source coder.

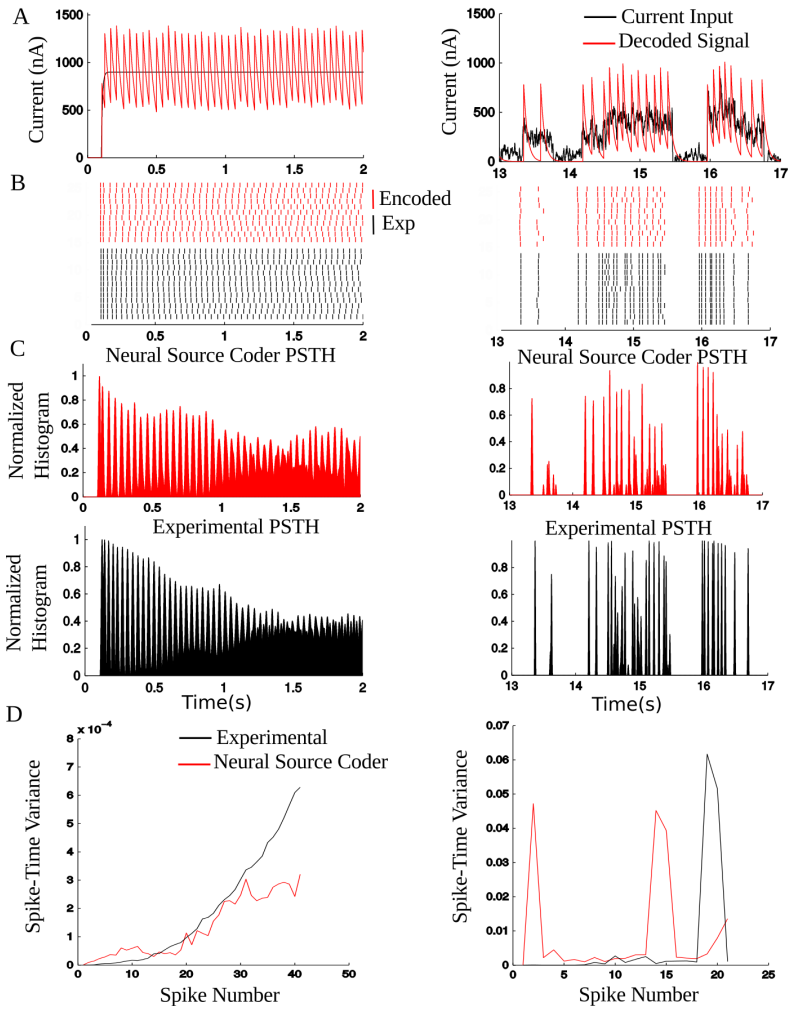

Figure 6.8: *In vitro* responses of a cortical pyramidal neuron, and matched neural source coder. Panel A displays the stimulus current (black) and reconstructed waveform (red) are shown for a DC stimulus (left) and frozen-noise stimulus (right). Panel B shows the raster plots of the experimental and neural source coder spike-trains. The DC stimulus (left) shows increased variability in spike times as the stimulus progresses, resulting in high trial-to-trial variability. The experimental data and neural source coder have spike trains with less variability for the frozen-noise stimulus (right). Panel C plots the smoothed, normalized PSTHs for the DC stimulus and frozen noise stimulus. For the DC stimulus, the trial-to-trial spike-trains progressively decorrelate. For the frozen noise, the times remain relatively precise. Panel D plots the variance of the spike times as a function of the spike number (from the start of the stimulus). For the DC stimulus, there is a growth in variance with spike number. The frozen-noise stimulus shows low variance for most spikes, with a few peaks. These peaks are largely due to missing spikes.

Although noisy thresholds only increase encoding error in single neural source coders, populations of neural source coders with noisy thresholds show reduced encoding error. This is a stochastic facilitation effect. In the proposed population reconstruction, the reconstructed waveforms are simply averaged together. This approach implicitly models a downstream neuron in the electrosensory lateral line lobe, which is innervated by a number of P-type afferents. By weighting and summing the input signals, the model roughly approximates reconstruction of input stimuli by these neurons. Although this is a reasonable first approximation, this does not capture all known aspects of synaptic processing [18] and filtering. The population reconstruction approach also assumes that all neurons are identical and encode the same baseline stimulus. Although nearby electroreceptors are stimulated with highly correlated signals under natural conditions [116], the signal stimulating each electroreceptor is not perfectly correlated. Further work will be required to study encoding of correlated input signals by a population with variable encoding parameters.

Previous studies [106, 108] have investigated stochastic resonance and dithering effects in populations of spiking neuron models, also showing improved performance metrics for noisy populations. Unlike previous studies, which used models such as the FitzHugh-Nagumo model, this study investigated the effect of threshold noise on the optimal spike-times generated by the neural source coder. The model closely predicts the statistics of experimental spike-trains, and simulations suggest that these statistics may play a key role in minimum-error population encoding.

Anti-correlations in spike trains have been observed in a wide range of sensory systems and animals [91, 90]. Anti-correlations have been suggested to increase information transfer [27] or improve detection of weak signals [93]. The neural source coder with stochastic threshold can be used to model these spike-train statistics, and the encoding model suggests that these statistics are important for minimum-error population coding. Spiking neuron models with adaptive thresholds have also been used to model the strong anti-correlations seen in experimental spike trains [28, 14, 117]. These models are mathematically similar to the neural source coder, but do not time spikes for minimum-error reconstruction. Although this work studies the encoding error of spike trains with these statistics, previous work has shown that strong anti-correlations leads to optimal detection of weak signals [91, 93].

The problem of sensory coding can be viewed from either the detection perspective or from the perspective of estimation (reconstruction) of the sensory signal. Further theoretical work will be required to study the optimal noise distributions for the neural source coder from a detection [118] and estimation [119] perspective.

Even though spike trains are often modeled as Poisson point processes, high spike-time reliability has been observed in many neurons, both cortical and peripheral [110, 120]. A neural source coder with noisy threshold predicts both the decorrelation of spike times in response to step stimuli and the reliable spike times in response to fluctuating stimuli. This raises some interesting questions about the role of precise spike-times in neural coding. Even though the step stimulus has decreasingly correlated spike-times, it may be encoded with low error by a population of neurons with decorrelated spike-trains. The lack of reliability does not necessarily mean the population-encoding error is poor. It is still unclear, however, how the intuition of population encoding in sensory afferents can be translated to cortical neurons.

For the neural source coder, the threshold noise was modeled as a low-pass or band-pass Gaussian random process. This additive threshold noise can be viewed as a model of internal noise, due to the random fluctuations within the neuron. A major noise source is the random opening and closing of the ion channels which determine the membrane potential [121, 122]. Due to the thousands of individual channels, the law of large numbers suggests that the aggregate effect on the membrane potential will be approximately Gaussian. The bandwidth of the noise process would be related to the rate at which channels open and close. There may still be further noise sources to consider. Modeling spike-train statistics with first serial correlation coefficients less than -0.5 required the introduction of a band-pass component. Biophysical mechanisms to generate band-pass noise will require further investigation, but this effect could also be due to a band-pass component in the input signal. Prior work has also demonstrated this behavior in resonate-and-fire neurons [117]. Further experimental evidence will be required to understand the true sources of noise in sensory encoding by populations, which may involve many ionic currents [123]. A final source of noise not studied here is quantal synaptic release, where a post-synaptic potential of random height is generated in response to a single spike [18]. Quantal synaptic failure has been

suggested as a mechanism to improve neural coding [124]. Further modeling work should incorporate this effect.

A model of optimal neural source coding which predicts deterministic spike times can be extended to generate jittered spike trains using a stochastic threshold. The parameters of the neural encoding model and noise process can be tuned to generate spike trains which match the range of spike-interval statistics observed in the spike trains of P-type sensory afferents of a weakly electric fish. The statistics are non-Poisson and non-renewal, showing strong correlations between intervals. Introducing stochastic spike-firing does not improve the encoding error of a single simulated neural source coder. However, simulated populations of these neural models show reduced encoding error for nonzero noise power, which is a clear noise-enhancement effect. A simple averaging of the population reconstructions improved encoding error. The neural source coder with stochastic threshold also models observations of spike-time reliability in response to constant and rapidly fluctuating stimuli. Further experiments involving population recordings in sensory systems will be required to further study the role of spike-time variability in optimal sensory encoding.

CHAPTER 7

POTENTIAL APPLICATION OF MINIMUM-ERROR ENCODING TO COCHLEAR IMPLANTS

The previous chapters of this thesis have proposed a model of optimal, energy-constrained neural encoding, compared the predictions to electrophysiological recordings, and proposed extensions to the original model. This approach has proven to accurately capture many aspects of sensory coding seen in experimentally recorded neurons. The precisely timed spikes predicted by this approach allow for minimum-error decoding of sensory stimuli. An interesting question is whether or not an improved understanding of sensory neural encoding can be applied to improve engineered systems, such as cochlear implants, which interact with sensory neurons. This chapter proposes a potential strategy for cochlear-implant sound-coding using the neural source coder and presents initial validation of this model using a vocoding experiment with normal-hearing subjects.

Here, the hypothesis is that the neural source coder can be used to time electrical pulses in cochlear implants to improve sound-coding. Little prior work has applied spiking neuron models to the problem of sound-coding for cochlear implants, but this emerging model may prove to be a good candidate. The proposed approach would be a new way to do sound-coding in cochlear implants. Precisely controlling the pulse-times following an optimal neural encoding strategy may be critical to improving speech and pitch perception for cochlear implants.

Cochlear implants are Brain Machine Interfaces (BMIs) which partially restore hearing for profoundly deaf or severely hard-of-hearing individuals [125, 126]. These implants are by far the most ubiquitous invasive BMI, with hundreds of thousands of devices implanted worldwide. Cochlear implant users, however, still suffer from poor perception, particularly for pitch and music [127, 128]. These devices are limited by physical constraints such as the number of possible electrodes [125], but also by sound-coding mechanisms which do not accurately transform sound signals into electrical pulses

to stimulate the auditory nerve [129]. The physical realities of battery life and processing power also limit performance [125]. Although there has been considerable success in restoring speech perception, there are still shortcomings in cochlear implants. For example, the perception of pitch and music is poor, and cochlear implant patients perform worse than hearing aid users at melody and pitch perception tests [127].

Much prior work on binaural cochlear-implants has focused on studying and overcoming the physical limitations of cochlear-implant devices. The number of electrodes and electrode configuration have been studied extensively in cochlear-implant patients [130] and in vocoding simulations [131, 132]. Another critical parameter is the electrode insertion depth [133], which can affect the area stimulated by each channel. The spatial spread of current is also a major area of study, as it is linked to frequency resolution in the cochlear implant [134]. The exact configuration of electrodes and the configuration during stimulation can have a direct affect on speech threshold levels [135]. However, it is critical to note that once a device is implanted in the subject, it is no longer possible to increase the number of channels, alter insertion depth, or change the electrode orientation. Due to the physical limitations of already implanted devices, it is important that sound-coding schemes be optimized for the best possible performance given existing devices.

Cochlear implants stimulate the auditory nerve by coding sound signals as electrical pulses. Each channel of the cochlear implant corresponds to a frequency band which is closely related to the tonotopic mapping of nearby auditory fibers. Typically, the sound is first passed through a filter bank, generating a band-pass filtered waveform for each channel. These filters can be designed with varying overlaps [136] and design methods [137], although a common model is simply a bank of IIR filters with a constant Q factor (center frequency to bandwidth ratio). Many current sound-coding approaches, such as Continuous-Interleaved-Sampling (CIS), use the amplitude of the signal envelope in each channel to modulate the pulse height [125]. ACE, another common coding strategy [129], builds off CIS by adding a channel selection block to preserve frequency features. A more recent strategy, Envelope Enhancement (EE), has been developed to enhance the encoded pulses at critical times, such as the onset of a stimulus [129]. To improve pitch perception, strategies have been developed to specifically modulate the

pulses with the detected pitch [128]. The sound-coding strategy then produces pulses with varying amplitudes and interpulse intervals. Interestingly, most of these models are ad-hoc and not directly based off the current understanding of encoding of signals by the inner hair cells and auditory nerve neurons.

Very rarely have spiking neuron models been applied to cochlear implant encoding, and in practice most coding strategies are similar to CIS. Modeling the inner hair cells, Meyer-Baese et al. [138] proposed two FPGA-based models to capture impulse generation by the hair cells and the adaptation in the spike rate using a two time-constant model. Further work by Grayden et al. [139], proposed sound-coding based on models of the auditory system, implementing a zero-crossing detector to generate spikes. Although interesting approaches, these works have not yet supplanted standard cochlear processing approaches such as CIS. The assumptions of these previous attempts, however, do not guarantee a close match to spike times observed in sensory afferents. The neural source coding approach provides a possible way to time pulses such that the spike times of sensory afferents are closely modeled. In particular, many existing sound-coding approaches do not fully exploit the timing of pulses, which could play a key role in phase locking for binaural processing and pitch processing [140].

For many cochlear-implant patients, it is not realistic to modify the implant to improve performance, and current sound-coding strategies often do not provide adequate performance for noisy speech and music perception. This chapter proposes an extension of the neural source coder which can be used to time pulses for cochlear implants, using pulses of a constant amplitude. This is in contrast to many common strategies such as CIS, which rely on amplitude modulation. It is possible that timing pulses using a modified neural source-coding strategy will result in spike times in the sensory afferents which mimic experimentally observed spike-times. If successful, this approach could result not only in improved perceptual performance, but also a new outlook on stimulus encoding for a wide variety of BMIs. Although tests with cochlear-implant patients have not yet been conducted, initial vocoding experiments with normal-hearing subjects suggest further work is well warranted.

7.1 Sound-Coding Strategy Using Neural Source Coders

This section proposes a stimulation strategy for cochlear implants based on the neural source coder. The goal is to time pulses from the implant such that the spikes generated in the auditory neurons will follow the encoding principles observed in the previous chapters. Here, the asymptotic form of the neural source coder introduced in Chapter 3 is used to generate desired spike times. Adapting the neural source coder to create a stimulation strategy, however, first requires an understanding of the responses of auditory-nerve neurons to electrical stimulation.

In healthy ears, the inner hair cells of the auditory system transduce mechanical vibrations of the cochlear into release of neurotransmitter to stimulate auditory neurons. Different spatial segments of the cochlear respond to different stimulation frequencies, resulting in a form of frequency analysis. This transduction process is complicated, and is often modeled in cochlear implants with several signal-processing blocks. There is often an automatic gain control block to account for the dynamic range of the signal, a pre-emphasis filter, and a filter bank with frequency bands corresponding to the spatial positions of the electrodes along the cochlear.

Although the auditory transduction process is complicated, the effects of direct electrical stimulation of individual sensory neurons have been studied in mammals. Experiments in cats show that the spiking probabilities of auditory neurons in response to biphasic electrical pulses is quite high [141]. A strong, biphasic pulse shows a high probability of generating a single spike with a relatively fixed delay. Smaller pulses generate spikes with lower probability. Due to the spatial spread of the current, many nearby afferents are likely affected. In the presence of a damaged cochlear, these spikes are particularly predictable [142, 143]. Repeated pulses can generate repeated spikes, with refractory periods of less than one millisecond [144]. There is also strong phase locking to direct sinusoid electric stimulation of auditory nerves [145]. Given these experiments, it is quite likely that human auditory neurons, in humans with damaged cochlears, also spike once with high probability in response to a large biphasic pulse. Therefore, the pulse times predicted by the neural source coder can be translated into electrical stimulation pulses of relatively large amplitude. This will result in a spiking pattern for nearby

auditory afferents which will follow, with high probability, the desired spiking pattern. Neurons which are further separated from the electrode will also be stimulated, but with a lower probability of spiking, introducing a potential complication. This sound-coding strategy is fundamentally different from common CIS strategies which pulse at fixed intervals and instead vary the amplitude to vary the probability of spiking. This is much like a rate-coding strategy, which is often a poor model of sensory neural coding, as argued in Chapters 4 and 5.

The proposed neural coding strategy is shown in Fig. 7.1. The fundamental idea is that after the standard auditory filterbank, a neural source coder can be used on each channel to generate pulse times with properties similar to the spike times of sensory afferents. A current source then generates a biphasic pulse, with fixed amplitude, to drive spikes on the auditory nerve with high probability. The experimental work in the cat auditory nerve [141, 142] suggests such a strategy will generate spike times on the auditory nerve following the predictions of the neural source coder.

In Fig. 7.1, the first two stages of processing are shared with standard cochlear implants. The first stage of processing is a pre-processing block, representing the standard pre-processing steps for cochlear implants. The most important of these steps is automatic gain control, which is necessary due to the limited dynamic range of neural responses to electrical stimuli [125]. After this, the signal is passed through a filterbank corresponding approximately to the frequency ranges stimulated by each electrode channel. The number of channels and the precise frequency mapping vary from patient to patient, and can be considered fixed for the purposes of introducing a neural source coder for cochlear implant sound-coding.

After analysis using the filterbank, a neural source coder is used to encode each channel independently. The output of the filterbank is used as the input signal $s(t)$, and it is assumed that the reconstruction $r(t)$ tracks the envelope of the signal. The asymptotic form of $\gamma = A/2$ is used. To determine the parameters A_i and τ_i for each channel, it is assumed some training data are available. The parameters are then selected as

$$\{A_i^*, \tau_i^*\} = \text{argmin}_{A,\tau} \frac{1}{T} \int_0^T (\hat{s_i(t)} - r_i(t))^2 dt \tag{7.1}$$

$$\text{subject to } N_{\text{spikes}}/T < R_i \tag{7.2}$$

where $\hat{s_i}(t)$ is the envelope of the output of each channel of the filter bank, and R_i is the maximum average rate allowed for each channel in spikes per second. One approach to choosing the values of R_i is to assume an overall average number of spikes per sensory neuron expected in response to stimulation at reasonable levels. In auditory sensory neurons, this would be approximately 150-200 spikes per second. This level is multiplied by the total number of channels to get an overall rate R. Spikes are then assigned to each channel as

$$R_i = \frac{||s_i(t)||_2^2}{||s(t)||_2^2} R \tag{7.3}$$

This procedure, assuming small overlap between filters, assigns the overall spikes to each channel proportionally to the power of that channel in the training data. This strategy prevents a large number of pulses being assigned to channels where the overall signal is small and dominated by noise.

A final consideration is that the pulses must be scheduled for output to the implant. Implants cannot drive pulses faster than a maximum rate, and cannot typically drive pulses on multiple channels simultaneously. Moreover, rapid stimulation of adjacent channels typically results in unexpected behavior due to the spatial spread of current. Therefore, it is necessary to introduce a refractory period Δ which restricts simultaneous pulses on multiple channels. A simple strategy to accomplish this is to allow the channel with the largest error to fire a spike, then lock out all firing for a period of Δ seconds. Thus, channel i will fire a pulse at time t if the following conditions are met:

1. $e_i(t) \geq A_i/2$
2. $t - \max_{i,j} t_{i,j} > \Delta$, where $t_{i,j}$ is the time of the jth pulse on the ith channel
3. $e_i(t) \geq e_j(t)$, where j ranges from 1 to the number of channels

Simulations of this strategy, shown in Fig. 7.2, show significant difference between the proposed method and standard CIS strategies. In this example, a segment of music was processed using a 20-channel filter bank of second-order Butterworth filters. The filters covered frequencies from 188 to 7938 Hz. The envelope was estimated using half-wave rectification and filtering with

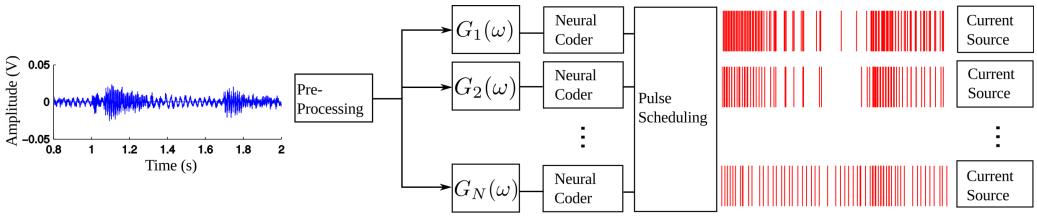

Figure 7.1: The signal processing chain for the proposed method of using neural source coders for sound-coding with cochlear implants. The figure flows from the left to the right. The raw audio signal is first passed through the standard pre-processing steps. This signal is then processed by the filterbank to create band-pass signals. These first two stages are identical to standard cochlear implant strategies, and the number of filters and filter frequency bands are already determined for each patient. After the filterbank, this thesis proposes using a neural source coder on each channel to generate pulse times. A pulse-scheduling algorithm assures that pulses do not occur too rapidly, which is determined by the hardware limitations of each implant. The pulse times are then used as the input to a current source which generates biphasic pulses. These pulses will drive individual spikes in the sensory afferents with high probability, in principle resulting in spike trains which follow the predictions of the neural source coder.

a low-pass filter with a 160 Hz cutoff frequency. Assuming an average rate of 150 spikes per second, rates were allocated to each channel as described above. For the channel shown in Fig. 7.2, the rate was 175 spikes per second. The parameter A was 0.0023 V and the time constant was 16 milliseconds. A CIS strategy was simulated, also using 175 spikes per second. For the CIS strategy, the amplitude of each pulse is equal to the value of the envelope at that time instant. Both pulse trains were reconstructed using the filter $h(t)$ of the neural source coder, although the filter was rescaled for the CIS pulses. Figure 7.2B and C highlight the differences in pulses generated by the two methods. The pulse train generated by the neural source coder shows spike-rate adaptation to positive changes in the signal, and a low pulse rate when the signal is small. When reconstructed, Fig. 7.2D shows that the neural source coder follows the envelope much more precisely than the CIS strategy, despite the CIS strategy encoding the exact envelope level. The slight error between the neural source coder reconstruction and the envelope is due to the fact that neural source coder input signal is the output of the filterbank, not the envelope itself. The CIS reconstruction does not rise rapidly enough in response to changes in the signal. The reconstruction error

for the CIS strategy is -5.3 dBV compared to -7.5 dBV for the neural source coder.

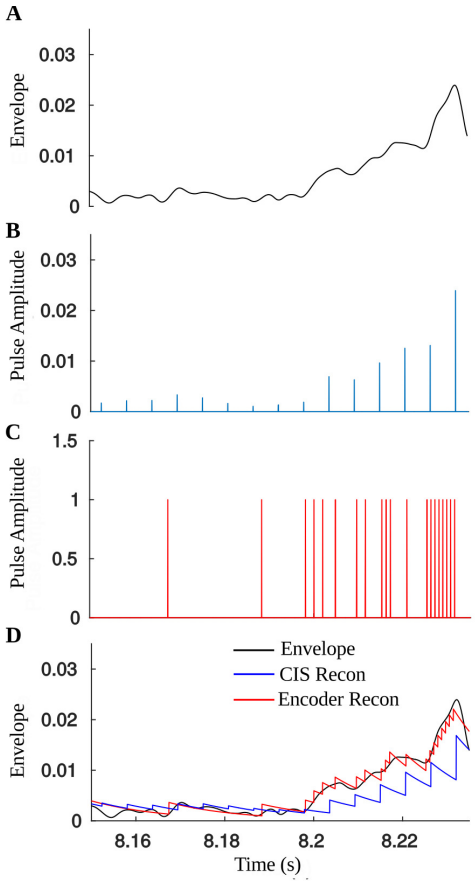

Figure 7.2: Simulated encoding of one cochlear-implant channel using a CIS strategy and a neural source-coding strategy. Panel A shows the signal envelope for one channel of the filterbank. The envelope is estimated using half-wave rectification and a low-pass filter. Panel B shows a CIS encoding of this envelope, using a pulse rate of 175 pulses per second (the same as the neural source coder). Pulses are equally spaced with amplitude equal to the signal envelope. Panel C shows the pulse times generated by the neural source coder. In this case, the amplitudes of all the pulses are the same, and the information is encoded in time. This strategy shows aspects of sensory neural coding, such as the increase in spike rate when the envelope rapidly increases. Panel D shows the original envelope, along with the reconstructions of the neural source encoder and CIS strategies. The CIS strategy lags when the envelope suddenly changes, and does not follow the envelope as closely. This results in an encoding error of -5.3 dBV compared to -7.5 dBV for the neural source coder.

7.2 Hearing-in-Noise Test Using a Vocoding Simulation

Although this sound-coding strategy must obviously be tested on existing cochlear-implant speech processors, a reasonable first step to assessing this approach is to reconstruct the sound waveform and present the vocoded example to normal-hearing listeners. Due to the difficulty of testing algorithmic developments on large populations of cochlear-implant patients, vocoding experiments involving normal-hearing subjects are often used as a preliminary assessment of processing strategies for cochlear implants. Previously, vocoding experiments have found noise and sine-wave vocoding result in similar hearing thresholds [146]. Further work has investigated the number of channels required for accurate speech recognition [131, 132]. Other vocoding strategies have been used to investigate electrode insertion depth [133] and filter bank design [137].

Here, the Hearing In Noise Test (HINT) [147] is used to assess the difference in hearing thresholds for the neural source vocoder and a standard noise vocoder. To reconstruct the spike trains generated by the system in Fig. 7.1, the pulses are first filtered by the neural source-coding filter $h(t)$. This generates, in the limit of high spike-rates, an optimal estimate of the envelope of the signal. Secondly, the pulses are filtered by the frequency response of the filterbank for that channel, $g_i(t)$, scaled to create a unity-gain filter. This creates an estimate of the carrier frequency for each channel. The theoretical analysis of the optimal source coder does not provide any guarantees on this reconstruction, but it appears to work well in practice. The carrier is then modulated by the envelope to estimate the signal for that channel. The signal in each channel is summed together and played to the listener. The reconstruction process for a signal channel is shown in Fig. 7.3.

The noise vocoder is related to CIS and other strategies which stimulate proportionally to the signal envelope. The same pre-processing and filter bank is used for the noise vocoder as for the neural source vocoder. The signal in each band is then half-wave rectified and low-pass filtered with a cutoff of 160 Hz to estimate the signal envelope. The envelope is then used to modulate colored noise, which is generated by passing independent, Gaussian, white noise through the band-pass filter for each channel, normalized to unity gain. The modulated signals are then summed together and played to the listener. This strategy preserves the envelope in each frequency band.

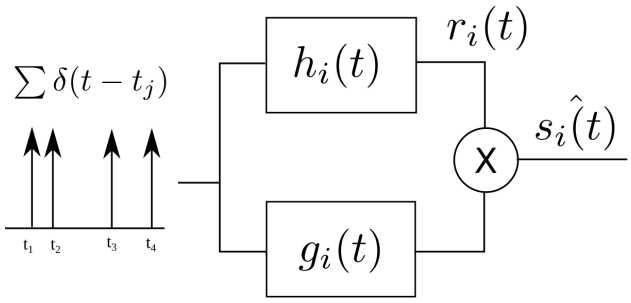

Figure 7.3: The reconstruction process for each channel in the proposed neural source vocoder. The pulse train generated for each channel using the system shown in Fig. 7.1 is passed through two different filters. The first is the low-pass filter $h(t)$ used by the neural source coder. This reconstruction provides an estimate of the signal envelope, as predicted by the neural source coder. The second filter is the band-pass filter $g_i(t)$ for the channel, which is corresponds to the filter in Fig. 7.1 normalized to unity gain. This provides an estimate of the carrier frequency of the signal. These two signals are multiplied together to estimate the signal for this channel.

For the spike encoder, the spike rate varied from 73 to 228 spikes per second, with an average of 153 spikes per second. The value of A ranged form 0.0019 to 0.0025 and τ ranged from 20 to 30 milliseconds. A refractory period of 1 millisecond was used. The parameters A and τ were chosen for each channel using the procedure described above with one of the practice sentences used as training data.

The HINT was administered to nine subjects in the laboratory of Justin Aronoff (University of Illinois IRB, #14035). The subjects were all college undergraduates with pure-tone thresholds in a normal range, as tested with a standard audiogram. All subjects except Subject 6 spoke English as a native language. Subject 6 was removed from the study for this reason. Subjects were first allowed to practice the HINT using the signal without vocoding. One of the two vocoders was then selected at random, and three sentence lists were presented to the listener. The listener was then presented with three sentence lists using the other vocoder.

For all listeners, eight channels were used. No preprocessing steps were used in this experiment. The filter banks were implemented as fourth-order Butterworth filters. The frequencies covered by the filter bank ranged from 200 Hz to 7000 Hz. Each sentence list consisted of 20 sentences. A threshold of 50% of words identified correctly was used to determine whether to increase or decrease the signal power. Speech-shaped noise was presented at a fixed

Table 7.1: Results of HINT with Normal-Hearing Subjects (dB SNR)

	Noise Vocoder	Neural Source Vocoder	Difference
Subject 1	3.29	-0.23	3.53
Subject 2	2.82	1.65	1.18
Subject 3	4.83	1.41	3.41
Subject 4	1.53	0.59	0.94
Subject 5	4.59	0.71	3.88
Subject 7	2.94	1.53	1.41
Subject 8	1.29	0.82	0.47
Subject 9	2.24	-0.47	2.71

level of 60 dB, and the signal level adjusted. Using the first sentence, the signal power was increased by 4 dB until the listener could recognize 50% of the words. For the remaining 19 sentences, the SNR was adjusted by 2 dB.

The results of this first experiment are summarized in Table 7.1. The data from eight subjects are shown. The mean threshold for the noise vocoder was 2.90 dB SNR. The mean threshold for the neural source vocoder was 0.80 dB SNR, a difference of 2.10 dB. For every subject, the neural source coder had a lower threshold. The difference between the two encoders was found to be significant using a one-sample t-test of the difference ($p = 0.0012$). Although this result does not necessarily imply improvement in cochlear implants, it does suggest that the neural source coder is preserving important aspects of the signal. It also outperforms the noise vocoder, which relies solely on the envelope of the signal.

7.3 Future Directions

The next step is to implement this strategy for testing with cochlear-implant patients. This will require the ability to precisely control the pulse times of the implant. Although the initial vocoder results are promising, it is absolutely critical to investigate this strategy for actual cochlear-implant users.

Further experiments will also be needed to assess the neural source coder for binaural processing and pitch perception. The precise timing of the neural source coder may preserve interaural time differences which are not used by

strategies which rely solely on the envelope. Envelope-based strategies are likely relying primarily on interaural level differences. Since the neural source coder input signal is the output of each filter, spikes will tend to be generated at the peaks of the signal. The phase locking predicted by the neural source coder may also play a role in pitch and music perception.

Beyond cochlear implants, the neural source coder may have implications for a large number of BMI systems. Few BMIs currently consider direct neural feedback, and the user receives only ad hoc visual or haptic feedback. A principled approach to optimally encoding stimuli for BMI systems which directly stimulate sensory neurons could alter the design of devices such as prosthetic arms. Feedback in these systems is usually visual, audio, or tactile. Sometimes, cortical feedback is provided by implanted electrodes, known as intracortical micro stimulation [148, 149]. In these cases, feedback tends to use a rate code of electrical pulses, where the pulse rate is proportional to the stimulus intensity. It is possible that the neural source coder could be applied to generate spike trains which follow the principles of sensory neural encoding.

CHAPTER 8

CONCLUSIONS AND FUTURE DIRECTIONS

This work has argued that sensory neurons follow an encoding principle which simultaneously attempts to minimize encoding error while limiting the expended energy. Over millions of years of evolution, selective pressure has likely favored the development of neural codes which represent sensory signals with maximum fidelity. Yet at the same time, neural activity is metabolically expensive, which provides selective pressure to minimize neural activity. Since neurons communicate with each other by firing action potentials, this suggests the spikes must be timed to minimize error while simultaneously limiting the rate at which they are fired.

The trade-off between minimum error encoding and energy consumption can be modeled as a constrained optimization problem. This problem involves minimizing the average, squared encoding error subject to a constraint on the average spike-rate. For a first-order reconstruction filter in the limit of high spike-rates, a solution to the constrained optimization problem is found by tracking the encoding error and firing spikes when a threshold level is reached. This approach suggests that neurons must track the reconstructed signal internally to compute the reconstruction error, possibly using an adaptive threshold mechanism. In the limit of high spike-rates, this neural source coder is capable of optimizing the trade-off between error consumption and encoding error.

Comparing the predictions of the neural source coder to experimental data, several key features of experimental spike-trains were replicated which were not explicitly modeled in the optimization problem. The neural source coder was able to predict spike times with millisecond precision in both a peripheral sensory neuron and a cortical neuron. The accuracy of the predictions for the cortical neuron were particularly surprising, as the spike rate was quite low. Additionally, the neural source coder predicts the asymmetric spike-rate adaptation observed in experimental data.

Further analysis of the neural source coder yielded an alternative view of the encoder as an instantaneous-rate coder of a function which depends on the signal, signal derivative, and encoding parameters. This model shows rate coding properties when the signal is slowly varying and temporal coding properties due to spike-rate adaptation when the signal is rapidly varying. The addition of a noisy threshold results in spike times which closely match the interval statistics observed in experimental neurons. Overall, the neural source coder predicts many experimental phenomenon which are not explicitly modeled by the constrained optimization approach.

Introducing the noisy threshold also reduced encoding error in a simulated neural population, where reconstruction was performed by averaging across neurons. This noise enhancement suggests that while deterministic times may minimize encoding error in individual neurons, populations may benefit from jittered spiking. Further work will be necessary to examine minimum-error, energy-constrained encoding in populations. This will require more detailed modeling of the synapse and dendrites, to understand how signals from multiple neurons are integrated before being encoded as a spike train. It is also possible that populations with inter-neuron communication could outperform populations of neurons which do not have interconnections [58], and it will be important to investigate encoding error in both of these situations.

More experimental work is also necessary. This work suggests that there is a range of possible trade-offs between encoding error and energy consumption. This likely varies from sensory system to sensory system, and may also change with time. Experimental work in different sensory afferents may lead to a better understanding of this trade-off. Intracellular recordings may be needed to better understand how such a mechanism could be implemented biophysically. This might allow for experiments to better understand spike-threshold adaptation and the relationship to minimum-error, energy-constrained neural encoding.

APPENDIX A

ENERGY-CONSTRAINED, MINIMUM-ERROR ENCODING WITH L^P NORMS

What is the appropriate error metric when studying neural coding? In many prior studies, such as stimulus reconstruction studies [38], encoding error is studied using a squared-error criterion. A squared-error, or mean squared-error, criterion has been well studied and is mathematically tractable. However, it is unclear what criterion is actually optimized in the process of neural coding. This appendix shows that the results of Chapter 3 using the linearized model of the error can be extended to the class of L^p norms, for a real number $p \geq 1$. These norms are defined by

$$\|x(t)\|_p = \left(\int_0^T |x(t)|^p dt \right)^{1/p} \tag{A.1}$$

for a function $x(t)$ defined from 0 to T.

In terms of the L^P norms, Problem 3.1 can be written as

$$\min_{\gamma(s(t),t),A,\tau} \frac{1}{T}(\|s(t) - r(t)\|_p)^p \tag{A.2}$$
$$\text{subject to } R = \frac{E-b}{k}$$

Here, the norm is raised to the pth power, which is monotonically increasing and preserves the minimizing value. In the limit of high spike-rates, it is possible to take the approach of Chapter 3 and linearize the error. The same assumptions on the input signal $s(t)$ are required.

As the choice of norm does not affect the linearization of the input signal and reconstruction, Lemma 1 still holds. Then with small error for a high spike-rate, the error can be expressed as

$$\hat{e}(t) = (s'(0) + \frac{s(0) + A - \gamma}{\tau})t - (A - \gamma) \tag{A.3}$$

Assuming $s(t) >> A - \gamma$, the result of Lemma 2 still holds, and the time until the next spike is given with small error by

$$\hat{\Delta} = \frac{A}{s'(0) + s(0)/\tau} \tag{A.4}$$

The average error for the L^p norm criterion in Problem A.2 over the interval 0 to $\hat{\Delta}$ is then given by

$$\frac{1}{\hat{\Delta}} \int_0^{\hat{\Delta}} \left| \big(s'(0) + \frac{s(0)}{\tau}\big)t - (A - \gamma) \right|^p dt \tag{A.5}$$

The linear form of the error is always increasing over the interval from 0 to $\hat{\Delta}$, under the assumptions on the input signal stated in Chapter 3. Therefore, the error undergoes a sign transition at most once. The transition point, where $\hat{e}(t) = 0$, can be defined as $t = \delta$ with $0 \leq \delta \leq \hat{\Delta}$. The integral can then be written as

$$\begin{aligned} \frac{1}{\hat{\Delta}} \Bigg(\int_0^{\delta} (-\big(s'(0) + \frac{s(0)}{\tau}\big)t + (A - \gamma))^p dt + \\ \int_{\delta}^{\hat{\Delta}} \big(\big(s'(0) + \frac{s(0)}{\tau}\big)t - (A - \gamma)\big)^p dt \Bigg) \end{aligned} \tag{A.6}$$

Evaluating the integral gives

$$\begin{aligned} \frac{1}{\hat{\Delta}} \Bigg(- \frac{(-\big(s'(0) + \frac{s(0)}{\tau}\big)\delta + (A - \gamma))^{p+1}}{(s'(0) + \frac{s(0)}{\tau})(p+1)} + \frac{(A - \gamma)^{p+1}}{(s'(0) + \frac{s(0)}{\tau})(p+1)} + \\ \frac{\big(\big(s'(0) + \frac{s(0)}{\tau}\big)\hat{\Delta} - (A - \gamma)\big)^{p+1}}{(s'(0) + \frac{s(0)}{\tau})(p+1)} - \frac{(\big(s'(0) + \frac{s(0)}{\tau}\big)\delta - (A - \gamma)\big)^{p+1}}{(s'(0) + \frac{s(0)}{\tau})(p+1)} \Bigg) \end{aligned} \tag{A.7}$$

Since at the transition point δ the linearized error is zero, this expression is reduced to

$$\frac{1}{\hat{\Delta}} \Bigg(\frac{(A - \gamma)^{p+1}}{(s'(0) + \frac{s(0)}{\tau})(p+1)} + \frac{\big(\big(s'(0) + \frac{s(0)}{\tau}\big)\hat{\Delta} - (A - \gamma)\big)^{p+1}}{(s'(0) + \frac{s(0)}{\tau})(p+1)} \Bigg) \tag{A.8}$$

Substituting the value of $\hat{\Delta}$, taking the derivative with respect to γ, and

setting the derivative to zero gives

$$(A-\gamma)^p = (\gamma)^p \tag{A.9}$$

which is satisfied by $\gamma^* = A/2$, regardless of p. The second derivative with respect to γ is given by

$$\frac{p(A-\gamma)^{p-1}}{A} + \frac{p\gamma^{p-1}}{A} \tag{A.10}$$

which is greater than 0 for all $0 < \gamma < A$. The point γ^* is therefore a unique minimum over the range of interest, for all values of $p \geq 1$. For the limiting case of $p \to \infty$, the L^∞ norm is the maximum of the absolute value of the error function over the interval. This is also minimized by $\gamma^* = A/2$, as any other value results in an absolute value of the error greater than $A/2$ either just before or just after the spike. The rate constraint is still satisfied by applying the results of Theorem 2. When analyzing the linearized model in the limit of high spike-rates, the results of Chapter 3 hold for the class of L^P norms.

REFERENCES

[1] D. Purves, G. Augustine, D. Fitzpatrick, W. Hall, A. LaMantia, J. McNamara, and L. White, *Neuroscience*. Sunderland, MA: Sinauer Associates, 2008.

[2] F. Rieke, D. Warland, R. de Ruyter van Steveninck, and W. Bialek, *Spikes*. Cambridge, MA: Massachusetts Institute of Technology, 1997.

[3] F. Gabbiani and C. Koch, "Principles of spike train analysis," *Methods in Neuronal Modeling*, pp. 313–360, 1998.

[4] F. Gabbiani and C. Koch, "Coding of time-varying signals in spike trains of integrate-and-fire neurons with random threshold," *Neural Computation*, vol. 8, no. 1, pp. 44–66, 1996.

[5] S. B. Laughlin, "Energy as a constraint on the coding and processing of sensory information," *Current Opinion in Neurobiology*, vol. 11, no. 4, pp. 475–480, 2001.

[6] J. E. Niven and S. B. Laughlin, "Energy limitation as a selective pressure on the evolution of sensory systems," *Journal of Experimental Biology*, vol. 211, no. 11, pp. 1792–1804, 2008.

[7] B. Hille, *Ion Channels of Excitable Membranes*. Sunderland, MA: Sinauer Associates, 2001.

[8] J. Eggermont, P. Johannesma, and A. Aertsen, "Reverse-correlation methods in auditory research," *Quarterly Reviews of Biophysics*, vol. 16, no. 03, pp. 341–414, 1983.

[9] A. L. Hodgkin and A. F. Huxley, "A quantitative description of membrane current and its application to conduction and excitation in nerve," *The Journal of Physiology*, vol. 117, no. 4, pp. 500–544, 1952.

[10] D. Attwell and S. B. Laughlin, "An energy budget for signaling in the grey matter of the brain," *Journal of Cerebral Blood Flow & Metabolism*, vol. 21, no. 10, pp. 1133–1145, 2001.

[11] B. Sengupta, M. Stemmler, S. B. Laughlin, and J. E. Niven, "Action potential energy efficiency varies among neuron types in vertebrates and invertebrates," *PLoS Computational Biology*, vol. 6, no. 7, p. e1000840, 2010.

[12] W. B. Levy and R. A. Baxter, "Energy efficient neural codes," *Neural Computation*, vol. 8, no. 3, pp. 531–543, 1996.

[13] R. Kobayashi, Y. Tsubo, and S. Shinomoto, "Made-to-order spiking neuron model equipped with a multi-timescale adaptive threshold," *Frontiers in Computational Neuroscience*, vol. 3, 2009.

[14] R. Brandman and M. E. Nelson, "A simple model of long-term spike train regularization," *Neural Computation*, vol. 14, no. 7, pp. 1575–1597, 2002.

[15] S. S. Goldstein and W. Rall, "Changes of action potential shape and velocity for changing core conductor geometry," *Biophysical Journal*, vol. 14, no. 10, p. 731, 1974.

[16] T. Sasaki, N. Matsuki, and Y. Ikegaya, "Action-potential modulation during axonal conduction," *Science*, vol. 331, no. 6017, pp. 599–601, 2011.

[17] M. S. Lewicki, "A review of methods for spike sorting: The detection and classification of neural action potentials," *Network: Computation in Neural Systems*, vol. 9, no. 4, pp. R53–R78, 1998.

[18] L. Abbott and W. G. Regehr, "Synaptic computation," *Nature*, vol. 431, no. 7010, pp. 796–803, 2004.

[19] N. Brunel and M. C. Van Rossum, "Lapicques 1907 paper: From frogs to integrate-and-fire," *Biological Cybernetics*, vol. 97, no. 5-6, pp. 337–339, 2007.

[20] J. Benda and A. V. Herz, "A universal model for spike-frequency adaptation," *Neural Computation*, vol. 15, no. 11, pp. 2523–2564, 2003.

[21] R. B. Stein, "Some models of neuronal variability," *Biophysical Journal*, vol. 7, no. 1, p. 37, 1967.

[22] J. Benda, A. Longtin, and L. Maler, "Spike-frequency adaptation separates transient communication signals from background oscillations," *The Journal of Neuroscience*, vol. 25, no. 9, pp. 2312–2321, 2005.

[23] E. M. Izhikevich, "Which model to use for cortical spiking neurons?" *IEEE Transactions on Neural Networks*, vol. 15, no. 5, pp. 1063–1070, 2004.

[24] B. Katz, "Depolarization of sensory terminals and the initiation of impulses in the muscle spindle," *The Journal of Physiology*, vol. 111, no. 3-4, pp. 261–282, 1950.

[25] S. Hagiwara, "Analysis of interval fluctuation of the sensory nerve impulse." *The Japanese Journal of Physiology*, vol. 4, no. 3, pp. 234–240, 1954.

[26] A. Buller, J. Nicholls, and G. Ström, "Spontaneous fluctuations of excitability in the muscle spindle of the frog," *The Journal of Physiology*, vol. 122, no. 2, pp. 409–418, 1953.

[27] M. J. Chacron, A. Longtin, and L. Maler, "Negative interspike interval correlations increase the neuronal capacity for encoding time-dependent stimuli," *The Journal of Neuroscience*, vol. 21, no. 14, pp. 5328–5343, 2001.

[28] M. J. Chacron, K. Pakdaman, and A. Longtin, "Interspike interval correlations, memory, adaptation, and refractoriness in a leaky integrate-and-fire model with threshold fatigue," *Neural Computation*, vol. 15, no. 2, pp. 253–278, 2003.

[29] D. Madison and R. Nicoll, "Control of the repetitive discharge of rat CA 1 pyramidal neurones in vitro." *The Journal of Physiology*, vol. 354, no. 1, pp. 319–331, 1984.

[30] D. Brown and P. Adams, "Muscarinic suppression of a novel voltage-sensitive K+ current in a vertebrate neurone," *Nature*, vol. 283, no. 5748, pp. 673–676, 1980.

[31] Y.-H. Liu and X.-J. Wang, "Spike-frequency adaptation of a generalized leaky integrate-and-fire model neuron," *Journal of Computational Neuroscience*, vol. 10, no. 1, pp. 25–45, 2001.

[32] J. Benda, L. Maler, and A. Longtin, "Linear versus nonlinear signal transmission in neuron models with adaptation currents or dynamic thresholds," *Journal of Neurophysiology*, vol. 104, no. 5, pp. 2806–2820, 2010.

[33] R. Brette and W. Gerstner, "Adaptive exponential integrate-and-fire model as an effective description of neuronal activity," *Journal of Neurophysiology*, vol. 94, no. 5, pp. 3637–3642, 2005.

[34] R. Jolivet, T. J. Lewis, and W. Gerstner, "Generalized integrate-and-fire models of neuronal activity approximate spike trains of a detailed model to a high degree of accuracy," *Journal of Neurophysiology*, vol. 92, no. 2, pp. 959–976, 2004.

[35] B. Fontaine, J. L. Peña, and R. Brette, "Spike-threshold adaptation predicted by membrane potential dynamics in vivo," *PLoS Computational Biology*, vol. 10, no. 4, p. e1003560, 2014.

[36] W. Gerstner and R. Naud, "How good are neuron models?" *Science*, vol. 326, no. LCN-ARTICLE-2009-014, pp. 379–380, 2009.

[37] J. J. Eggermont, "Is there a neural code?" *Neuroscience & Biobehavioral Reviews*, vol. 22, no. 2, pp. 355–370, 1998.

[38] W. Bialek, F. Rieke, R. de Ruyter van Steveninck, and D. Warland, "Reading a neural code," *Science*, vol. 252, no. 5014, pp. 1854–1857, 1991.

[39] A. A. Lazar, E. A. Pnevmatikakis, and Y. Zhou, "Encoding natural scenes with neural circuits with random thresholds," *Vision Research*, vol. 50, no. 22, pp. 2200–2212, 2010.

[40] A. A. Lazar, "Population encoding with Hodgkin–Huxley neurons," *IEEE Transactions on Information Theory*, vol. 56, no. 2, pp. 821–837, 2010.

[41] A. A. Lazar and E. A. Pnevmatikakis, "Video time encoding machines," *IEEE Transactions on Neural Networks*, vol. 22, no. 3, pp. 461–473, 2011.

[42] J. Shin, C. Koch, and R. J. Douglas, "Adaptive neural coding dependent on the time-varying statistics of the somatic input current," *Neural Computation*, vol. 11, no. 8, pp. 1893–1913, 1999.

[43] J. Shin, "Adaptation in spiking neurons based on the noise shaping neural coding hypothesis," *Neural Networks*, vol. 14, no. 6, pp. 907–919, 2001.

[44] J. Shin, "A unifying theory on the relationship between spike trains, EEG, and ERP based on the noise shaping/predictive neural coding hypothesis," *Biosystems*, vol. 67, no. 1, pp. 245–257, 2002.

[45] R. Schreier and G. C. Temes, *Understanding Delta-Sigma Data Converters*. Piscataway, NJ: IEEE Press, 2005.

[46] A. Hasenstaub, S. Otte, E. Callaway, and T. J. Sejnowski, "Metabolic cost as a unifying principle governing neuronal biophysics," *Proceedings of the National Academy of Sciences*, vol. 107, no. 27, pp. 12 329–12 334, 2010.

[47] P. Lennie, "The cost of cortical computation," *Current Biology*, vol. 13, no. 6, pp. 493–497, 2003.

[48] S. B. Laughlin, R. de Ruyter van Steveninck, and J. C. Anderson, "The metabolic cost of neural information," *Nature Neuroscience*, vol. 1, no. 1, pp. 36–41, 1998.

[49] B. Sengupta, S. B. Laughlin, and J. E. Niven, "Balanced excitatory and inhibitory synaptic currents promote efficient coding and metabolic efficiency," *PLoS Computational Biology*, vol. 9, no. 10, p. e1003263, 2013.

[50] H. B. Barlow, "Possible principles underlying the transformation of sensory messages," *Sensory Communication*, pp. 217–234, 1961.

[51] A. Borst and F. E. Theunissen, "Information theory and neural coding," *Nature Neuroscience*, vol. 2, no. 11, pp. 947–957, 1999.

[52] B. A. Olshausen and D. J. Field, "Sparse coding of sensory inputs," *Current Opinion in Neurobiology*, vol. 14, no. 4, pp. 481–487, 2004.

[53] M. S. Lewicki, "Efficient coding of natural sounds," *Nature Neuroscience*, vol. 5, no. 4, pp. 356–363, 2002.

[54] P. Crotty and W. B. Levy, "Energy-efficient interspike interval codes," *Neurocomputing*, vol. 65, pp. 371–378, 2005.

[55] T. Berger and W. B. Levy, "A mathematical theory of energy efficient neural computation and communication," *IEEE Transactions on Information Theory*, vol. 56, no. 2, pp. 852–874, 2010.

[56] J. Xing, T. Berger, and T. J. Sejnowski, "A Berger-Levy energy efficient neuron model with unequal synaptic weights," in *IEEE International Symposium on Information Theory Proceedings (ISIT), 2012*. IEEE, 2012, pp. 2964–2968.

[57] J. Xing and T. Berger, "Energy efficient neurons with generalized inverse Gaussian conditional and marginal hitting times," in *IEEE International Symposium on Information Theory Proceedings (ISIT), 2013*. IEEE, 2013, pp. 1824–1828.

[58] M. Boerlin, C. K. Machens, and S. Denève, "Predictive coding of dynamical variables in balanced spiking networks," *PLoS Computation Biology*, vol. 9, no. 11, p. e1003258, 2013.

[59] S. Deneve, "Bayesian spiking neurons I: Inference," *Neural Computation*, vol. 20, no. 1, pp. 91–117, 2008.

[60] T. M. Cover and J. A. Thomas, *Elements of Information Theory*. John Wiley & Sons, 2012.

[61] T. Berger and J. Gibson, "Lossy source coding," *IEEE Transactions on Information Theory*, vol. 44, no. 6, pp. 2693–2723, 1998.

[62] R. Baddeley, L. F. Abbott, M. C. Booth, F. Sengpiel, T. Freeman, E. A. Wakeman, and E. T. Rolls, "Responses of neurons in primary and inferior temporal visual cortices to natural scenes," *Proceedings of the Royal Society of London. Series B: Biological Sciences*, vol. 264, no. 1389, pp. 1775–1783, 1997.

[63] M. Nelson, Z. Xu, and J. Payne, "Characterization and modeling of p-type electrosensory afferent responses to amplitude modulations in a wave-type electric fish," *Journal of Comparative Physiology A*, vol. 181, no. 5, pp. 532–544, 1997.

[64] W. Kistler, W. Gerstner, and J. Hemmen, "Reduction of the Hodgkin-Huxley equations to a single-variable threshold model," *Neural Computation*, vol. 9, no. 5, pp. 1015–1045, 1997.

[65] D. Yager and C. Hopkins, "Directional characteristics of tuberous electroreceptors in the weakly electric fish, hypopomus (gymnotiformes)," *Journal of Comparative Physiology A*, vol. 173, no. 4, pp. 401–414, 1993.

[66] P. Delmas and D. A. Brown, "Pathways modulating neural KCNQ/M (Kv7) potassium channels," *Nature Reviews Neuroscience*, vol. 6, no. 11, pp. 850–862, 2005.

[67] Z. Pan, T. Kao, Z. Horvath, J. Lemos, J.-Y. Sul, S. D. Cranstoun, V. Bennett, S. S. Scherer, and E. C. Cooper, "A common ankyrin-G-based mechanism retains KCNQ and NaV channels at electrically active domains of the axon," *The Journal of Neuroscience*, vol. 26, no. 10, pp. 2599–2613, 2006.

[68] E. Balaguer-Ballester, N. R. Clark, M. Coath, K. Krumbholz, and S. L. Denham, "Understanding pitch perception as a hierarchical process with top-down modulation," *PLoS Computational Biology*, vol. 5, no. 3, p. e1000301, 2009.

[69] R. P. Rao and D. H. Ballard, "Predictive coding in the visual cortex: A functional interpretation of some extra-classical receptive-field effects," *Nature Neuroscience*, vol. 2, no. 1, pp. 79–87, 1999.

[70] T. S. Lee and D. Mumford, "Hierarchical Bayesian inference in the visual cortex," *JOSA A*, vol. 20, no. 7, pp. 1434–1448, 2003.

[71] J. Gautrais and S. Thorpe, "Rate coding versus temporal order coding: A theoretical approach," *Biosystems*, vol. 48, no. 1, pp. 57–65, 1998.

[72] R. Van Rullen and S. J. Thorpe, "Rate coding versus temporal order coding: What the retinal ganglion cells tell the visual cortex," *Neural Computation*, vol. 13, no. 6, pp. 1255–1283, 2001.

[73] E. D. Adrian, "The impulses produced by sensory nerve endings," *The Journal of Physiology*, vol. 61, no. 1, pp. 49–72, 1926.

[74] M. London, A. Roth, L. Beeren, M. Häusser, and P. E. Latham, "Sensitivity to perturbations *in vivo* implies high noise and suggests rate coding in cortex," *Nature*, vol. 466, no. 7302, pp. 123–127, 2010.

[75] D. M. MacKay and W. S. McCulloch, "The limiting information capacity of a neuronal link," *The Bulletin of Mathematical Biophysics*, vol. 14, no. 2, pp. 127–135, 1952.

[76] T. Gollisch and M. Meister, "Rapid neural coding in the retina with relative spike latencies," *Science*, vol. 319, no. 5866, pp. 1108–1111, 2008.

[77] C. Kayser, N. K. Logothetis, and S. Panzeri, "Millisecond encoding precision of auditory cortex neurons," *Proceedings of the National Academy of Sciences*, vol. 107, no. 39, pp. 16 976–16 981, 2010.

[78] Z. N. Aldworth, A. G. Dimitrov, G. I. Cummins, T. Gedeon, and J. P. Miller, "Temporal encoding in a nervous system," *PLoS Computational Biology*, vol. 7, no. 5, p. e1002041, 2011.

[79] S. P. Strong, R. Koberle, R. de Ruyter van Steveninck, and W. Bialek, "Entropy and information in neural spike trains," *Physical Review Letters*, vol. 80, no. 1, p. 197, 1998.

[80] S. A. Prescott and T. J. Sejnowski, "Spike-rate coding and spike-time coding are affected oppositely by different adaptation mechanisms," *The Journal of Neuroscience*, vol. 28, no. 50, pp. 13 649–13 661, 2008.

[81] P. Dayan and L. F. Abbott, *Theoretical Neuroscience*. Cambridge, MA: MIT Press, 2001, vol. 806.

[82] A. Nabatiyan, J. Poulet, G. De Polavieja, and B. Hedwig, "Temporal pattern recognition based on instantaneous spike rate coding in a simple auditory system," *Journal of Neurophysiology*, vol. 90, no. 4, pp. 2484–2493, 2003.

[83] A.-M. M. Oswald, B. Doiron, and L. Maler, "Interval coding. I. Burst interspike intervals as indicators of stimulus intensity," *Journal of Neurophysiology*, vol. 97, no. 4, pp. 2731–2743, 2007.

[84] D. L. Jones, E. C. Johnson, and R. Ratnam, "A stimulus-dependent spike threshold is an optimal neural coder," *Frontiers in Computational Neuroscience*, vol. 9, p. 61, 2015.

[85] E. C. Johnson, D. L. Jones, and R. Ratnam, "Minimum squared-error, energy-constrained encoding by adaptive threshold models of neurons," in *IEEE International Symposium on Information Theory Proceedings (ISIT), 2015.* IEEE, June 2015, pp. 1337–1341.

[86] N. Y.-S. Kiang, T. Wantanabe, E. C. Thomas, and L. F. Clark, *Discharge Patterns of Single Fibers in the Cat's Auditory Nerve.* Cambridge, MA: MIT Press, 1965.

[87] S. Panzeri and S. R. Schultz, "A unified approach to the study of temporal, correlational, and rate coding," *Neural Computation*, vol. 13, no. 6, pp. 1311–1349, 2001.

[88] M. Rudolph and A. Destexhe, "Tuning neocortical pyramidal neurons between integrators and coincidence detectors," *Journal of Computational Neuroscience*, vol. 14, no. 3, pp. 239–251, 2003.

[89] N. Masuda and K. Aihara, "Duality of rate coding and temporal coding in multilayered feedforward networks," *Neural Computation*, vol. 15, no. 1, pp. 103–125, 2003.

[90] F. Farkhooi, M. F. Strube-Bloss, and M. P. Nawrot, "Serial correlation in neural spike trains: Experimental evidence, stochastic modeling, and single neuron variability," *Physical Review E*, vol. 79, no. 2, p. 021905, 2009.

[91] R. Ratnam and M. E. Nelson, "Nonrenewal statistics of electrosensory afferent spike trains: Implications for the detection of weak sensory signals," *The Journal of Neuroscience*, vol. 20, no. 17, pp. 6672–6683, 2000.

[92] N. Lüdtke and M. E. Nelson, "Short-term synaptic plasticity can enhance weak signal detectability in nonrenewal spike trains," *Neural Computation*, vol. 18, no. 12, pp. 2879–2916, 2006.

[93] J. Goense and R. Ratnam, "Continuous detection of weak sensory signals in afferent spike trains: the role of anti-correlated interspike intervals in detection performance," *Journal of Comparative Physiology A*, vol. 189, no. 10, pp. 741–759, 2003.

[94] W. H. Nesse, L. Maler, and A. Longtin, "Biophysical information representation in temporally correlated spike trains," *Proceedings of the National Academy of Sciences*, vol. 107, no. 51, pp. 21 973–21 978, 2010.

[95] N. S. Jayant and P. Noll, *Digital Coding of Waveforms: Principles and Applications to Speech and Video.* Englewood Cliffs, NJ: Prentice Hall, 1984.

[96] M. N. Shadlen and W. T. Newsome, "The variable discharge of cortical neurons: implications for connectivity, computation, and information coding," *The Journal of Neuroscience*, vol. 18, no. 10, pp. 3870–3896, 1998.

[97] R. de Ruyter van Steveninck, G. D. Lewen, S. P. Strong, R. Koberle, and W. Bialek, "Reproducibility and variability in neural spike trains," *Science*, vol. 275, no. 5307, pp. 1805–1808, 1997.

[98] G. L. Gerstein and B. Mandelbrot, "Random walk models for the spike activity of a single neuron," *Biophysical Journal*, vol. 4, no. 1, p. 41, 1964.

[99] J. B. Goense, R. Ratnam, and M. E. Nelson, "Burst firing improves the detection of weak signals in spike trains," *Neurocomputing*, vol. 52, pp. 103–108, 2003.

[100] J. Von Neumann, "Probabilistic logics and the synthesis of reliable organisms from unreliable components," *Automata Studies*, vol. 34, pp. 43–98, 1956.

[101] L. Schuchman, "Dither signals and their effect on quantization noise," *Communication Technology, IEEE Transactions on*, vol. 12, no. 4, pp. 162–165, December 1964.

[102] K. Wiesenfeld, F. Moss et al., "Stochastic resonance and the benefits of noise: From ice ages to crayfish and squids," *Nature*, vol. 373, no. 6509, pp. 33–36, 1995.

[103] M. D. McDonnell and D. Abbott, "What is stochastic resonance? Definitions, misconceptions, debates, and its relevance to biology," *PLoS Computational Biology*, vol. 5, no. 5, p. e1000348, 2009.

[104] H. Chen, L. R. Varshney, and P. K. Varshney, "Noise-enhanced information systems," *Proceedings of the IEEE*, vol. 102, no. 10, pp. 1607–1621, 2014.

[105] A. Longtin, "Stochastic resonance in neuron models," *Journal of Statistical Physics*, vol. 70, no. 1-2, pp. 309–327, 1993.

[106] J. Collins, C. C. Chow, T. T. Imhoff et al., "Stochastic resonance without tuning," *Nature*, vol. 376, no. 6537, pp. 236–238, 1995.

[107] J. J. Collins, T. T. Imhoff, and P. Grigg, "Noise-enhanced information transmission in rat SA1 cutaneous mechanoreceptors via aperiodic stochastic resonance," *Journal of Neurophysiology*, vol. 76, no. 1, pp. 642–645, 1996.

[108] D. R. Chialvo, A. Longtin, and J. Müller-Gerking, "Stochastic resonance in models of neuronal ensembles," *Physical Review E*, vol. 55, no. 2, p. 1798, 1997.

[109] J. E. Levin and J. P. Miller, "Broadband neural encoding in the cricket cereal sensory system enhanced by stochastic resonance," *Nature*, vol. 380, no. 6570, pp. 165–168, 1996.

[110] Z. F. Mainen and T. J. Sejnowski, "Reliability of spike timing in neocortical neurons," *Science*, vol. 268, no. 5216, pp. 1503–1506, 1995.

[111] G. E. Uhlenbeck and L. S. Ornstein, "On the theory of the Brownian motion," *Phys. Rev.*, vol. 36, pp. 823–841, Sep 1930.

[112] D. Cox and P. Lewis, *The Statistical Analysis of Series of Events*. London, UK: Chapman Hall, 1966.

[113] O. Avila-Akerberg and M. J. Chacron, "Nonrenewal spike train statistics: Causes and functional consequences on neural coding," *Experimental Brain Research*, vol. 210, no. 3-4, pp. 353–371, 2011.

[114] O. Avila-Akerberg and M. J. Chacron, "Noise shaping in neural populations." *Physical Review. E, Statistical, Nonlinear, and Soft Matter Physics*, vol. 79, no. 1, pp. 011 914–011 914, 2009.

[115] C. A. Shumway, "Multiple electrosensory maps in the medulla of weakly electric gymnotiform fish. I. Physiological differences," *The Journal of Neuroscience*, vol. 9, no. 12, pp. 4388–4399, 1989.

[116] M. E. Nelson and M. A. Maciver, "Prey capture in the weakly electric fish apteronotus albifrons: Sensory acquisition strategies and electrosensory consequences," *Journal of Experimental Biology*, vol. 202, no. 10, pp. 1195–1203, 1999.

[117] T. Schwalger and B. Lindner, "Patterns of interval correlations in neural oscillators with adaptation," *Frontiers in Computational Neuroscience*, vol. 7, 2013.

[118] H. Chen, P. K. Varshney, S. M. Kay, and J. H. Michels, "Theory of the stochastic resonance effect in signal detection: Part I fixed detectors," *IEEE Transactions on Signal Processing*, vol. 55, no. 7, pp. 3172–3184, 2007.

[119] H. Chen, P. K. Varshney, and J. H. Michels, "Noise enhanced parameter estimation," *IEEE Transactions on Signal Processing*, vol. 56, no. 10, pp. 5074–5081, 2008.

[120] R. VanRullen, R. Guyonneau, and S. J. Thorpe, "Spike times make sense," *Trends in Neurosciences*, vol. 28, no. 1, pp. 1–4, 2005.

[121] E. Neher and C. F. Stevens, "Conductance fluctuations and ionic pores in membranes," *Annual Review of Biophysics and Bioengineering*, vol. 6, no. 1, pp. 345–381, 1977.

[122] J. A. White, J. T. Rubinstein, and A. R. Kay, "Channel noise in neurons," *Trends in Neurosciences*, vol. 23, no. 3, pp. 131–137, 2000.

[123] K. Fisch, T. Schwalger, B. Lindner, A. V. Herz, and J. Benda, "Channel noise from both slow adaptation currents and fast currents is required to explain spike-response variability in a sensory neuron," *The Journal of Neuroscience*, vol. 32, no. 48, pp. 17 332–17 344, 2012.

[124] W. B. Levy and R. A. Baxter, "Energy-efficient neuronal computation via quantal synaptic failures," *The Journal of Neuroscience*, vol. 22, no. 11, pp. 4746–4755, 2002.

[125] F.-G. Zeng, S. Rebscher, W. Harrison, X. Sun, and H. Feng, "Cochlear implants: System design, integration, and evaluation," *IEEE Reviews in Biomedical Engineering*, vol. 1, pp. 115–142, 2008.

[126] P. C. Loizou, "Mimicking the human ear," *IEEE Signal Processing Magazine*, vol. 15, no. 5, pp. 101–130, 1998.

[127] V. Looi, H. McDermott, C. McKay, and L. Hickson, "Music perception of cochlear implant users compared with that of hearing aid users," *Ear and Hearing*, vol. 29, no. 3, pp. 421–434, 2008.

[128] J. Laneau, J. Wouters, and M. Moonen, "Improved music perception with explicit pitch coding in cochlear implants," *Audiology and Neurotology*, vol. 11, no. 1, pp. 38–52, 2006.

[129] J. Wouters, H. McDermott, and T. Francart, "Sound coding in cochlear implants: From electric pulses to hearing," *IEEE Signal Processing Magazine*, vol. 32, no. 2, pp. 67–80, March 2015.

[130] J. A. Bierer and J. C. Middlebrooks, "Auditory cortical images of cochlear-implant stimuli: Dependence on electrode configuration," *Journal of Neurophysiology*, vol. 87, no. 1, pp. 478–492, 2002.

[131] M. F. Dorman, P. C. Loizou, and D. Rainey, "Speech intelligibility as a function of the number of channels of stimulation for signal processors using sine-wave and noise-band outputs," *The Journal of the Acoustical Society of America*, vol. 102, no. 4, pp. 2403–2411, 1997.

[132] P. C. Loizou, M. Dorman, and Z. Tu, "On the number of channels needed to understand speech," *The Journal of the Acoustical Society of America*, vol. 106, no. 4, pp. 2097–2103, 1999.

[133] M. F. Dorman, P. C. Loizou, and D. Rainey, "Simulating the effect of cochlear-implant electrode insertion depth on speech understanding," *The Journal of the Acoustical Society of America*, vol. 102, no. 5, pp. 2993–2996, 1997.

[134] A. Kral, R. Hartmann, D. Mortazavi, and R. Klinke, "Spatial resolution of cochlear implants: The electrical field and excitation of auditory afferents," *Hearing Research*, vol. 121, no. 1, pp. 11–28, 1998.

[135] R. L. Snyder, J. C. Middlebrooks, and B. H. Bonham, "Cochlear implant electrode configuration effects on activation threshold and tonotopic selectivity," *Hearing Research*, vol. 235, no. 1, pp. 23–38, 2008.

[136] P. C. Loizou, O. Poroy, and M. Dorman, "The effect of parametric variations of cochlear implant processors on speech understanding," *The Journal of the Acoustical Society of America*, vol. 108, no. 2, pp. 790–802, 2000.

[137] V. L. Ming and L. L. Holt, "Efficient coding in human auditory perception," *The Journal of the Acoustical Society of America*, vol. 126, no. 3, pp. 1312–1320, 2009.

[138] U. Meyer-Baese, A. Meyer-Baese, and H. Scheich, "Auditory neuron models for cochlea implants," in *AeroSense'97*. International Society for Optics and Photonics, 1997, pp. 582–593.

[139] D. B. Grayden, A. N. Burkitt, O. P. Kenny, J. C. Clarey, A. G. Paolini, and G. M. Clark, "A cochlear implant speech processing strategy based on an auditory model," in *Intelligent Sensors, Sensor Networks and Information Processing Conference, 2004.* IEEE, 2004, pp. 491–496.

[140] A. Dreyer and B. Delgutte, "Phase locking of auditory-nerve fibers to the envelopes of high-frequency sounds: Implications for sound localization," *Journal of Neurophysiology*, vol. 96, no. 5, pp. 2327–2341, 2006.

[141] R. V. Shannon, "Multichannel electrical stimulation of the auditory nerve in man. I. Basic psychophysics," *Hearing Research*, vol. 11, no. 2, pp. 157–189, 1983.

[142] R. Hartmann, G. Topp, and R. Klinke, "Discharge patterns of cat primary auditory fibers with electrical stimulation of the cochlea," *Hearing Research*, vol. 13, no. 1, pp. 47–62, 1984.

[143] C. Van den Honert and P. Stypulkowski, "Temporal response patterns of single auditory nerve fibers elicited by periodic electrical stimuli," *Hearing Research*, vol. 29, no. 2, pp. 207–222, 1987.

[144] C. A. Miller, P. J. Abbas, and B. K. Robinson, "Response properties of the refractory auditory nerve fiber," *JARO-Journal of the Association for Research in Otolaryngology*, vol. 2, no. 3, pp. 216–232, 2001.

[145] S. B. Dynes and B. Delgutte, "Phase-locking of auditory-nerve discharges to sinusoidal electric stimulation of the cochlea," *Hearing Research*, vol. 58, no. 1, pp. 79–90, 1992.

[146] F. Chen and P. C. Loizou, "Predicting the intelligibility of vocoded speech," *Ear and Hearing*, vol. 32, no. 3, p. 331, 2011.

[147] M. Nilsson, S. D. Soli, and J. A. Sullivan, "Development of the hearing in noise test for the measurement of speech reception thresholds in quiet and in noise," *The Journal of the Acoustical Society of America*, vol. 95, no. 2, pp. 1085–1099, 1994.

[148] J. E. O'Doherty, M. Lebedev, T. L. Hanson, N. Fitzsimmons, and M. A. Nicolelis, "A brain-machine interface instructed by direct intracortical microstimulation," *Frontiers in Integrative Neuroscience*, vol. 3, p. 20, 2009.

[149] M. L. Homer, A. V. Nurmikko, J. P. Donoghue, and L. R. Hochberg, "Implants and decoding for intracortical brain computer interfaces," *Annual Review of Biomedical Engineering*, vol. 15, p. 383, 2013.